A CONTINUUM PATH INTEGRAL APPROACH TO THE SIMULATION OF A
UNITARY GAS

BY

ADAM CHRISTOPHER KNAPP

DISSERTATION

Submitted in partial fulfillment of the requirements
for the degree of Doctor of Philosophy in Chemical Physics
in the Graduate College of the
University of Illinois at Urbana-Champaign, 2015

Urbana, Illinois

Doctoral Committee:

      Professor David M. Ceperley, Chair
      Assistant Professor Bryan K. Clark
      Professor Martin H. W. Gruebele
      Professor Philip W. Phillips

Abstract

This thesis presents an investigation by simulation of a unpolarized fermionic unitary gas system composed of two interacting fermionic species. While these species do not interact amongst themselves, they interact with each other using a pairwise zero-range delta function potential that has been tuned to unitarity i.e.the scattering length $a_s = -\infty$. A path integral Monte Carlo simulation of such a system is performed using an exact novel zero-range, delta function pair propagator which has been tuned to the unitary limit so that essentially all interactions amongst the interacting particles are comprised of s-wave interactions. This tuning in some sense yields the simplest imaginable interacting fermionic system which out to display features that would apply universally to interacting fermionic particles with particular interest within this field of study being in understanding the unitary BCS-BEC crossover. Numerical and ergodic challenges to sampling a divergent approximate path integral are discussed and solutions are proposed, implemented and explored. This thesis represents a step closer to this understanding by investigating this system with this novel propagator in a fixed-node path integral Monte Carlo framework and comparing to earlier work.

To my parents, Joan and Leonard, and my sister and brother-in-law, Amelia and John and niece, Coral,

whose first year more or less bookends this project. Your love and support has been everything to me.

Acknowledgments

Professionally, I would like to thank my committee Profs. David Ceperley, Bryan Clark, Martin Gruebele, and Philip Phillips for their steadfastness and patience through this process. In particular, Prof. Ceperley's guidance as my advisor has been critical to the completion of this this thesis as has Prof. Clark's willingness to help me through the intricacies of the interaction between my simulation and the PIMC++ source code. Dr. Norm Tubman's guidance and patience has also been remarkably helpful throughout this project and has been and remains greatly appreciated. I would like to thank the other members of the computational condensed matter group for the valuable conversations and support throughout the years. In particular, I would like to thank ChangMo (David) Yang for the late night talks and discussions of science and scientific computing. Dr. Lucas Wagner for being able and willing to answer my questions about scientific computing and directions condensed matter simulations. Dr. Hitesh Changlani for valuable external advice and Huihuo Zheng for so graciously listening to my conversations with ChangMo.

On a more personal note, graduate school has been a long, and frequently, tortured road for me. The advice and camaraderie of good friends and family has been critical to me throughout my years in the Midwest and Champaign-Urbana. My friends and fellow graduate students, who are invariably one and the same, have provided a great deal of support and fun over the years among them are: Nick Salovich, Chris Corcoran, and Joe Gezo. Thank you guys for everything. My former roommates, Andrew Dubar, Rusty Connor, and Jeff Carter provided much needed perspective when need during my early years here. My aunts, uncles, cousins and grandmother for so graciously letting me stay and visit their homes over these years while I've been so far from anyplace I would willingly consider home. I cannot express how important those trips were for my sanity. Finally, I'd like to thank my family Joan and Leonard Knapp and my sister Amelia (Mia) Redmond, brother-in-law John Redmond, and niece, Coral Redmond. You rode this roller coaster with me and were always there for me. I cannot express my gratitude for your unwavering support. You were there with me through the good times and the bad. I love all of you.

Table of Contents

List of Abbreviations

MC   Monte Carlo.

PI   Path Integral

PIMC   Path Integral Monte Carlo.

Chapter 1

An Introduction to the Physics of Cold Atom Systems

1.1 Motivating Background and Applications

While the bulk of this thesis concerns the path integral Monte Carlo (PIMC) simulation and study of an unpolarized fermionic cold atom system in the unitary limit, it is worthwhile to review the origins of the physics which underlies and justifies this study, what is broadly referred to as "cold atom systems" – a field of study which has seen tremendous growth over the past two decades. This introductory chapter is intended as a broad, non-exhaustive overview of the history, applications, and experimental methodology of trapped cold atom systems; theoretical concerns will be considered in subsequent chapters.

1.1.1 A Historical Introduction

As has already been noted, the past two decades have seen tremendous advancement and growth in advancements, growth and interest in the physics of cold atom systems. Within the physics community, the general interest in this field has grown so much that it has been termed to be a "third quantum revolution [1]," which possible hyperbole aside, nonetheless, demonstrates the clear excitement generated by work within this field. Consequently, adopting a prudent outlook towards this field, it seems very worthwhile to take a closer look at the particulars of this field, particularly when due consideration is given to the prior relative sleepiness (in this author's opinion) of AMO (atomic, molecular, and optical) physics.

The arguable transformation of traditional AMO physics from a peripheral field to a central one within the physics community has generally followed two great changes. The initial cause of this upsurge of interest was a technical one and happened in 1995. In that year, a Bose-Einstein condensate (BEC) in dilute atomic gases was first made [2–4], and ultimately resulted in Nobel prizes for the principle investigators of that work, Cornell, Wieman and Ketterle. BECs had until 1995 remained an object solely of theoretical curiosity and were subject to considerable debate in terms of whether or not they were experimentally realizable. The second great change in AMO physics was a financial one and followed naturally from the first: this field saw an increase in funding by 26% in inflation adjusted terms from 1995 to 2005 within the United States in

an era when other physical science funding stayed roughly constant or decreased (significantly in the case of high energy physics) in those same terms [5]. Thus, this increase in funding naturally brought about a flurry of activity and brought interest to this specialty from outside its traditional confines [5].

After BECs were first observed, the proverbial flood gates opened, and further stimulated by the aforementioned funding increase, other advances soon followed. To give just a few highlights: the fermionic corollary to BECs, the Fermi-Dirac condensates (FDCs) were first observed in 1999 by DeMarco and Jin [6], Feschbach resonances were used to tune interactions between constituent trapped atoms [7, 8]. A pairing scale gap measurement was performed in 2004 [9], which was soon followed by a measurement of vortices to identify the superfluid state in 2005 by Zwierlein et. al. [10]. Concurrent with these experimental advancements, modern theoretical work in this now experimentally fertile area soon blossomed due to the possibility of experimental verification and the funding increase.

However, much of this theoretical work was aimed not so much at the intrinsic possibilities of AMO type-systems, but at problems in other fields of physics. This was possible because many toy models from other areas of physics became experimentally accessible due to the technical and experimental advances in AMO physics, of course, one could argue the converse that these advances happened because other fields saw potential in cold atom systems to access systems. From either standpoint, the theoretical considerations of other fields lead naturally to the applications of cold atom systems within the physics community.

1.1.2   Applications of Cold Atom Systems

In this author's view as has already been alluded to, much of the worked performed within the cold trapped atom portion of the AMO subfield has ultimately been performed to serve and enhance programs of research from outside of the AMO specialty with a particular emphasis upon the goals and interests of condensed matter physics community. This statement is not meant as a criticism, but as a point of departure for understanding the orientations, inclinations, and motivations of this nascent field.

The growth of this specialty has been something of a windfall for modern condensed matter physics. Condensed matter physics as a field of inquiry has been severely challenged by the theoretical and, in many cases experimental, intractability of its modern signature problems. Many of these problems ultimately stem from many-body theory such as strongly correlated electron systems and result in a cascade of further complications as in the fermionic pairing of high-temperature superconductivity to give an example. Because cold atom systems allow experimentalists to deftly tune the interactions among their cold atom particles, much hope within condensed matter physics that these systems will allow the eventual direct simulation many of the intractable toy models used in condensed matter physics by means of direct experimentation.

Specifically, since cold atom systems have tunable interactions which can be made to mimic many of the idealized relationships and interactions typically imposed upon the toy model systems, they may be used to physically simulate many of these same models. In essence, these systems are analog quantum computing devices for the simulation of very specific toy models and can be viewed as the first experimentally realizable and scalable many-body rung of quantum computing, albeit with the understanding that these are single use, analog devices. In recent years, observations to this effect have led to serious inquiries into the computational complexity of model Hamiltonians [11] as well as the full extent and ultimate physical relevance of underlying toy models within condensed matter and other physical fields of inquiry such as nuclear or particle physics [12].

A Listing of Applications

Amongst the systems in condensed matter, materials, and chemical physics that have seen applications and/or interest for study with cold atom systems are [1]:

One-dimensional systems: One dimensional systems are a well-developed and classical area of theoretical condensed matter physics (CMP) research and feature many exactly solvable models and approaches. In particular, this area has been a test bed for many developments in theoretical CMP. In particular, Bethe ansatz and quantum inverse scattering methods have allowed the exact solution of many systems [13], the density matrix renormalization group has been remarkably effective for the numerical solution of one-dimensional systems [14], and approximate analytical methods such as conformal field theory and bosonization [15] have further investigation into otherwise intractable systems and regimes. Nonetheless, many experimental questions remain and are being addressed by one-dimensional cold atoms gases in particular TonksGirardeau gases which are repulsive bosonic systems and are interesting due to their superficially counterintuitive property of being fermion-like have been studied in experimental detail with cold atoms [16] as they are a system which is difficult to study experimentally in any other way to compare with theoretical and numerical results.

Phase-transitions in two-dimensional systems: The Mermin-Wagner-Hohenberg theorem predicts that continuous systems do not exhibit long-range order in temperatures above absolute zero. They do however allow for possibility of undergoing a transition which decays algebraically instead of exponentially, the Kosterlitz-Thouless-Berezinskii transition. While said transition has already been observed in a macroscopic liquid helium system, an atomic scale resolution of the system was not accessible, and had to wait to be observed in a cold atom gas system [17].

Various perturbations upon spin and Hubbard-type models: Due to the tunability of the interactions amongst the constituents of cold atom gases, a natural goal has been the experimental detection and ob-

servation of the various spin and Hubbard-type models which serve as models for condensed matter spin and strongly correlated systems. Because these models are unsolved even in their most basic form in 2 or 3 dimensions, using cold atom systems to simulate these "simple" systems is highly desirable [13, 15].

Direct observation of anyons and other fractional quantum Hall effect related phenomena: While fractional quantum hall effects are well studied today and have served to even secure a Nobel prize for Laughlin, Störmer, and Tsui in 1998 [18], many of their correlated effects as well as anyonic excitations remain to be directly observed. Rotating cold atomic gas states have been suggested to realize and observe various aspects of fractional quantum hall effects [19].

Realizing systems whose disorder is directly probeable and reproducible: The possibility of experimentally probing exactly tuned and experimentally reproducible disordered systems is a tantalizing one due to the importance that disorder plays in the phenomena condensed matter physics. In particular, cold atom systems have been proposed or used to observe disordering phenomena as diverse as Anderson localization and Bose glasses. More importantly due to the previously mentioned tunability of the underlying systems, cold atom systems justify as experimentally realizable the theoretical exploration of potentially novel and unimagined disordered physical states and regimes.

Quantum computation and topological systems:Amongst the grand goals of modern physics is the construction and physical understanding in detail of a quantum computer as these computational systems are expected to have significant advantages over classical computers [20]. Unfortunately, realizing quantum computers using standard quantum states has proven to be difficult due to decoherence [20]. Consequently, topological states which cannot be locally decohered are of considerable interest. Certain spin systems which possess topological states are theoretically realizable as cold atom systems and hence there is hope that they may be eventually realized in these same systems and made to perform quantum computations [21, 22].

Superchemistry: Cold atom gas systems also present opportunities for chemistry. Specifically, they allow the creation and careful control of simple two-body and higher chemical reactions from a controlled intial state to a controlled final state. Effimov trimers have already been observed in trapped Cs atoms [23] and further work on the creation of deeply bound molecules has been done by Danzl et.al. [24].

Of course, in order to realize the preceding systems much work both theoretical, and in particular, experimental will be required to advance the art of the field. Consequently, to fully respect this work, an introduction to the experimental methodology and its theoretical underpinnings is desirable which is the subject of the next section. Suffice to say these systems are relevant as experimental probes for many-body systems because they allow for a hitherto unprecedented degree of tunability of their underlying interactions and structure.

1.2 Methods in Cold Atom Systems

In this section, the experimental methods used to create and probe cold atom systems will be presented in two subsections. The first subsection will qualitatively describe the experimental methods used to create cold atom systems via optical trapping. The second subsection will present the underlying technical details to these methods and flesh them out from a physical standpoint. Theoretical approaches to cold atom systems with an emphasis on those applied to cold fermionic unitary gases will be detailed in a subsequent chapter.

1.2.1 Experimental Methods for Cold Atom Systems: A Qualitative Overview

Trapped cold atom systems are an important means to investigate specific aspects and effects of many-body quantum statistical mechanics. Due to their tunability, they allow experimentalists to probe physical regimes that had prior to their development been only investigated from a theoretical standpoint or under very restricted and system specific conditions. Cold atoms are typically trapped using either magnetic fields or the external potentials created with laser light.Typically the atoms are cooled using evaporative and laser cooling. In the evaporative case, the cooling effect works by allowing the atoms to redistribute their energy amongst themselves so that the fastest and hence most energetic are allowed to escape the trap and carry their energy away. In the case of laser cooling, an atom is hit by a specially tuned laser beam of photons which causes the atom to re-radiate a photon of higher energy and thus cool down i.e. slow the atom in question. These methods have been combined to create systems with temperatures in the nanoKelvin range. Of particular importance to the scientific viability of these systems are Feschbach resonances between particles which allow the interaction strength between those same atoms to be tuned utilizing an external magnetic field. Combining these tuned interactions with clever choices in the trapping laser arrangements, choice in constituent atoms, and the external magnetic field allows for a wide variety of interesting cold atom systems to be probed [1].

1.2.2 A Technical Approach to Experimental Methods for Cold Atom Systems

That said many of the technical specifics of cold atom interactions are required for a deeper understanding of this field. This next section serves to act as a deeper technical description of the experimental methodology of cold atom systems and draws from unless otherwise cited Pethick and Smith [25] and Pitaevskii and Stringari [26] [1].

---

[1]This subsection closely follows the presentation given by Shenquan Zhou in his thesis [27].

Methods for Atomic Cooling

Many of the constraints and requirements for atomic cooling are dictated by ultimate requirements of the underlying traps. Of particular importance for cold atomic systems are the experimental constraints on magnetic field strength which are much less than 1 T, this results in a constraint on the average energy of the atoms and hence the temperature. Assuming a 1 T magnetic field requires that in order for the atoms to be trapped that they be cooled to about a temperature $T < \mu_B B \approx 0.67$ K/T $\times 1$T $= 0.67K$. For optical traps, the experimental constraints require that the frequency of the trapping laser be chosen away from atomic resonances. Moreover, due to the energetic shallowness of the optical traps, on the order of a μK, the atoms must be cooled by other means before trapping [1, 25, 26].

As an added complication the effectiveness of these cooling methods are typically applied in a hierarchical fashion due to the standard tradeoff between efficiency/effectiveness and performance. In this case, Doppler cooling can cool the most number atoms with the finest control, Sisyphus cooling cools fewer atoms but to a lower temperature and finally, evaporative cooling can reach temperatures low enough for Bose-Einstein condensates to form, but is the least efficient of the investigated methods [25].

Doppler Cooling: Doppler cooling is an optical cooling technique which utilizes the Doppler wave effect to cool atoms. In this method, the atom subject to cooling is effected by two counter-propagating laser beams of equivalent frequency and intensity. The frequency of these beams are slightly offset from the energy of electronic transition between an excited state and ground state.

The laser radiation field of the beam can be thought of as exerting a frictional force on the atoms in a configuration known as optical molasses. In essence, the laser beams are tuned such that a transition is more likely to occur if the atom in question is moving such that the detuned laser beams' frequency is matched with the energy of the related transition by the Doppler shift induced by the atom's movement. As this effect occurs in either of the direction's of the atom's one dimensional Cartesian movement, it localizes narrows range of the average kinetic energy of the atom and hence cools the system. The lowest temperature reachable by this technique is found by balancing the the heating rate with the cooling rate and relating the resulting momentum's mean-square value to a diffusive random walk which ultimately allows the decay rate of the excited state transition state to be related directly to the temperature as,

$$kT = \frac{\hbar\Gamma_i}{2},\tag{1.1}$$

where Γ_i is the constant associated with decay transition's Lorentzian description from excited state $|i\rangle$. For the case of ^{6}Li the, the Doppler cooling temperature floor is 140 μK; for point of comparison in Na it is 480

μK.

Sisyphus Cooling: Sisyphus cooling while related to and incidentally discovered by analyzing data from Doppler cooling is a mechanism through which atoms can be cooled using laser beams below the temperatures expected to be achieved by Doppler cooling. When it was first observed as a byproduct of Doppler cooling, it was both welcomed since that technique seemed to work better than expected and disquieting because something was clearly wrong with the underlying analysis of Doppler cooling. Eventually, Sisyphus cooling was explained by considering the energy lost by moving the atoms through an inhomogeneous laser radiation field since in effect the laser radiation induces not a constant but an oscillating periodic potential. In effect the atoms lose kinetic energy by being repeatedly being moved via optical pumping from periodic potential maximas to lower energy states which obviously decreases kinetic energy and thus temperature resulting in a thermal energy of about the recoil energy,

$$E_R = kT_{Sisyphys} = \frac{\hbar^2 q^2}{2m},\qquad(1.2)$$

where E_R describes the energy added to that of the atom after absorbing a photon of momentum $\hbar q$. This results in a cooling effect which can reach temperatures several orders of magnitude less than that of Doppler cooling which typically range from 0.1 to 1.0 μK.

Evaporative Cooling:

Finally after laser cooling has been applied to cold atom systems, the next and typically final stage of cooling applied to these systems is evaporative cooling. The method works in essentially the same way that helium boils off from the earth at ambient temperatures, with a modicum of control provided by a radiofrequency (RF) induced spin flip which on the atomic spin state which can be used to eject the heated atoms in question. In essence, evaporative cooling works bleeding atoms with higher than average energy from the trap. The experimenter allows the atoms to collide and scatter and exchange energy so that a Boltzmann-Maxwell distribution is achieved. Next because the Zeeman effect in an inhomogeneous magnetic field causes a resonant frequency dependent upon the position of the atom when a tuned RF pulse is applied to the system and the internal spin state of an atom is changed from a low-field to a high-field seeker, the higher energy atoms may be selectively ejected by being more likely to be in higher energy positions in the magnetic trap. This method can then be applied repeatedly to the same system by tuning the RF pulse to selectively eject atoms with lower and lower internal energies.

Further complicating this cooling technique are the quantum statistics or wavefunction symmetry of the particles being cooled. In the case of fermions, the antisymmetry of the particles' wavefunction prevents

the collision of the underlying particles so an intermediary particle to help with the energetic rearrangement must be included in the system, and then once the system of interest is cooled, these helper particles must be depending on the specific experiment ignored, ejected or have the secondary particles used be the same fermionic species in a different hyperfine state which themselves must then be ignored, ejected, or transitioned into the state of actual interest. This secondary form of evaporative cooling is called sympathetic cooling.

Background Data on Atoms Used in Traps

Much current and past experimentation in fermionic cold atom systems have occurred in cold alkali atom systems such as rubidium, Rb, sodium, Na, and potassium, K. These are neutral atoms containing an equivalent number of electrons and protons. Due to this equivalence in electrons and protons, it is the neutron number within the nucleus which determines the particle statistics of this composite atomic system. Specifically, if the number of neutrons is even, the atom is a boson; if the number of neutrons is odd, it is a fermion. The table below lists various alkali metals along with experimentally relevant values [25, 26]

Table 1.1: Neutral Alkali Metals: *This table presents various alkali metals used in optical trapping experiments. Z denotes the proton number, N is the neutron number, I is the nuclear magnetic moment in units of the nuclear magneton $\mu_N = e\hbar/2_{,p}$ and $\nu_{textrmhf}$ is the hyperfine splitting*

Isotope	Z	N	I	μ/μ_N	ν_{hf} (MHz)
^{1}H	1	0	1/2	2.793	1420
^{6}Li	3	3	1	0.822	228
^{7}Li	3	4	3/2	3.256	804
^{23}Na	11	12	3/2	2.218	1772
^{39}K	19	20	3/2	0.391	462
^{40}K	19	21	4	-1.298	-1286
^{41}K	19	22	3/2	0.215	254
^{85}Rb	37	48	5/2	1.353	3036
^{87}Rb	37	50	3/2	2.751	6835
^{133}Cs	55	78	7/2	2.579	9193

Hyperfine Splitting: An Introduction

The underlying effect used for the trapping and subsequent tuning of the interactions between trapped atoms is hyperfine splitting. Hyperfine splitting may be described as the collection of effects due to external electromagnetic field and spin couplings which result in small energetic shifts in the level structure of ions, atoms, and molecules. These effects are important in cold atom systems as they give experimentalists ways to manipulate and control systems using external fields. Specifically, because they are so important for the

performance of cold atom experiments an overview will be given in the following sub-subsections.

Hyperfine Splitting for Alkali Atoms without an External Field

Due to their relatively simplified hyperfine splitting structure, alkali atoms are frequently used in cold atom systems. This simplified hyperfine structure for alkalis descends from their simple ground state electronic structure composed of closed shells and a single electron in an s-shell so that electron has an angular momentum quantum number $L = 0$ which is important for subsequent investigation. As an example, starting with the typical ground state electronic configuration of Li a simple alkali atom is $1s^2 2s^1$. Hyperfine interactions in this context arise when the electron spin couples to the nuclear spin and the electromagnetic splitting is particularly strong for alkali metals because the open-shell electron is in an s orbital configuration has a comparatively high probability of being close to the nucleus. Moreover, since the valence electron has no angular momentum, it doesn't induce a magnetic field on the nucleus. Thus, the coupling electron-nuclei coupling is due solely to the magnetic field caused by the electron spin. The coupling of the electronic spin $S = 1/2$ to the nuclear spin I then yields $F = \pm 1/2$ for the quantum number F for the total spin, according to the rules for addition of angular momentum.

The simplest Hamiltonian used to model hyperfine interactions is given by

$$\hat{H}_{\mathrm{hf}} = A\mathbf{I} \cdot \mathbf{J}, \tag{1.3}$$

where A is the system specific hyperfine constant and $\mathbf{I}$ and $\mathbf{J}$ are the nuclear spin and electronic angular momentum operators. The terms given in eqn. (1.3) may be expressed in terms of the total angular momentum operator $\mathrm{F} = \mathbf{I} + \mathbf{J}$ as,

$$\mathbf{I} \cdot \mathbf{J} = \frac{1}{2} \left(F(F+1) - I(I+1) - J(J+1) \right). \tag{1.4}$$

For the alkali metals given in table (1.1), the absolute magnitude for the electronic spin, S and electronic angular momentum J is 1/2 which leads to the evaluation of eqn. (1.3) for splitting between $F = \pm 1/2$ is given as,

$$\Delta E_{\mathrm{hf}} = E_{I+\frac{1}{2}} - E_{I-\frac{1}{2}} = h\nu_{\mathrm{hf}} = A\left(I + 1/2\right). \tag{1.5}$$

The values of ΔE_{hf} for relevant alkali metals are given in the aforementioned table (1.1).

9

Hyperfine Splitting for Alkali Atoms with an External Field: The Magnetic Trapping of Atoms

Within trapped cold atom systems, atoms are typically trapped within external magnetic fields via the Zeeman effect. Consequently when trapping atoms in an external magnetic field the hamiltonian given by eqn. (1.3) must be augmented to account for the effects of that same field as,

$$\hat{H}_{\text{hf}} = A\mathbf{I} \cdot \mathbf{J} + CJ_z + DI_z, \tag{1.6}$$

where

$$C = g\mu_B B, \tag{1.7}$$

and

$$D = -\frac{\mu}{I}B, \tag{1.8}$$

where z is the orientation of the magnetic field, $\mu_B = |e|\hbar/2m_e$ is the Bohr magneton, and g is the electron structure factor and is about $g = 2 + 2\alpha/\pi$ to the leading order term; the effects of nuclear spin are small and despite being typically neglected are presented here for point of reference and to include effects of the magnetic field on the nucleus. The energetic contribution of the first perturbative term may then be solved for as,

$$\langle F, m_F | 2\mu_B J_z B | F, m_F \rangle = g_L \mu_B m_F B, \tag{1.9}$$

where m_F is the eigenvalue of F_z and

$$g_L = \frac{F(F+2) + J(J+2) - I(I+1)}{2F(F+1)} \tag{1.10}$$

is the Lande factor.

Furthermore, the entirety of eqn. (1.6) may be solved via diagonalization for arbitrary magnetic fields [25, 26] using a complete set of states denoted by $|m_I\, m_J\rangle$, the solution of which will be suppressed here due to lengthy algebra. Once solved, however, the solution and its description of energy levels and states serve as a convenient guide to tuning the external magnetic field and optimizing the trap. The depth of a magnetic trap is determined by the minimum of the Zeeman energy and due to experimental constraints on magnetic fields are typically on an energy scale much less than 1 K. Thus, the atoms must be cooled prior to magnetic trapping typically by either evaporative or laser techniques.

Optical Trapping of Atoms

Optical traps utilize the interaction of atoms with electromagnetic radiation fields typically emitted by lasers tuned away from resonance and higher than the hyperfine splittings to trap atoms in an external potential. The Hamiltonian describing this atom-laser field interaction is the dipole approximation,

$$\hat{H}_{Dipole} = -\mathbf{d} \cdot \mathcal{E}, \tag{1.11}$$

where $\mathcal{E}$ is the electric field operator and $\mathbf{d}$ is the dipole operator. Ultimately, using second-order perturbation theory this dipole interaction causes an energy shift in the ground state as

$$\Delta E_0 = -\frac{1}{2}\alpha(\omega)\langle\mathcal{E}^2(\mathbf{r},t)\rangle_t \tag{1.12}$$

where $\langle\cdots\rangle_t$ means the time average and

$$\alpha(\omega) = \sum_{i\neq 0} |\langle i|\mathbf{d}\cdot\hat{\epsilon}|0\rangle|^2 \left(\frac{1}{E_i - E_0 + \hbar\omega} + \frac{1}{E_i - E_0 - \hbar\omega}\right) \tag{1.13}$$

is the dynamical polarizability. If the frequency of $\alpha(\omega)$ is close to an atomic resonance, it is reasonable to ignore the non-resonant transitions and reduce eqn. (1.13) to

$$\alpha(\omega)|_{near\,resonance} \approx \frac{|\langle i|\mathbf{d}\cdot\hat{\epsilon}|0\rangle|^2}{E_i - i\hbar\Gamma_i/2 - E_0 - \hbar\omega} \tag{1.14}$$

where $-i\hbar\Gamma_i/2$, the finite lifetime due to spontaneous emission of photons, is put in using phenomenological considerations by allowing the excited state energy to have both real and imaginary terms.

The energy level shift in this formalism is then given by

$$V_0(\mathbf{r}) = -\frac{1}{2}\mathcal{R}[\alpha(\omega)\langle\mathcal{E}^2(\mathbf{r},t)\rangle_t] \tag{1.15}$$

where under the previous approximation scheme, the detuning δ the difference between the laser frequency and the resonant frequency may be defined as

$$\delta = \omega - \frac{E_i - E_0}{\hbar} = \omega - \omega_{i,0}. \tag{1.16}$$

and red and blue detuning refer to $\delta < 0$ and $\delta > 0$, respectively. The perturbative methodology remains used to derive these equations remains valid so long as $|\langle i|\mathbf{d}\cdot\hat{\epsilon}|0\rangle| << \hbar\sqrt{\delta^2 + \Gamma_i/4}$, which is typically true

due to the weak electric fields present in most cold atom experiments.

These atom-laser field interactions allow an experimentalist to create a radiation field with a maximal intensity in space. Detuning the laser light to the red causes the ground-state atom-laser field potential to have a spatial mininum in $V_0(\mathbf{r})$ which serves as a trap for those atoms. These traps are useful because they allow atoms to interrogated by both external light interactions and magnetic field potentials. This state of affairs is convenient since at least for the alkali atoms the ground state is virtually independent of the magnetic substate, due to the ground state being in an s-orbital state. This independence subsequently allows the experimentalist to change the magnetic field depending upon the underlying needs of the experiment. An example is that one may cool the system using an inhomogeneous field and then apply a uniform magnetic field for the purposes of utilizing Feschbach resonances.

Chapter 2

Cold Fermi Gases with Attractive Interactions and the BCS-BEC Crossover

2.1 Introduction and Overview

Cold fermionic gases with attractive interactions are currently being explored within the context of condensed matter physics due their ability to mimic many of the fundamental features underlying strongly correlated electron systems. These systems present, to both experimentalist and theorists, forms of strongly correlated interactions, which may be considered to be "simplified" from a theoretical standpoint due to the rudimentary and on/off nature of their interactions, features which are not typical of traditional, experimental condensed matter interactions. Often, these systems require quantum statistical mechanical analysis, and thus, must necessarily satisfy certain requirements to be considered within this regime. In the case of cold fermi gases, the systems are quantum degenerate and thus feature an interparticle separation $r_0 \propto \rho^{-1/d}$, where ρ is the density of a d-dimensional system which is comparable to the de Broglie wavelength, $\lambda_{dB} = \sqrt{\hbar^2/mk_bT}$, of the comprised particles which results in a high probability of fermionic particle exchange in their study and thus requires the inclusion of this phenomenon in their analysis. Within the context of condensed matter physics, superconductivity and superfluidity in liquid ^{3}He are among the systems which satisfy these requirements. For this chapter, however, the main subject of interest will be cold fermionic gases at unitary.

From an abstract point of view, binding all of these systems together are their propensity to form composite bosonic particles due to a weakly attractive interaction that is either innate to the the system in question or which arises as a composite force due to other excitations. After the formation of these composite bosons, subsequent macroscopically detectable states, like superfluids, may be formed. Within this chapter and thesis, two forms of fermionic pairing are being studied strongly bound and weakly bound pairs. Roughly speaking, a the strongly bound fermionic pair have a spacing which is much less than the interparticle spacing of the system in question such that these pair may be considered to be a dimer as is seen in a Bose-Einstein condensate of composite bosons. A weakly bound pair is a little more conceptually subtle where the composite boson is formed of weakly bound fermionic pairs in position space, although they can be strongly bound in momentum space [28].

Within condensed matter physics, it has been of historical interest to understand and probe the regime in which weakly bound fermionic pair transition to strongly bound pairs both as a function of temperature and other parameters [29, 30]. This thesis will specifically focus upon results related to a temperature based transition, although results from other orientations such as those seen in the $T = 0$ BCS variational wave function will be considered as well. To consider this effect, this chapter is structured as follows: The first section will present a rudimentary background on quantum mechanics for fermions. The next section will consider Bose-Einstein condensation bosonic and composite bosonic particles; this will be followed by a section which describes and derives the BCS theory of superconductivity. Finally, a brief overview of the crossover between BCS states and Bose-Einstein condensation will be presented, which will be followed by a more in depth presentation of experimental results and theoretical results related to this crossover.

2.2   Quantum Statistical Mechanics for Fermions

A basic description for non-interacting fermionic statistical mechanics may be begun with the average occupation number for a fermion species given as

$$f(\epsilon, T) = \frac{1}{e^{\beta(\epsilon - \mu)} + 1} \tag{2.1}$$

where ϵ is the quantum state energy and T is the temperature. $\beta = \frac{1}{k_B T}$ and the chemical potential μ is determined implicitly by

$$N = \int g(\epsilon) f(\epsilon, T) d\epsilon, \tag{2.2}$$

where $g(\epsilon)$ is the density of states as a function of quantum state energy. Moreover this density of states formalism may be used to calculate other thermodynamic quantities as follows

$$\langle u \rangle = \int U(\epsilon) f(\epsilon, T) d\epsilon \tag{2.3}$$

where $\langle u \rangle$ is a general thermal expectation value and $U(\epsilon)$ is a function which typically combines the density of states with an estimator for the quantity of interest as a function of energy, ϵ. Using these expressions with the standard thermodynamical formalism allows one to calculate any of the quantities typically associated thermodynamics for fermionic systems so long as one is able to calculate or otherwise has available the density of states $g(\epsilon)$.

As an example for a non-interacting, non-relativistic fermionic system of spin S the density of states for arbitrary dimensions, d, is given by

$$g(\epsilon) = \frac{(2S+1)V\pi^{d/2}(2m)^{d/2}}{(2\pi\hbar)^d\Gamma(\frac{d}{2})}\epsilon^{d/2-1},$$ (2.4)

which allows the calculation of the Fermi energy ϵ_F at $T = 0$ as

$$\epsilon_F = \frac{\hbar^2 k_F^2}{2m} = \frac{\hbar^2}{2m}\left(\frac{\Gamma(1+\frac{d}{2})(2\pi)^d}{(2S+1)\pi^{d/2}}\frac{N}{V}\right)^{2/d}$$ (2.5)

using eqn. (2.2) and the definition of fermi energy as being chemical potential μ at $T = 0$. Specializing this equation to 3 dimensions yields

$$\epsilon_{F3D} = \frac{\hbar^2}{2m}\left(\frac{(6\pi)^3}{(2S+1)}\frac{N}{V}\right)^{2/3}.$$ (2.6)

for the Fermi energy and

$$E_0 = \int_0^{\epsilon_F}\epsilon g(\epsilon)d\epsilon = \frac{d}{d+2}N\epsilon_F$$ (2.7)

for the energy after returning to arbitrary dimension, d, which by definition is the ground state energy. The grand canonical potential, $\Phi(T,\mu)$, for this system is

$$\Phi(T,\mu) = -\frac{2}{d}E(T,\mu) = k_B T\int_0^\infty g(\epsilon)\ln\left(1 - e^{-\frac{(\epsilon-\mu)}{k_B T}}\right)d\epsilon$$ (2.8)

and the equation of state for this ideal fermi gas is

$$P(T,\mu)V = \frac{2}{d}E(T,\mu).$$ (2.9)

Naturally, at high enough temperatures the quantum nature of the ideal fermi gas should subside and one ought to recover the equation of state for the ideal gas. In this case one may rewrite the grand canonical potential in terms of the fugacity $z = e^{\mu/k_B T}$ as

$$\Phi \approx -k_B T z\int_0^\infty g(\epsilon)e^{-\frac{\epsilon}{k_B T}}d\epsilon = -k_B T z\frac{V}{\lambda_{th}T^d}.$$ (2.10)

Using the preceding equation one may perform low order corrections to the equation of state of the ideal

gas to get

$$P(T, \frac{N}{V}) = \frac{2}{d} \frac{E(T, \frac{N}{V})}{V} = \frac{N k_B T}{V} \left(1 + \frac{N \lambda_{th} T^d}{2^{1+d/2}(2S+1)V} \right). \tag{2.11}$$

The second quantum term is typically quite small for atoms (although not for electrons) at ambient temperatures due to the small value of $\hbar$ implicitly present in the thermal wavelength λ_{th}. When that term is allowed to get large however, this term will contribute and deviations from the ideal gas will be observed as is the case when the volume or temperature tends towards zero.

On a slightly different note useful approximations for the non-interacting fermi gas for the purposes of comparison may be derived using the Sommerfeld expansion for low temperature [31] and are presented as follows:

$$\mu(T, V, N) = \epsilon_F \left(1 - \frac{\pi^2}{12} \left(\frac{k_B T}{\epsilon_F} \right)^2 + \ldots \right) \tag{2.12}$$

is the first order expression for the non-interacting ideal fermi gas for the chemical potential.

$$E(T, V, N) = \frac{3}{5} N \epsilon_F \left(1 + \frac{5\pi^2}{12} \left(\frac{k_B T}{\epsilon_F} \right)^2 + \ldots \right) \tag{2.13}$$

is the first order expression for the non-interacting ideal fermi gas for the energy, and

$$S(T, V, N) = N k_B \frac{\pi^2}{2} \frac{k_B T}{\epsilon_F} \left(1 - \frac{\pi^2}{24} \left(\frac{k_B T}{\epsilon_F} \right)^2 + \ldots \right) \tag{2.14}$$

is the first order expression for the non-interacting ideal fermi gas for the entropy.

2.3 Bose-Einstein Condensation of Bosonic and Composite Bosonic Particles

Within noninteracting bosonic systems, the Bose-Einstein condensate (BEC) arises as the macroscopic manifestation and occupation of a ground single-particle quantum state; in effect, within such systems, all or some significant fraction of the bosons occupy the same state and such systems in the guise of superfluid helium represent one of the few macroscopically observable quantum effects available to the (relatively) unaided human observer. In order to begin probing this phenomenon, the BEC is typically described in terms

of the single-particle reduced density matrix formalism [32] as,

$$\rho_1(\mathbf{r}, \mathbf{r}') = N \sum_s p_s \int d\mathbf{r}_2 \mathbf{r}_3 \ldots \mathbf{r}_N \Psi_s^*(\mathbf{r}, \mathbf{r}_2, \ldots, \mathbf{r}_N) \Psi_s(\mathbf{r}', \mathbf{r}_2, \ldots, \mathbf{r}_N). \tag{2.15}$$

Eqn. (2.15) defines a positive-definite Hermitian reduced density matrix for the system in question. When the system is not in a BEC state, the reduced density matrix is said to be diagonally dominant, or concomitantly, that the off-diagonal terms decay to zero; whereas for a BEC state, the off-diagonal terms are non-zero and are,

$$\lim_{(\mathbf{r}-\mathbf{r}') \to \infty} \rho_1(\mathbf{r}, \mathbf{r}') = \phi^*(\mathbf{r})\phi(\mathbf{r}')\frac{N_0}{V}. \tag{2.16}$$

which can be considered to be an order parameter for BECs.

An explanation for why eqn. (2.16) may be considered to be an order parameter was given by Onsager and Penrose [33] who define the signature of off-diagonal long range order in a BEC as being due to a macroscopically large eigenvalue in the reduced density matrix i.e. the eigenvalue η_i allows η_i/N $O(1)$ as N gets large, the underlying cause of which may be directly traced to a macroscopic occupation of an underlying state.

This macroscopic occupation of a single state causes problems when one considers that the macroscopic occupation of a single state in fermionic systems is forbidden due to the Pauli exclusion principle Fermionic systems can, however, exhibit BEC through the condensation of composite bosons formed by paired fermions. This change in theoretical description from simple to composite particles necessitates that the single-particle reduced density matrix be replaced by a two-body reduced density matrix (2-RDM) to fully capture the new description. Following Onsager and Penrose, who also considered the case for paired fermions, the two-particle spin-$\frac{1}{2}$ reduced density matrix is given as

$$\rho_2(\mathbf{r}_1\sigma_1, \mathbf{r}_2\sigma_2|\mathbf{r}_1'\sigma_1', \mathbf{r}_2'\sigma_2') =$$
$$N(N-1) \sum_s p_s \sum_{\sigma_3 \cdots \sigma_N} \int d\mathbf{r}_3 d\mathbf{r}_4 \ldots_d \mathbf{r}_N \Psi_s^*(\mathbf{r}_1\sigma_1, \mathbf{r}_2\sigma_2, \ldots, \mathbf{r}_N\sigma_N) \Psi_s(\mathbf{r}_1'\sigma_1', \mathbf{r}_2'\sigma_2', \ldots, \mathbf{r}_N'\sigma_N') \tag{2.17}$$

This new two-particle reduced density matrix (2-RDM), which is antisymmetric under particle exchange, allows the extension of the Onsager-Penrose criterion The off-diagonal long range order is expressed in the same where the eigenvalue η_i allows η_i/N $O(1)$ as N gets large except that η_i is now the eigenvalue of a 2-RDM. Moreover, the criteria presented here can be specialized to the fixed-spin case. Considering the applicability of this formalism to the case presented in this thesis, the two particles in question are different

particle types one of which may be thought of as spin-up and the other as spin down. That said, this theory, in effect, describes the off-diagonal long range order for interacting fermionic particles and may be considered a theoretical probe of the intrinsic bonding strength between the two subject fermions[1].

2.4 A Brief Overview of BCS Theory

Having defined a methodology in the prior section for identifying the long range order of composite bosons comprised of bound fermionic dimers, these bound fermionic dimer systems have been and still are of considerable interest in the condensed matter physics community since they provide cornerstone subject and in some sense can be seen as a defining phenomenon for the field. For many interesting phenomena, the BCS approach to superconductivity has become a definitive theory and used to explain many other phenomena. In BCS theory, a weak attraction amongst fermions in the fermi sea causes a bound fermionic pair [28] to disrupt that sea and emerge. The following two-body Schrödinger equation describes this interaction [28],

$$\left(-\frac{\hbar^2}{2m}\nabla_1^2 - \frac{\hbar^2}{2m}\nabla_2^2 + \lambda V(1,2)\right)\psi(1,2) = E\psi(1,2), \tag{2.18}$$

where $\lambda < 0$ describes an attractive interaction and $V(1,2)$ describes a pair interaction with the eigenfunctions and energy values written as,

$$\psi(1,2) = \phi_0(1,2) + \sum_{n\neq 0}\phi_n(1,2)\frac{1}{E-E_n}\langle\phi_n|kV|\psi(1,2)\rangle \tag{2.19}$$

$$E - E_n = \langle\phi_0|\lambda V|\psi(1,2)\rangle. \tag{2.20}$$

For a homogeneous system, the total pair momentum is conserved and may be used to define a helpful

---

[1]As an aside, it seems quite likely that these methods may be (and may have been) further extended to incorporate entanglement and methods to scrutinize bonds.

coordinate transformation as [28],

$$\mathbf{P} = \mathbf{k}_1 + \mathbf{k}_2, \ \mathbf{k} = \frac{1}{2}(\mathbf{k}_1 - \mathbf{k}_2) \tag{2.21}$$

$$\mathbf{R} = \frac{1}{2}(\mathbf{x}_1 + \mathbf{x}_2), \ \mathbf{x} = \mathbf{x}_1 - \mathbf{x}_2 \tag{2.22}$$

$$v = mV\hbar^{-2} \tag{2.23}$$

$$E = \hbar^2\kappa^2 m^{-1} + \frac{1}{4}P^2 m^{-1} \tag{2.24}$$

After applying this set of substitutions to eqns (2.18) and (2.20), the wavefunction becomes [28],

$$\psi(1,2) = V^{-\frac{1}{2}}e^{i\mathbf{P}\cdot\mathbf{R}}V^{-\frac{1}{2}}\psi_{\mathbf{P},\mathbf{k}}(\mathbf{x}) \tag{2.25}$$

where V is the system volume and the plane-wave function describes the free particle motion of the center of mass term and $\psi_{\mathbf{P},\mathbf{k}}$ is the term which describes the interaction. Unlike the pair Schrödinger equation in free space, this transformation results in a formulation which uses the filled Fermi sea as a frame of reference so that upon back-substitution in the Schrödinger equation (2.18) yields [28],

$$\psi_{\mathbf{P},\mathbf{k}} = e^{i\mathbf{k}\cdot\mathbf{x}} + \frac{\lambda}{(2\pi)^3}\int_\Gamma dt^3 e^{-\mathbf{t}\cdot\mathbf{x}}\frac{\langle\mathbf{t}|v|\psi_{\mathbf{P},\mathbf{k}}\rangle}{\kappa^2 - t^2} \tag{2.26}$$

$$\kappa^2 - k^2 = \lambda V^{-1}\langle\mathbf{t}|v|\psi_{\mathbf{P},\mathbf{k}}\rangle \tag{2.27}$$

which are subject to the conditions

$$\frac{1}{2}\mathbf{P} \pm \mathbf{t}| < k_F, \Gamma = |\frac{1}{2}\mathbf{P} \pm \mathbf{t}| > k_F. \tag{2.28}$$

The pair Schrödinger equation is thus transformed into the Bethe-Goldstone equation which may be solved in the case when $\mathbf{P}$ (a full solution must be typically performed via numerical methods) [28] to yield [28],

$$\kappa^2 = k_F^2 - \frac{m\Delta}{\hbar^2} \tag{2.29}$$

19

where Δ is given by

$$\Delta = \frac{\hbar^2 k_F^2}{2m} e^{-\frac{4\pi^2}{k_F|\lambda|u_F^2}} \tag{2.30}$$

with an energy shift for an interacting pair given by

$$\Delta E = \frac{\hbar^2(\kappa^2 - k^2)}{m} \tag{2.31}$$

and $u(\mathbf{k})$ is the Fourier transform of a separable term $u(x)$ associated with the potential which is derived by considering that $V(1,2)$ is short-ranged and well approximated as $V(1,2) \approx u(1)u(2)$ [28].

The physical interpretation for this preceding stream of equations (2.18, 2.20, 2.24, 2.25, 2.27, 2.28, 2.29, 2.31) begins with the energy shift, ΔE, for the interacting pair, which indicates that a bound Fermi pair arises within the Fermi sea of this toy two-particle model since by doing so the ground state lowers its overall energy and leads to the conclusion that fermionic pairing and hence bosonic phenomena can arise within fermionic systems while making the most minimal of assumptions concerning the interaction amongst the fermions, namely that an attraction exist.

That this situation was originally derived for a fermionic pair interaction and not for a multiparticle system is only a temporary inconvenience as the general case of a Fermi gas may be subsequently considered for an interacting system by using a Bogoliubov transformation to decouple the interactions within the system.

First the system is presented in a second quantized form in terms of the grand canonical potential operator because using the thermodynamic potential allows one to consider a system with a mutable number of particles which is convenient as [28],

$$\hat{K} = \hat{H} - \mu \hat{N}$$
$$= \sum_{k,\sigma} a_{k\sigma}^\dagger a_{k\sigma}(\epsilon_k^0 - \mu) - \frac{1}{2} \sum_{\mathbf{k}_1+\mathbf{k}_2-\mathbf{k}_3+\mathbf{k}_4, \sigma_1\sigma_2\sigma_3\sigma_4} \langle \mathbf{k}_1\sigma_1\mathbf{k}_2\sigma_2|V|\mathbf{k}_3\sigma_3\mathbf{k}_4\sigma_4\rangle a_{\mathbf{k}_1\sigma_1}^\dagger a_{\mathbf{k}_2\sigma_2}^\dagger a_{\mathbf{k}_4\sigma_4} a_{\mathbf{k}_3\sigma_3} \tag{2.32}$$

where $\mathbf{K}$ denotes a momentum states and σ denotes the spin state; V is assumed to be attractive. Canonical transformations for these states with explicit spin states may be defined as [28],

$$\alpha_{\mathbf{k}} = u_k a_{\mathbf{k}\uparrow} - v_k a_{-\mathbf{k}\downarrow}^\dagger \quad \beta_{-\mathbf{k}} = u_k a_{-\mathbf{k}\downarrow} + v_k a_{-\mathbf{k}\uparrow}^\dagger. \tag{2.33}$$

where their commutation relations and the equations relating their constants are given by [28],

$$\{\alpha_{\mathbf{k}}, \alpha_{\mathbf{k'}}^{\dagger}\} = \{\beta_{\mathbf{k}}, \beta_{\mathbf{k'}}^{\dagger}\} = \delta_{\mathbf{kk'}} \tag{2.34}$$

$$\{a_{\mathbf{k}\sigma}, a_{\mathbf{k'}\sigma'}^{\dagger}\} = \delta_{\mathbf{kk'}}\delta_{\sigma\sigma'} \tag{2.35}$$

Inverting these relations to the original operators yields [28],

$$a_{\mathbf{k}\uparrow} = u_k \alpha_{\mathbf{k}} + v_k \beta_{-\mathbf{k}}^{\dagger} \ a_{-\mathbf{k}\downarrow} = u_k \beta_{-\mathbf{k}} + v_k \alpha_{\mathbf{k}}^{\dagger} \tag{2.36}$$

where the equation relating the associated c-numbers or constants is

$$u_k^2 + v_k^2 = 1. \tag{2.37}$$

Applying these relations to the grand canonical potential's first term with fixed spins given by eqn. (2.32) yields,

$$\sum_{\mathbf{k}} \left(\epsilon_k^0 - \mu\right) \left(a_{\mathbf{k}\uparrow}^{\dagger} a_{\mathbf{k}\uparrow} + a_{-\mathbf{k}\downarrow}^{\dagger} a_{-\mathbf{k}\downarrow}\right) =$$

$$\sum_{\mathbf{k}} \left(\epsilon_k^0 - \mu\right) \left[2v_k^2 + N(a_{\mathbf{k}\uparrow}^{\dagger} a_{\mathbf{k}\uparrow}) + N(a_{-\mathbf{k}\downarrow}^{\dagger} a_{-\mathbf{k}\downarrow})\right] =$$

$$\sum_{\mathbf{k}} \left(\epsilon_k^0 - \mu\right) \left[2v_k^2 + (u_k^2 - v_k^2)(\alpha_{\mathbf{k}}^{\dagger}\alpha_{\mathbf{k}} - \beta_{\mathbf{k}}^{\dagger}\beta_{\mathbf{k}}) + 2u_k v_k (\beta_{-\mathbf{k}}\alpha_{\mathbf{k}} + \alpha_{\mathbf{k}}^{\dagger}\beta_{-\mathbf{k}}^{\dagger})\right] \tag{2.38}$$

where N denotes normal ordering. The potential energy operator may be re-written in terms of these canonical transformations as well as

$$\hat{V} = -\frac{1}{2} \sum_{\mathbf{kk'q}} \langle \mathbf{kk'}|V|\mathbf{k+q,k'-q}\rangle [a_{\mathbf{k}\uparrow}^{\dagger} a_{\mathbf{k'}\uparrow}^{\dagger} a_{\mathbf{k'-q}\uparrow} a_{\mathbf{k+q}\uparrow} + a_{-\mathbf{k}\downarrow}^{\dagger} a_{-\mathbf{k'}\downarrow}^{\dagger} a_{-\mathbf{k'-q}\downarrow} a_{-\mathbf{k-q}\downarrow}]$$

$$- \sum_{\mathbf{kk'q}} \langle \mathbf{k-k'}|V|\mathbf{k+q,k'-q}\rangle [a_{\mathbf{k}\uparrow}^{\dagger} a_{-\mathbf{k'}\downarrow}^{\dagger} a_{-\mathbf{k'-q}\downarrow} a_{\mathbf{k+q}\uparrow}], \tag{2.39}$$

which may be further reduced using the normal ordering formalism. Ultimately, the Hamiltonian in eqn. (2.32) may be given by the following [28]

21

$$K = U + H_1 + H_2 + N(\hat{V}) \tag{2.40}$$

$$U = 2\sum_{\mathbf{k}} \xi_k v_k^2 + \sum_{\mathbf{k},\mathbf{k'}} v_k^2 v_{k'}^2 \langle \mathbf{kk'}|\hat{V}|\mathbf{kk'}\rangle - \sum_{\mathbf{k}} u_k v_k \Delta_k \tag{2.41}$$

$$H_1 = \sum_{\mathbf{k}} (\alpha_{\mathbf{k}}^\dagger \alpha_{\mathbf{k}} + \beta_{-\mathbf{k}}^\dagger \beta_{-\mathbf{k}})[(u_k^2 - v_k^2)\xi_k + 2u_k v_k \Delta_k] \tag{2.42}$$

$$H_2 = \sum_{\mathbf{k}} (\alpha_{\mathbf{k}}^\dagger \beta_{-\mathbf{k}}^\dagger + \beta_{-\mathbf{k}}\alpha_{\mathbf{k}})[2u_k v_k \Delta_k - (u_k^2 - v_k^2)\xi_k], \tag{2.43}$$

where $\xi_k = \epsilon_k - \mu$ is the energy measured relative to the chemical potential and Δ_k is energy gap given by

$$\Delta_k = \sum_{\mathbf{k'}} \langle \mathbf{k}, -\mathbf{k}|\hat{V}|\mathbf{k'}, -\mathbf{k'}\rangle u_{k'} v_{k'}. \tag{2.44}$$

The various terms of $\mathcal{K}$ are physically explained as follows: U's first two terms are the Hartree-Fock ground state energy of an interacting Fermi gas. H_1 describes the quasi-particle dispersions and excitations and H_2 is a factor which may be eliminated by judicious choice of the transformation constants u_k and v_k.

To find the appropriate values for u_k and v_k so that $H_1 = 0$ and $\mathcal{K}$ becomes described by a set of oscillators allow [28], allow

$$2\xi_k u_k v_k = \Delta_k(u_k^2 - v_k^2) \tag{2.45}$$

and set $H_2 = 0$ so that

$$\mathcal{K} = U + H_1 = U + \sum_{\mathbf{k}} E_k (\alpha_{\mathbf{k}}^\dagger \alpha_{\mathbf{k}} + \beta_{-\mathbf{k}}^\dagger \beta_{-\mathbf{k}}), \tag{2.46}$$

where $E_k = \sqrt{\Delta_k + \xi_k^2}$ and is referred to as the quasi-particle dispersion energy. The energy gap Δ_k transforms into a non-linear integral equation given by

$$\Delta_k = \sum_{\mathbf{k'}} \langle \mathbf{k}, -\mathbf{k}|\hat{V}|\mathbf{k}, -\mathbf{k}\rangle \frac{\Delta_{k'}}{2E_{k'}}. \tag{2.47}$$

Further steps in the derivation requires the the number of particles and hence the chemical potential μ be set which is done as

$$\langle \mathcal{N} = \sum_{\mathbf{k}\sigma} \langle \mathbf{O}|a_{\mathbf{k}\sigma}^\dagger a_{\mathbf{k}\sigma}|\mathbf{O}\rangle = \sum_{\mathbf{k}} \left(1 - \frac{\xi_k}{E_k}\right). \tag{2.48}$$

22

The BCS gap and number equations given by (2.47) and (2.48) respectively are general for interacting ferminons in the BCS pairing regime of weak attractive interaction and are the fundamental equations underlying BCS theory.

These equations are typically simplified because in their most common manifestations in electrons in metal systems the potential is only contributes in a major way in the momentum shell close to the Fermi surface [28]. The energy gap may then be written as

$$\Delta_k = \Delta_0 \theta(\hbar\omega_D - |\xi_k|), \tag{2.49}$$

where the thickness of the shell is given by the Debye frequency, $\hbar\omega_D$, which is limit of the phonons which give rise to the attractive interaction in the metal system. Assuming $\hbar\omega_D << \epsilon_F$, Δ_0 may be written as

$$
\begin{aligned}
\Delta_0 &= \frac{g}{2V} \sum_{\mathbf{k}} \theta(\hbar\omega_D - |\xi_k|) \frac{1}{\sqrt{\Delta_0^2 + \xi_k^2}} \\
&= \frac{g}{2} \int \frac{d^3k}{(2\pi)^3} \theta(\hbar\omega_D - |\xi_k|) \frac{1}{\sqrt{\Delta_0^2 + \xi_k^2}} \\
&= \frac{gN(0)}{2} \int_{-\hbar\omega_D}^{\hbar\omega_D} \frac{d\xi}{\sqrt{\Delta_0^2 + \xi^2}} \\
&\approx gN(0)ln\left(\frac{2\hbar\omega_D}{\Delta_0}\right),
\end{aligned}
\tag{2.50}
$$

where $N(0)$ is the density of states for the energy density at the Fermi surface for a spin projection and $g = \frac{4\pi\hbar^2 a_s}{m}$ as the effective interaction. Rearranging these expressions yields

$$\Delta_0 = 2\hbar\omega_D e^{-\frac{1}{N(0)g}} \tag{2.51}$$

$$E_s - E_n = \frac{VN(0)\Delta_0^2}{2}, \tag{2.52}$$

where Δ_0 is the energy gap and $E_s - E_n$ is the energetic difference between the normal and gapped solution for the ground state.

This energy gap's opening gives rise to the instability in the Fermi surface which results in the formation

of Cooper pairs in the ground state and the BCS variational wave function given by

$$\Psi_0 = \prod_k u_k + v_k a_{\mathbf{k}\uparrow}^\dagger a_{-\mathbf{k}\uparrow}^\dagger |0\rangle \tag{2.53}$$

$$\tag{2.54}$$

$$= c \times \prod_k 1 + \eta_k a_{\mathbf{k}\uparrow}^\dagger a_{-\mathbf{k}\uparrow}^\dagger |0\rangle \tag{2.55}$$

where $|0\rangle$ is a vacuum state and u_k and v_k are functions used in the variational process. Performing a variational procedure upon the thermodynamic expectation values of this ground state results in the recovery of gap and number equations identical to those just derived via Bogoliubov transformations.

Rounding out this section are relations for finite temperature quantities related to transition phenomena for BCS superconductivity. While the precise methodology for performing this is beyond the scope of this thesis, they are typically found using finite temperature Green functions and T-matrix methods [28].

The gap function for a uniform system at finite temperature is given by the following equation as [28],

$$\Delta(T) = \frac{g}{\beta\hbar} \sum_n \int \frac{d^3k}{(2\pi)^3} \frac{\hbar\Delta(T)}{\sqrt{(\hbar\omega_n)^2 + E_k^2}}, \tag{2.56}$$

where $\omega_n = (2n+1)\pi/\beta\hbar$ describes the fermionic Matsubara frequencies. Applying the same Debye frequency cutoff, yields the simplified finite temperature gap equation,

$$1 = \frac{gN(0)}{2} \int_{-\hbar\omega_D}^{\hbar\omega_D} \frac{d\xi}{\sqrt{\Delta^2 + \xi_k^2} \tanh \frac{\sqrt{\Delta^2 + \xi_k^2}}{2k_B T}}. \tag{2.57}$$

Setting $\Delta = 0$ gives the superconducting transition temperature as [28],

$$k_B T_c = \frac{2e^\gamma}{\pi} \hbar\omega_D e^{-1/N(0)g} \approx 1.13\hbar\omega_D e^{-1/N(0)g}, \tag{2.58}$$

and gap equation for the transition as

$$\Delta(T) = k_B T_c \left(\frac{8}{7\zeta(3)}\right)^{1/2} \left(1 - \frac{T}{T_c}^{1/2}\right). \tag{2.59}$$

2.5 Introduction to Fermionic Gases and Unitarity

Unitarity or describing a system to be at unitarity or the unitary limit is a phrase or phrasing which defines a two-component fermionic system with a potential comprised of attractive pairwise interaction system in

which the interparticle interaction is dominated by s-wave scattering due to the zero-range of the pairwise interactions and in which the resulting scattering length of that s-wave interaction diverges. In theory, the unitary limit is applicable to all two-component, short range fermionic systems when they become dilute enough as the dilution causes the pair interactions to become effectively zero-range upon rescaling. This interaction rescaling effect, in turn, results in the dominance of the s-wave scattering interaction between the attractive short-range pair interactions of the fermionic particles [12, 34].

Since by definition, a unitary system has a divergent scattering length, ζ, the unitary limit was the subject of considerable consternation when first derived in the 1950's as this system counterintuitively possesses a zero-range interaction with an infinite range effect [12, 34]. Causing further concern, a unitary system possesses only a single dimensional scale to define it, which within the literature, is typically defined by the cube root the density n of the system [12]. This single length scale causes considerable difficulty for many of the standard analytic perturbative techniques in probing the unitary limit due to the lack of an appropriate, small parameter to work. That said this not to paint the situation as entirely bad from an analytic theory standpoint as this single dimensional scale has also been a source of strength due to the applicability of scaling arguments [12]. Nonetheless, due to the theoretical difficulties presented by unitarity, it remains a limit uniquely well-suited for investigation by computational techniques.

When unitarity was first investigated in the late 1940's and early 1950's, it was considered to be little more than a curiosity for condensed matter systems due to the requirement that the scattering length be so large that the s-wave interactions dominate the higher order terms. Moreover, searching for such an effect among the plethora of available condensed matter systems was felt to be nothing more than a fool's errand. Consequently, unitarity as a field of investigation was developed in its early years within the nuclear physics community where by happenstance a dilute neutron gas reveals a unitary interaction amongst its constituents [34]. The interest of the condensed matter community in unitary fermions only arose when cold atom systems made experimental realizations of such systems possible due to the tunability of the their constituent interactions.

2.6   The BCS-BEC Crossover

Naturally, because unitarity involves an attractive interaction among fermions it is natural to consider how its composite bosonic pairing and resultant Bose-Einstein condensation behaves; moreover, it is important to note that because the unitary system is so simple from the standpoint of its pairwise interactions that it offers the possibility to treat this system as a platform for understanding and suggesting avenues of attack for

more complicated but related systems like high-temperature superconductors. That said, contained within the classical BCS theory is the germ of understanding for pairing in unitary systems at a microscopic level. It has long been noted [32, 35] that the variational BCS wave function

$$\Psi_0 = \prod_k u_k + v_k a_{\mathbf{k}\uparrow}^\dagger a_{-\mathbf{k}\uparrow}^\dagger |0\rangle \tag{2.60}$$

$$\tag{2.61}$$

$$= c \times \prod_k 1 + \eta_k a_{\mathbf{k}\uparrow}^\dagger a_{-\mathbf{k}\uparrow}^\dagger |0\rangle \tag{2.62}$$

may have its region of applicability extended from weak BCS type coupling to the strong dimer interactions of the BEC regime by increasing the bare interaction U and observing the evolution of this ground state wave function. Rewriting eqn. (2.62) as

$$\Psi_0 = c \times \prod_k 1 + \eta_k a_{\mathbf{k}\uparrow}^\dagger a_{-\mathbf{k}\uparrow}^\dagger |0\rangle \qquad\qquad = c \times \exp\left(\sum_k \eta_k a_{\mathbf{k}\uparrow}^\dagger a_{-\mathbf{k}\uparrow}^\dagger\right)|0\rangle \tag{2.63}$$

Projecting the preceding onto a N-particle state allows, this expression to be written as

$$\Psi_0 = c \times \sum_k \left(\eta_k a_{\mathbf{k}\uparrow}^\dagger a_{-\mathbf{k}\uparrow}^\dagger\right)^{N/2}|0\rangle \tag{2.64}$$

which is a composite bosonic wave function of pair size η due to the the inherent pairing interaction created by the $a_{\mathbf{k}\uparrow}^\dagger a_{-\mathbf{k}\uparrow}^\dagger$. As U is increased, η decreases until a dilute gas of bosonic dimers is reached, while the remaining unpaired fermionic atoms are increasingly driven towards pairing due to the energetic benefits. This drive towards pairing results in interesting effects on the chemical potential μ of the underlying system. While initially within the BCS region $\mu = \epsilon_F$ as the interaction strength U is increased and the system becomes dominated by bosonic degrees of freedom due to the pairing effect, μ decreases and eventually becomes negative with the crossover region being described as the transition through $\mu = 0$. From a temperature dependent standpoint, it is inferred that the system becomes a mixture of free fermionic atoms and bound fermionic pairs which interact with and mediate interactions between the free fermionic atoms the relation between which are tuned by the temperature of the system. The underlying specifics with which superfluidity arises in these remain a subject of continuing interest in this area of study [30, 36]. Finally, from a microscopic point of view, it is important to investigate and determine the temperature at pairing and condensation occurs as this is a critical feature of BCS theory as it relates to these systems. Specifically, it is interesting to consider and will be subject of this thesis whether or not there is a direct observation in

26

system simulations of a discontinuous phase transition between the crossover from the BCS weakly paired regime to the strongly bound BCS regime at some transition temperature T_c.

2.7   Experimental Approaches and Results for Unitary Systems and the BCS-BEC Crossover

A bifermionic cold atom system may be tuned to display the signature of a system at unitarity and the BCS-BEC cross regime using the trapping techniques described in the prior chapter in conjunction with Feschbach resonances. Specifically, the interaction or channel between fermionic atoms may be altered by tuning an externally applied magnetic field to be close to the aforementioned Feschbach resonance of a trapped hyperfine species. These interactions between fermionic atoms may give rise to "channels" when the diagonal of the hyperfine indices for the interaction in question becomes dominant with channel being 'open' when for a given energy the particles are free asymptotically at large distance and 'closed' when a bound state appears at that energy.

When elastic scattering in an open channel occurs while energetically close to the bound state of a close channel, a Feschbach resonance appears. The magnetic moments of atoms in the open and closed channels are different as a consequence of the difference between the underlying hyperfine indices, which here is described as $\Delta\mu$, where μ is the magnetic moment and not the chemical potential. The resultant change in energy between these channels is given in reference to non-interacting atoms as [1, 32],

$$\Delta E = E_{closed}(\mathbf{r} \to \infty) - E_{open}(\mathbf{r} \to \infty) = \Delta\mu \cdot B. \tag{2.65}$$

Turning off the field described by B causes the bound state with binding energy $|E_b|$ to hybridize with that of the open state if $|E_b|$ is close to $E = 0$ as the off-diagonal terms couple the two channels. If the external field is turned on but is kept very small so that the detuning parameter δ becomes

$$\delta = \Delta E - |E_b| = \Delta\mu \cdot B - |E_b|. \tag{2.66}$$

As $|\delta|$ tends towards 0, second order processes between the open and closed channels appear due to the particles in the open channel scattering from the intermediate state of the closed channel so that the scattering

length of the particle interaction may be given by

$$a_s = \frac{C}{-\delta} \qquad (2.67)$$

which in effect results in a tunable scattering length as a function of the detuning parameter where C is a system specific constant. At unitarity when $\delta \to 0$ the scattering length becomes divergent and the system is best modeled as an interaction defined by a pairwise delta function interaction where the adjustable parameter $a_s \to \infty$.

2.8 Theoretical and Computational Realizations of Cold Atom and Unitary Systems and the BCS-BEC Crossover

Theoretical approaches to cold atom unitary systems have typically focused upon non-perturbative theoretical methods due to the lack of a small parameter in such systems around which to develop a perturbative theory. This has particularly been the case for the BCS-BEC crossover transition. Nonetheless perturbative approaches to the BCS and BEC limits of such systems do exist and will be explored here in the first subsection. While mean-field theory is typically inapplicable to these systems from a quantitative perspective due to the distinct lack of a phase transition in the crossover regime [12], the approach was important in the formative years in the late 1960's and early 1970's of the theoretical study of this field but is not considered here.

Moving on to the next subsection of this section, Akkineni has previously observed in a related thesis [36] that most theoretical/analytical approaches to the unitary transition begin with the BCS theory, an example of which is an approach due to Ohashi and Griffin [37] and may be generally described as an augmented BCS theory with a Feschbach resonance. This subsection will be followed by a functional integral formalism presented within [36] and originally by Randeria in [29] as well as a brief overview of lattice-type approaches.

So that, finally the computational methodologies, which in this author's view have come to dominate this field will be presented due to their quantitative character, which, at least in principle if not as frequently in practice, offers the possibility of *ab initio*-type results. First, an exploration of $T = 0$ Green's function Monte Carlo type studies on unitary systems. This will be followed by a brief investigation of lattice methods until finally prior work with path integral methods for these systems will be presented.

2.8.1 Perturbative Approaches

As has already been alluded to for the two limiting cases of the BCS-BEC crossover, perturbative methods may be applied in either limit. For a Bose-Einstein condensate, the system may be modeled as strongly-bound bosonic dimers or molecules and free leftover fermions so that further insights into the system may gained by solving the two-, three-, and four-body problems associated with these constituents so that the various binding energies and scattering lengths of the bosonic-dimer interaction, the dimer-fermion interaction, and the dimer-dimer interaction may be found. As a summation of these for the BEC limit, the energy is given as,

$$E(n_F, n_B) = -\frac{\hbar^2}{ma_s}n_B + \frac{3}{5}\frac{\hbar^2}{2m}(6\pi^2)^{2/3}n_F^{5/3} + f_{FB}n_Fn_B + \frac{1}{2}f_{BB}n_B^2 \qquad (2.68)$$

where n_B is the number of bosonic dimers, n_F is the number of free excess fermions and the factors given by f are couplings which may be determined from the scattering length using few-body methods [38,39] as

$$f_{BB} = \frac{\pi\hbar^2}{m}a_{BB}a_s \approx \frac{\pi\hbar^2}{m}1.2a_s \qquad (2.69)$$

$$(2.70)$$

$$f_{FB} = \frac{\pi\hbar^2}{m}a_{FB}a_s \approx \frac{\pi\hbar^2}{m}3.54a_s \qquad (2.71)$$

$$(2.72)$$

$$E_B = \frac{\hbar^2}{m}a_s^{-2} \qquad (2.73)$$

where a_{FB} and a_{BB} denote scattering length of a free fermion and bosonic dimer collision and of bosonic dimer-dimer collision respectively. As one ventures further into the BEC regime these couplings weaken and the application of perturbative techniques becomes reasonable when applied to the k_Fa_s parameter where $k_F = (3\pi^2\rho)^{1/3}$ and ρ is the particle number density.

Within the BCS regime, a similar weakly attractively interacting plateau may be reached as well where the scattering length a_s becomes small and is negative so that a pertubation series in this term becomes possible with the major caveat that the various infrared singularities associated with BCS instability must be handled. Complicating the interpretation of these singularities is that the specifics of the underlying polarized superfluid phases are still unknown even in the weak coupling regime [12] which makes comparing energies difficult as one needs to know the structure of the IR divergences in order to compare energies. While many new phases have been proposed it has been observed by Forbes that:

"In principle, the true ground state at finite polarization might be something [very different than previ-

ously proposed] and if it is separated by a first-order transition from the other states then there might not even be a perturbative signal in the form of an instability. To truly understand what is happening in these interesting regimes, one needs a reliable *ab initio* method or experiment."

As such a result would allow one to perturbatively approach the BCS regime of a unitary gas experiment. While other perturbative results on unitary gases exist, in particular an approach due to Son and Nishida exists based upon using a parameter ϵ perturbing about the dimension of the system [40]. Specifically since the 4-dimensional version of the system of Son and Nishida has no transition, this is used as the reference system and a perturbation in its dimensional term is performed. Unfortunately going to 3 or 2 dimensions is a perturbation which is not small so it is unclear how applicable these results are.

2.8.2 An Augmented BCS Approach

Non-perturbative approaches must be taken to studying the unitary transition due to the lack of a pertubative parameter at that transition. As has already been noted by Akkineni, these transitions usually result from considering the underlying BCS theory. In the work of Ohashi and Griffin [37], a Hamiltonian is formulated in a BCS-like framework which incorporates the Feshbach resonance as

$$\mathcal{K} = \sum_{\mathbf{k}\sigma} \left(\frac{\hbar^2 k^2}{2m} - \mu \right) a_{\mathbf{k}\sigma}^{\dagger} a_{\mathbf{k}\sigma} + \sum_{\mathbf{k}} (E_k^0 + 2\nu) b_{\mathbf{k}\sigma}^{\dagger} b_{\mathbf{k}\sigma}$$
$$- U \sum_{\mathbf{k},\mathbf{k'}} a_{\mathbf{k}\uparrow}^{\dagger} a_{-\mathbf{k}\downarrow}^{\dagger} a_{\mathbf{k'}\downarrow} a_{-\mathbf{k'}\uparrow} + g_r \sum_{\mathbf{k}\mathbf{k'}[b_{\mathbf{k}}^{\dagger}, a_{-\mathbf{k}+\frac{\mathbf{k'}}{2}\downarrow} a_{\mathbf{k}+\frac{\mathbf{k'}}{2}\uparrow} + h.c.]} . \tag{2.74}$$

This Hamiltonian has been formulated to specifically include the two-channel model which arises as a consequence of the Feshbach resonances and thus incorporates stable dimers as well as the interactions between the atoms and the dimers. The $a_{\mathbf{k}\sigma}^{\dagger}$ and $a_{\mathbf{k}\sigma}$ are the fermionic operators from the first and third terms of the BCS Hamiltonian. The $b_{\mathbf{k}}^{\dagger}$ and $b_{\mathbf{k}}$ are the bosonic operators which create and destroy the bound Feshbach dimers with center of mass momentum $\mathbf{k}$. 2ν denotes the binding energy of the dimers so that the second terms yields the kinetic and binding energy of those dimers. The system is setup so that the dimers will form when $2\nu \leq 2\epsilon_F$ and will not be able to decay unless $2\nu \geq 0$. The fourth term models the dimer-free fermion interaction and creates and destroys dimers while eating or regurgitating two fermions in the preocess. This ultimately results in the number operator for the system being described as

$$\mathcal{N} = \sum_{\mathbf{k}\sigma} a_{\mathbf{k}\sigma}^{\dagger} a_{\mathbf{k}\sigma} + 2 \sum_{\mathbf{k}} b_{\mathbf{k}}^{\dagger} b_{\mathbf{k}}. \tag{2.75}$$

2.8.3 A Functional Integral Formalism for Unitary Systems

A functional integral formalism for unitary systems has been summarized and described in [29] for continuum model with the intent to make quantitatively useful approximations to the couplings as a function of temperature above and below T_c for such unitary systems. Moreover, as of 1996 this formalism allowed its practitioners by their own statement [29] to recover all previously known results discovered by other methods and to go beyond them.

The imaginary time functional integral described by the action

$$S = \int_0^\beta d\tau \int d\mathbf{x} \bar{\psi}_\sigma(x) \partial_t \psi_\sigma(x) + \mathcal{K} \tag{2.76}$$

where $\mathcal{K}$ is given in eqn. (2.74) and $x = (\mathbf{x}, \tau)$ may be used to describe the partition function Z. The fermionic interactions may be decoupled by using a Hubbard-Stratonovich transformation which has an accompanying field $\Delta(\mathbf{x}, \tau)$ so that those fermions may be integrated out to obtain

$$Z = \int D\Delta D\bar{\Delta} e^{-S_{eff}[\Delta,\bar{\Delta}]} \tag{2.77}$$

where the effective action is

$$S_{eff}[\Delta(x)] = \frac{1}{g} \int_0^\beta d\tau \int d\mathbf{x} |\Delta(x)|^2 - \text{Tr} \log \mathbf{G}^{-1}[\Delta(x)] \tag{2.78}$$

and the inverse Nambu propagator is written as

$$\mathbf{G}^{-1}(x, x') = \begin{pmatrix} -\partial_t + \nabla^2/2m + \mu & \Delta(x) \\ \Delta^*(x) & -\partial_t - \nabla^2/2m \end{pmatrix}. \tag{2.79}$$

The functional integral can now be used to find the static, uniform saddle-points and the fluctuations about them. $\Delta = 0$ is the trivial saddle point and remains stable for all couplings even at high temperature, but becomes unstable below a temperature T_0 which is not T_c. T_0 may be found by solving

$$\frac{\delta S_{eff}}{\delta \Delta}[\Delta = 0] = 0 \tag{2.80}$$

to find

$$\frac{1}{g} = \sum_{\mathbf{k}} \frac{\tanh(\frac{\xi_{\mathbf{k}}}{2T_0})}{2\xi_{\mathbf{k}}}, \tag{2.81}$$

where $\xi_{\mathbf{k}} = \epsilon_{\mathbf{k}} - \mu$ and $\epsilon_{\mathbf{k}} = \frac{|\mathbf{k}^2|}{2m}$.

In order to use this solution, the ultraviolet divergences must be regulated by replacing the bare value for g with the low energy limit of the two-body T-matrix. For three dimensional systems, the following equation defines the regulator

$$\frac{m}{4\pi a_s} = -\frac{1}{g} + \sum_{|\mathbf{k}|<\Lambda} (2\epsilon_{\mathbf{k}})^{-1} \tag{2.82}$$

and defines the scattering length a_s as well. Applying this regulator to eqn. (2.81) results in

$$-\frac{m}{4\pi a_s} = \sum_{\mathbf{k}} \left(\frac{\tanh(\frac{\xi_{\mathbf{k}}}{2T_0})}{2\xi_{\mathbf{k}}} - \frac{1}{2\epsilon_{\mathbf{k}}} \right). \tag{2.83}$$

Since there are two unknowns T_0 and μ another equation is required to fix the solution. The suggested equation is $N = -\frac{\partial\Omega}{\partial\mu}$ which fixes the chemical potential for a given density. Finding this equation proceeds by first considering the thermodynamic potential $\Omega_0 = S_{eff}[\Delta = 0]/\beta$ and solving for the number equation as,

$$n = n_0(\mu, T) = \sum_{\mathbf{k}} \left(1 - \tanh(\frac{\xi_k}{2T}) \right). \tag{2.84}$$

Solving this equation in weak coupling limit, $1/k_F a_s \to -\infty$ allows the recovery of the BCS results as $\mu = \epsilon_F$ and $T_0 = 9e^{-2}\frac{\gamma\epsilon_F}{\pi}e^{-\pi/2k_F|a_s|}$ where $\gamma \approx 1.781$. In the strong coupling regime the roles of the gap and number equations reverse and one uses the gap equation to determine μ and the number equation to determine T_0. This limit results in $1/k_F a_s \to \infty$, the binding energy of the dimers are $E_b = 1/ma_s^2$, $\mu \approx -E_b/2$ and $T_0 \approx E_b/2\log(E_b/\epsilon_f)^{3/2}$. Ultimately by numerically solving the preceding equations an interpretation of T_0 becomes possible. In essence, T_0 describes the pairing scale or the temperature below which pairing effects become important; for systems above T_0 they may as well be described as unbound interacting fermions without dimer formation.

2.8.4 Lattice Methods for Unitary Systems

Lattice methods have also been applied to the study of the unitary Fermi gas and its associated phenomena. Typically, this approach proceeds using an Euclidean time lattice formalism [41–45] under which a lattice action is created with tunable parameters to find the proper interaction strengths to recreate the phase shifts in a given periodic box using the Lüscher formula [46],

$$k \cot \delta_k = \frac{1}{\pi L} S(\eta) \tag{2.85}$$

$$\eta = \left(\frac{Lk}{2\pi} \right)^2 \tag{2.86}$$

$$S(\eta) = \lim_{\Lambda \to \infty} \left(\sum_{\vec{n}} \frac{\theta(\Lambda^2 - n^2)}{n^2 - \eta} - 4\pi\Lambda \right). \tag{2.87}$$

The initial hope was that such lattice approaches would allow practitioners to probe the unitary limit even at small volumes by very carefully and judiciously tuning the associated parameters of this system. Unfortunately, this hope arguably did not entirely materialize as most of these results do not agree with experiment [47]. Moreover, there are issues of agreement for lattice methods with results from few-body methods [48] which have led Forbes to conclude [12] that current results and the methods used in lattice method approaches to unitary fermi systems are, "promising in principle [but require more understanding] before further progress is made."

2.8.5 Green Function or Diffusion Monte Carlo for Unitary Systems

While Monte Carlo approaches in principle are able to tackle unitary systems, they are hampered by the infamous fermionic sign-problem due to the antisymmetry of the underlying fermionic system wave function. That said much work has been performed on these systems using Green function or diffusion Monte Carlo as *ab initio* methods due to their ability to probe otherwise inaccessible regimes such a transitions without approximations or with only minimal assumptions.

From the standpoint of a theoretical approach to the unitary fermi gas, one of the first studies performed on such systems was by Carlson et. al. in [49, 50] were ground state properties at unitarity were simulated using fixed node Green function Monte Carlo.

Green function Monte Carlo proceeds by applying a Trotter discretized version of the Boltzmann projection operator $e^{-\tau \hat{H}}$ on some initial state $\Phi_i(\mathbf{R})$ that overlaps with the ground state. By integrating over
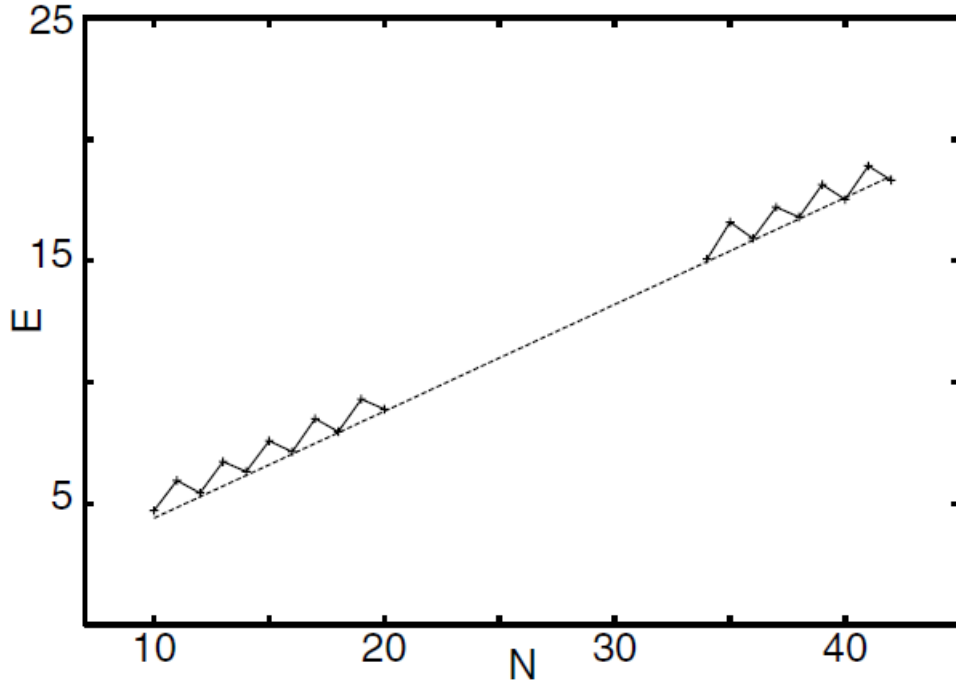
Figure 2.1: This plot presents Carlson et. al.'s [49] simulation of the the energy for different systems sizes at unitarity using the Green function Monte Carlo method.

many time steps of the projection operator, eventually one will be left with just the ground state as the contributions of all of the other higher excited states will have decayed to zero. This method is typically performed via a Markov chain process the details of which may be found in [51].

For fixed-node systems, the variational principle applies so that even if one had a correct wave function with incorrect fermionic nodes the energy calculated with these incorrect nodes would be higher than that calculated with the true nodes. Consequently, these fixed-node Green function Monte Carlo calculations represent an upper limit to the the true energy.

In the case of Carlson's calculations [49, 50], antisymmetrized BCS ground state nodes were used and are

defined by the following trial wave function as

$$\Psi_T(\mathbf{R}) = \mathcal{A}[\phi(\mathbf{r}_1^\uparrow - \mathbf{r}_1^\downarrow)\phi(\mathbf{r}_2^\uparrow - \mathbf{r}_{12}^\downarrow)\cdots\phi(\mathbf{r}_N^\uparrow - \mathbf{r}_N^\downarrow), \tag{2.88}$$

where the BCS pairing function is given by

$$\phi(\mathbf{r}) = \sum_{\mathbf{k}} \frac{v_k}{u_k} e^{i\mathbf{k}\cdot\mathbf{r}} \tag{2.89}$$

Eqn. (2.88) is multiplied by a parametrized Jastrow factor to model higher-order particle effects and to help improve the efficiency and convergence of the Monte Carlo procedure. The free parameters of the parametrized factors are optimized to minimize the energy and the resultant values associated with the ground state are calculated with the results being given in Fig. (2.1). The estimated energy per particle for a system with an even number of particles is $E = 0.44(l)\epsilon_{FG}$ and the quasiparticle gap for a system with an odd number of particles is $\Delta = 0.99(3)\epsilon_{FG}$.

2.8.6 Prior Path Integral Methods for Unitary Systems

Path integral Monte Carlo based approaches to unitary systems seem to have so far come in two forms either via auxilary field path integral Monte Carlo (AFPIMC) or by restricted node path integral Monte Carlo (RPIMC) when applied to the unitary fermi gas. The AFPIMC approach results in highly oscillatory integrals due to the Hubbard-Stratonovich transformation being applied to the fermionic fields being studied. Consequently, the errors with these methods have been quite large and will not be explored further in this thesis [12]. The RPIMC methodology does not suffer from these limitations so long as proper nodal forms are used and that these nodes are recognized as being an uncontrolled approximation being imposed on the system being considered.

For unitary Fermi gas systems, prior work within the Ceperley group has focused upon RPIMC methods. In particular the work of Akkineni [36] and Akkineni et. al. [52] focused upon RPIMC approaches to the unitary Fermi gas by simulating a fermionic system in periodic boundary conditions interacting with a short-range pair potential defined by the modified Pöschl-Teller potential [52],

$$v(r) = -\frac{2\hbar^2}{m}\frac{\mu^2}{\cosh(\mu r)} \tag{2.90}$$

where r is the distance between the particle pair in question, μ is a fitting parameter set to $\mu = 12$ and the system is set to a particle density of 0.238, which stays constant as the number of particles is varied.
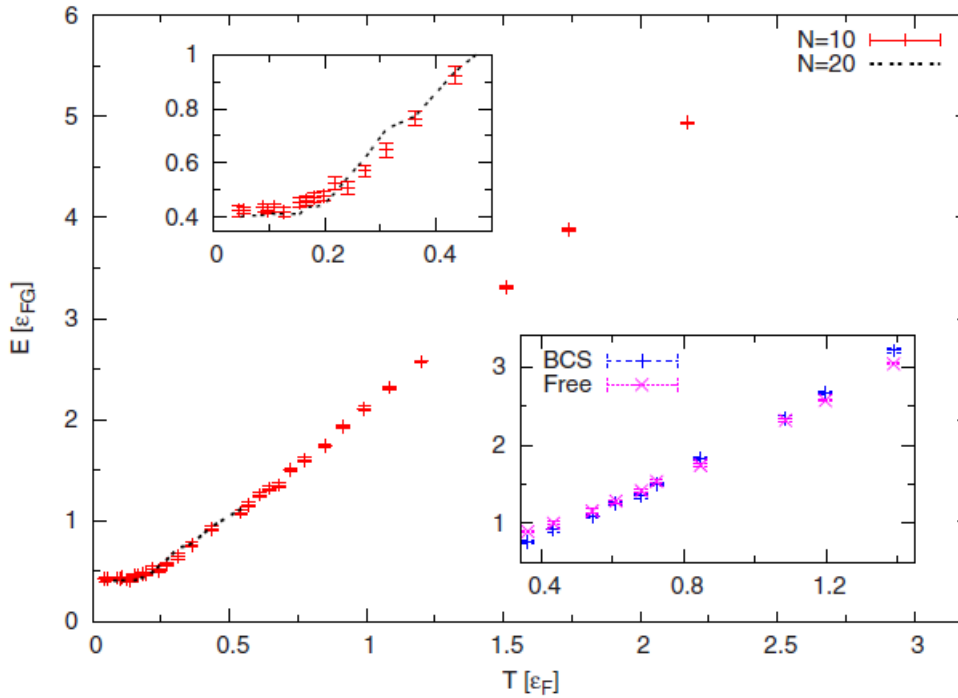
Figure 2.2: This plot compares system energy per particle for 10 and 20 particle systems using BCS nodes. With the upper inset magnifying the system at low temperature. The lower inset compares energy per particle for BCS and free particle nodes.

This setup results in an attractive divergent scattering length and hence satisfies the definition of a unitary system.

The nodes used to restrict the paths of the simulation originate from two sources. Free particle nodes are used for simulating the system at high temperature and BCS-type nodes are variational optimized at low temperature and used for pairing. Interpolating between these high and low temperature regime remain an open problem for this system and arguably for RPIMC methodology as well.

Akkineni simulates many quantities of interest to unitary fermi gas. In particular, he considers the energy per particle shows good agreement with prior computation. He also simulates pair correlation functions between the 2 different species of fermion for this system since the different weakly and strongly bound
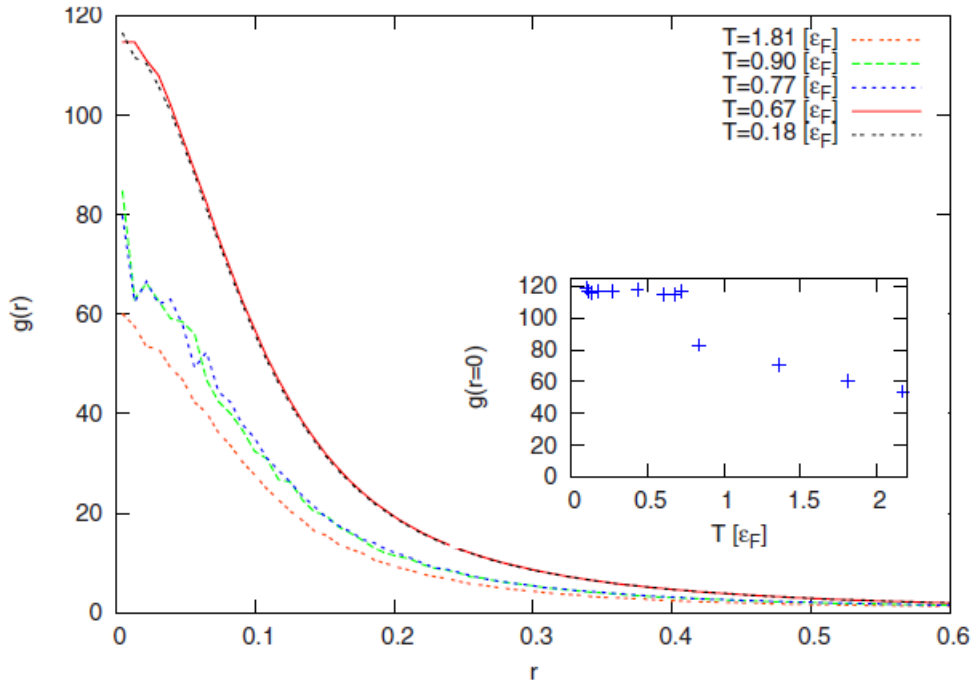
Figure 2.3: This plot presents Akkineni's simulation of the pair correlation function for the two species of fermions at different temperature through the presumable transition between the $0.67T_F$ and $0.54T_F$ simulations

pairing regimes should occur as a function of temperature and ought to appear as a function of temperature. Figure (2.3) shows that upon crossing a presumed T_c the pairing function narrows rapidly and the peak becomes more pronounced which is thought to be a signature of the system entering the strong pairing regime. The weak pairing regime in contrast is represented by a broad hump which extends out some radial distance.

Finally, Akkineni considers the temperature of the transition temperature T_c between the weakly and strongly paired regimes of the unitary gas, the BCS-BEC crossover. He attempts to probe them using the both superfluid fraction of the system as a function of temperature (Fig. (2.4)) and as estimated by comparing the superfluid density as a function of temperature (Fig. (2.5)) for systems of varying sizes
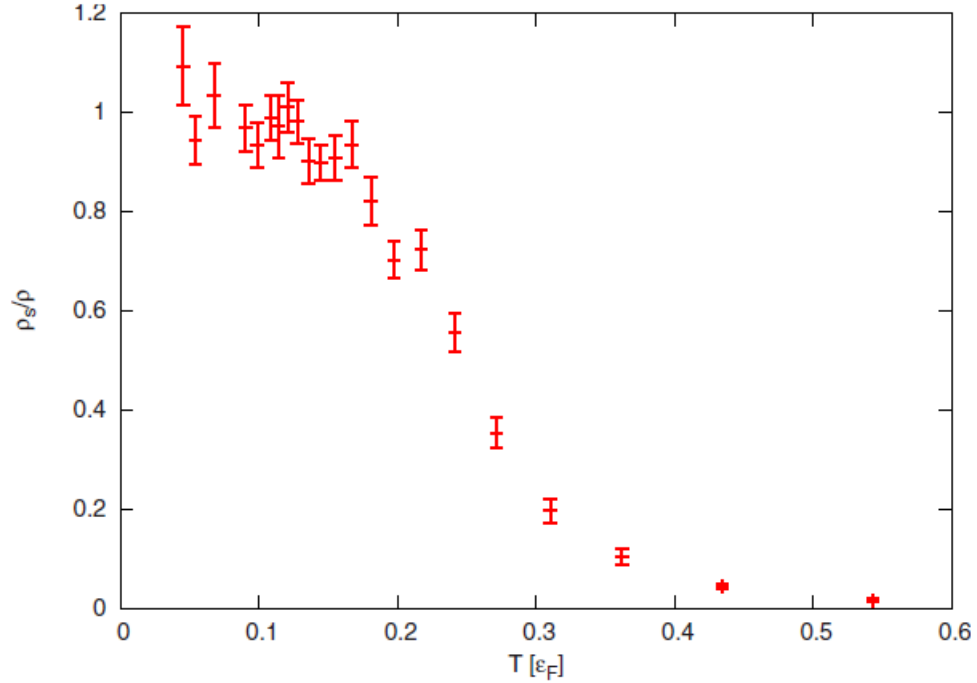
Figure 2.4: This plot presents Akkineni's simulation of the superfluid fraction ρ_s/ρ as function of temperature for a 20 particle system.

and estimating the $T_c \approx 0.255\epsilon_F$ from the crossover region of the plot. It compares relatively well to the theoretically determined value of $T_c = 0.22\epsilon_F$.

2.8.7 A Recent Variational and Diffusion Monte Carlo Approach to the Unitary Limit

At the end of 2014, an article concerning the application of variational and diffusion Monte Carlo to the unitary limit by Pessoa, Vitiello, and Schmidt appeared on the arXiv [53]. In this paper, a simulation of the ground state of the unitary limit of a zero-range fermionic gaseous system using a zero-range delta function pair potential is presented. Within diffsuion Monte Carlo, an approximate or trial ground state wavefunction is evolved using the corresponding imaginary-time propagator for the specific Bloch equation
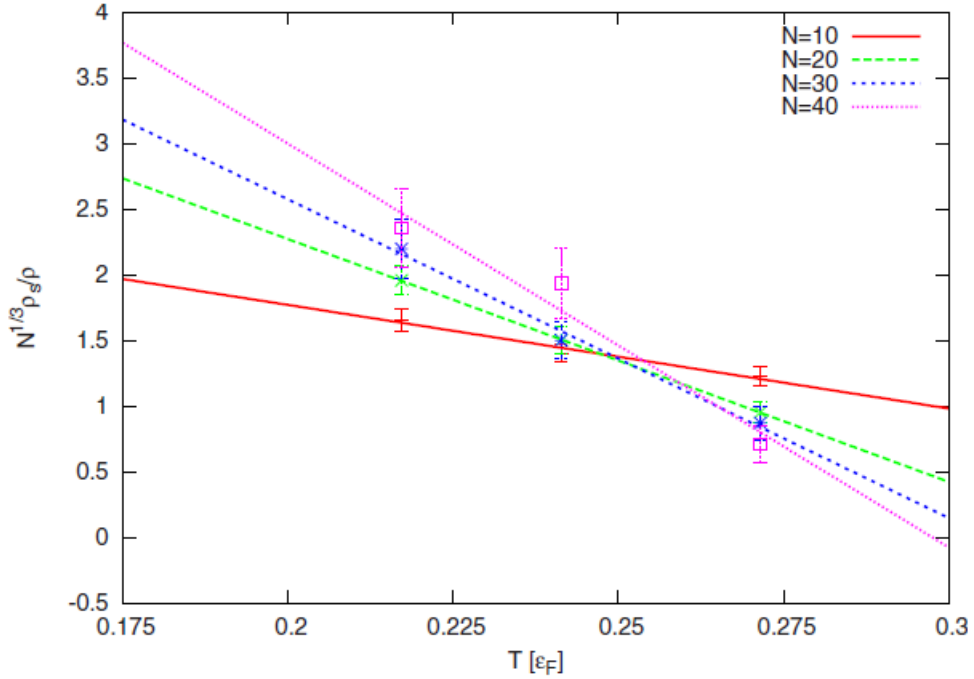
Figure 2.5: This plot presents Akkineni's simulation of the superfluid density ρ_s/ρ as function of temperature for a 10, 20, 30, and 40 particle system. The intersection of these densities occur at the presumed superfluid transition temperature of $T_c \approx 0.255\epsilon_F$.

which is defined by the Hamiltonian of the system under investigation. In simulation, the imaginary-time propagator is approximated using the Lie-Trotter discretization in a fashion similar to that used in path integral Monte Carlo which will be reviewed in chapter 4. This discretized operator is then used to evolve the approximate ground state wavefunction which in the paper under consideration is constructed using an approximate Jastrow-type wavefunction [53] to a state closer to the true ground state by causing the decay of the portions of the approximate wavefunction that a represented by excited states of the system.

For the part of the unitary DMC paper which concerns diffusion Monte Carlo, the propagator potion of the diffusion Monte Carlo scheme utilizes the same pair propagator as used in this thesis in chapter 6 for a

PIMC, which is given here as,

$$K(\mathbf{r}, \mathbf{r}'; \tau) = \left(\frac{\mu}{2\pi\hbar\tau}\right)^{3/2} e^{-\frac{\mu|\mathbf{r}-\mathbf{r}'|^2}{2\hbar\tau}} + \left(\frac{\tau\hbar}{\mu|\mathbf{r}||\mathbf{r}'|}\right)\left(\frac{\mu}{2\pi\hbar\tau}\right)^{3/2} e^{-\mu\frac{(|\mathbf{r}|+|\mathbf{r}'|)^2}{2\hbar\tau}}. \tag{2.91}$$

This is a convenient formalism as will be explored later in chapter 5; nonetheless, it will be explored here as Pessoa et. al.'s methodology for simulating fermionic systems at unitarity in the $T = 0$ limit. Moreover, just as will be discussed in chapters 5 and 6 the unitary nature of this simulation presents some challenges for sampling. In this paper, these are overcome by swapping particle pairings in the trial wavefunction and by a combined wavefunction-propagator sampling move which is used to roughly cancel the divergence due to the propagator [53]. Unfortunately, the particular form of this cancelling term does not appear to be applicable to just a path integral Monte Carlo simulation as it involves selectively tuning pairings in the trial wavefunction.

The key results at $T = 0$ obtained by Pessoa et. al. concern the calculated energy per particle, which is plotted for various system sizes in Fig. (2.6), and the radial distribution or pair correlation functions for the spin-up, spin-up particles and their interactions in Fig. (2.7) and for the spin-up, spin-down particles and their interactions in Fig. (2.8) [53].

For all of these simulations, the wavefunction was first variationally optimized and DMC simulations were performed using BCS-type nodes. Ultimately, an energy of $0.61(2)E_{FG}$ per particle was calculated which compared well with the variational upper bound $0.62(1)E_{FG}$ calculated by Chang et. al. in [54] using extrapolation. The pair correlation functions show similar agreement. A theoretical result for the free Fermi gas's pair correlation function [55]

$$g_{\uparrow\uparrow}(r) = g_{\downarrow\downarrow}(r) = 1 - \frac{9}{(k_F r)^4}\left(\frac{sin(k_F r)}{k_F r} - \cos(k_F r)\right)^2, \tag{2.92}$$

and plotted in Fig. (2.8) matches closely among like non-interacting particles. The spin-up, spin-down pair correlation function displays the expected $\frac{1}{(k_F r)^2}$ divergence at $r = 0$ [53].
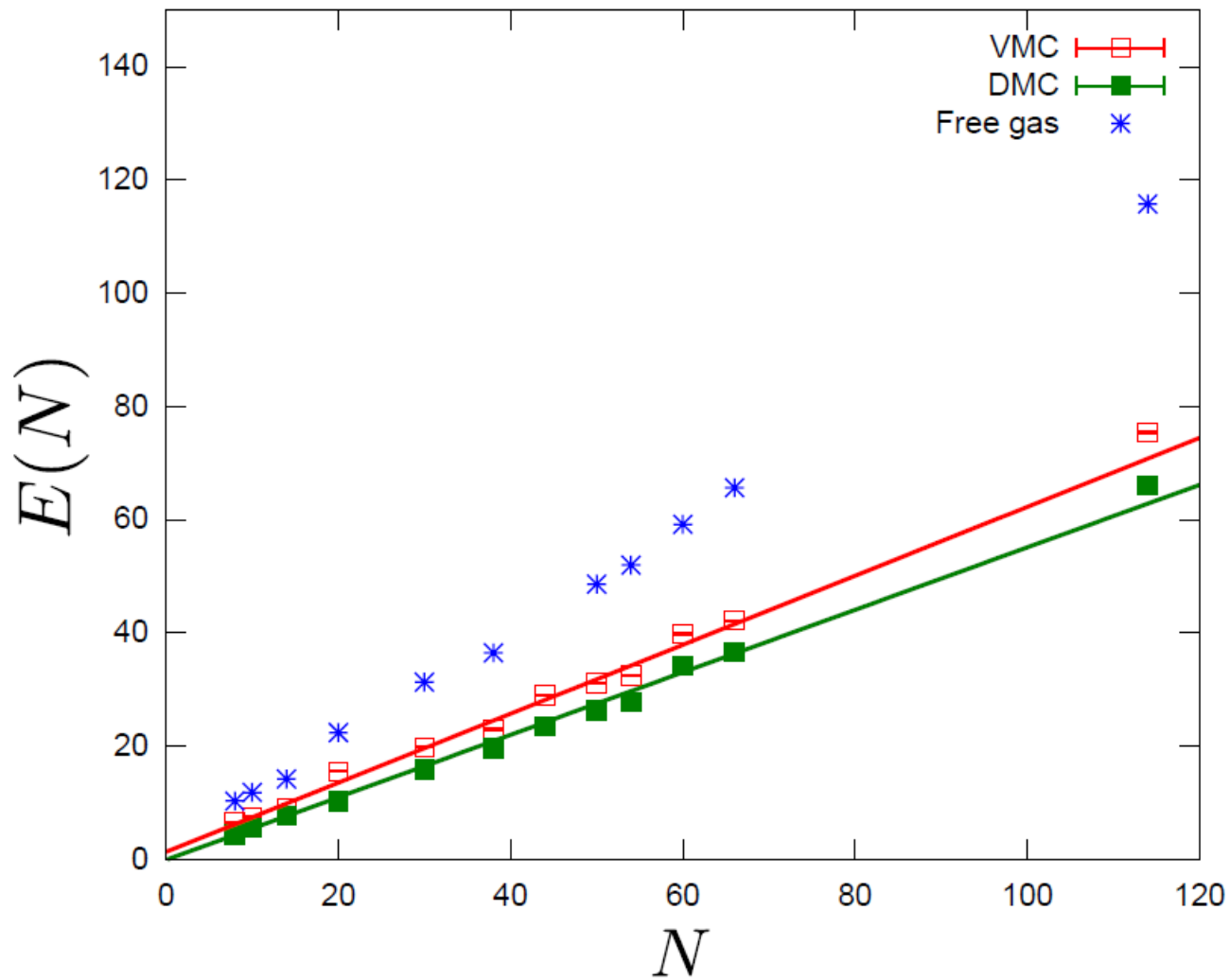
Figure 2.6: This plot from [53] details the calculated ground state energy per particle as a function of system size. N denotes the total number of particles in the system. Half of the particles are spin-up and the other half are spin-down. The energy is in units of E_{FG}. The hollow red square energies are calculated with variational Monte Carlo, the green square energies are calculated with diffusion Monte Carlo, and the blue asterisk energies are the corresponding free Fermi gas [53].
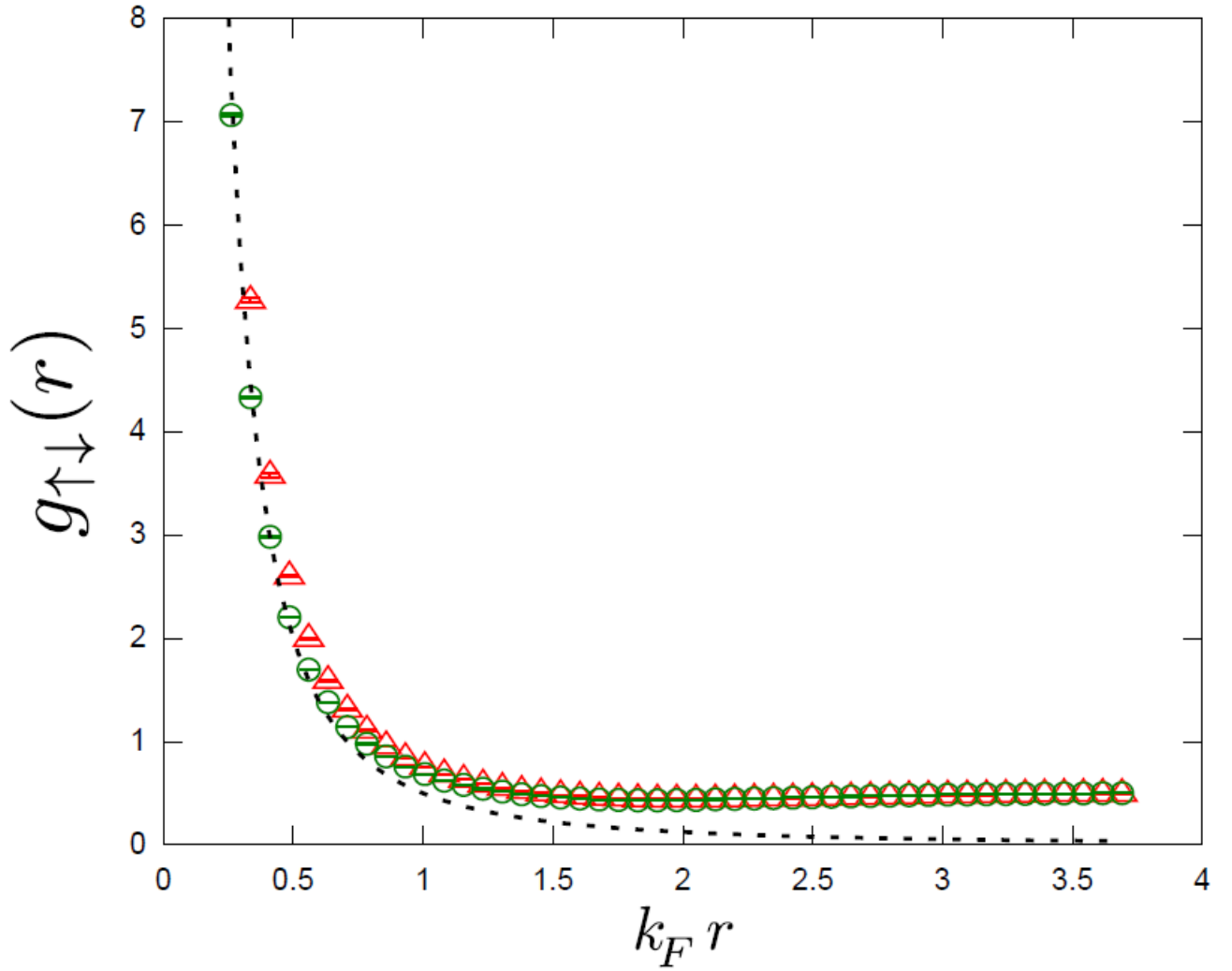
Figure 2.7: The plot of a radial distribution or pair correlation function for interaction between spin-up and spin-down particles in $N = 14$ system at unitarity. The blue line denotes the pair correlation function for the free Fermi gas; the results for VMC and DMC are denoted by the green circles and red triangles respectively [53].
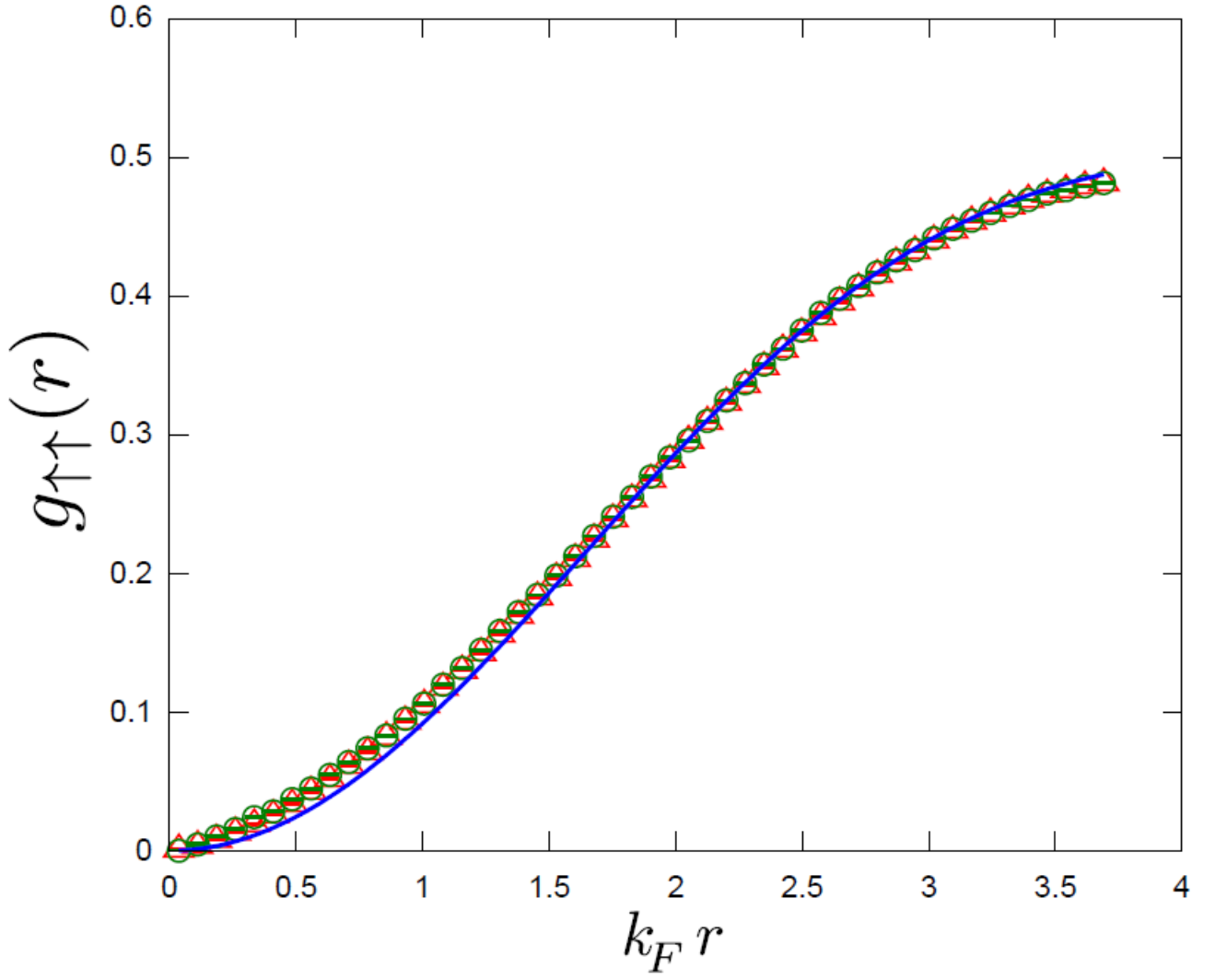
Figure 2.8: The plot of a radial distribution or pair correlation function for interaction between spin-up particles in $N = 14$ system at unitarity. The blue line denotes the pair correlation function for the free Fermi gas; the results for VMC and DMC are denoted by the green circles and red triangles respectively [53].

Chapter 3

Review of the Path Integral Approach to Quantum and Quantum Statistical Mechanics

3.1   Introduction

In a historical sense, one may argue that the path integral has been (re)-developed multiple times throughout the twentieth century and its story begins with Bachelier's work in finance studying stock prices with Brownian random walks in the early 1900's [56] and connects straight through to Wiener's related work on Brownian path summation in the late 1920's and 1930's [57, 58]. This chapter, however, will focus upon the conventional development of the subject from a physical point-of-view. This standard approach, like this chapter begins with the heuristic development of the path integral as a summation over the quantum probability amplitudes associated with classical trajectories, in work initiated by R.P. Feynman as part of his graduate thesis work on the quantum interpretation of the classical action in the early 1940's[1]. This chapter will then pivot to present the quantum statistical mechanical corollary to Feynman's path integral by deriving the quantum mechanical thermal density matrix using its relation to the Feynman path integral. Both of these formulations will then be mathematically justified using the Lie-Trotter operator-splitting spliting approach first suggested by E. Nelson in the early 1960's [59]. This chapter follows the presentation of this subject matter given in Feynman and Hibbs monograph [60] on the subject, that given by Kleinert in his massive tome on path integrals [58] as well as several doctoral theses that have covered similar content [61, 62].

3.2   From the Classical Action to the Path Integral

The simplest form of Feynman's path integral begins by considering the classical transition of a single particle in one dimension from a point x_1 at a time t_1 to a point x_2 at a time t_2. In classical mechanics, the path taken by this particle is described by the path which minimizes in the variational sense the classical action

---

[1]This approach was arguably first suggested by Dirac in his comments concerning the relationship of the classical action to the quantum propagator.

$S[\dot{x}(t), x(t); t]$ which is given by integrating the classical Lagrangian $\mathcal{L}$ over time as

$$S[\dot{x}(t), x(t); t] = \int_{t_1}^{t_2} \mathcal{L}(\dot{x}(t), x(t); t) \tag{3.1}$$

where the Lagrangian itself is defined as

$$\mathcal{L}(\dot{x}(t), x(t); t) = \frac{m}{2}\dot{x}(t)^2 - V(\dot{x}(t), xt, t) \tag{3.2}$$

In classical mechanics the Lagrangian provides a versatile compliment to Hamiltonian mechanics as the Hamilton's method is directly related to the Lagrangian by the Legendre transform.

Upon first encounter, this Lagrangian-action approach to classical systems would seem to have no direct mapping to quantum mechanics. Unlike Hamilton's approach to classical mechanics, which gave rise to the Schrödinger equation due to its inherent energy conservation. Due to the lack of an effective Legendre transform for quantum mechanics, the Lagrangian-action approach seems to be quite different as it necessarily minimizes an action and thus its quantum interpretation is seemingly somewhat muddled [58]. Nonetheless, as is frequently the case in early quantum theory, it was Dirac who first noticed/suggested a possible relation between the classical action, an integrated form of the Lagrangian, and the quantum mechanical propagator [63]. Namely that

$$|\psi(t)\rangle = e^{\frac{it}{\hbar}\hat{H}}|\psi\rangle \sim e^{\frac{i}{\hbar}S[x,t]}. \tag{3.3}$$

3.2.1 A Heuristic Description of the Path Integral

Building on this observation, Feynman made the intuitive connection between the classical action, the Lagrangian, and their interpretation in quantum mechanics [64,65]. In a classical context, the action describes the path taken by the particle which minimizes the energy requirement to get from the particle of interest's initial coordinates (x_1, t_1) to its final coordinates (x_2, t_2). Through a thought experiment where he considered the meaning of a particle subject to the non-classical rules of quantum mechanics, Feynman realized that the transition amplitude could be described as the sum of the action functionals given by eqn. (3.3) over all possible paths. Moreover, letting $\hbar \to 0$ allows the recovery the classical path of interest since this limit minimizes the now non-classical action functional and, thus, provides a direct link between time-dependent quantum and classical mechanics.

Using the formalism for the quantum amplitude of a path originally recognized by Dirac and given in eqn. (3.3) and summing over these amplitudes allows the approximate description of the total amplitude for the transition of a particle from its initial state 1 to its final state 2. In the "infinite limit" such that

an infinite number of screens are covered by an infinite number of holes, and thus free space is recovered, the summation of those infinite number of amplitudes associated with the infinite number of possible paths followed by the particle ought to yield the exact quantum transition amplitude of the particle in question.

Complicating this idealized free-particle situation is reality. If an external potential is added to the system, then the value of the external potential must be added to the Lagrangian associated with each point along the path in question so that the potential is accounted for in an appropriate fashion to the total transition amplitude. The case of multiparticle, interacting systems is handled in a very similar fashion, except that, paths for each particle must be considered and summed together to recover the transition amplitude. For the case of calculating a particle with a time-dependent potential, a time-ordering of the points along the path is required, so that the potentials appropriate time-dependent values are properly incorporated into the transition amplitudes for the paths in question.

Finally, the determination of the transition amplitude(s) associated with quantum particles whose spin is directly under consideration using a relativistic techniques are outside the scope of this thesis. Nonetheless, this case has been studied and in fact along with many other studies comprises the 1969 thesis of Leonard Schulman [66]. While the technical details may be considered to be generally outside the scope of this thesis, it is interesting to generally sketch them out here.

Spin was amongst the last quantum observable quantities to be described via path integration as it is an intrinsically quantum mechanical quantity arising from the interaction of quantum mechanics with special relativity and thus generally thought in the early years of postwar science to be outside the description of a methodology intrinsically rooted in classical mechanics. Nonetheless, the particles in question may be considered to be spinning in the classical sense and these spins may quantized using the logic of the path integral and thus incorporated into Feynman's methodological framework. Despite this success, to further explore the implications of spin in path integration requires the incorporation of special relativity into a path integral framework, and thus is firmly outside the scope of this thesis.

Before re-stating the insights gained from the preceding thought experiment in a more mathematical framework, it is interesting to consider the implications of what it actually means to sum paths using the Dirac functional form given by eqn. (3.3). Inspecting this form it is clear that the action associated with given particle path yields a value with the same units as $\hbar$ (energy·time). Replacing $S[(\cdot)]$ with this value in eqn. (3.3) yields an arbitrary complex phase.When a summation over a set of these complex phases is performed, the resulting value associated with quantum amplitude of the transitioning particle(s) from the initial state to the final state must occur due to the cancellation associated with the infinite number of oscillations associated with all of the unlikely (high-energy) paths associated with the particle(s).

While in our heuristic thought experiment this cancellation by phase oscillation does not seem to cause much of a problem. It seems quite plausible to many, including this author and has, in fact, been used for many years. It, nonetheless, is not mathematically well-founded because no intrinsic measure capable of describing the phase cancellation of these paths has been found from a mathematical perspective. This has led to a great deal of consternation within and without the physics community as well as to much work within the mathematical physics community. I mention this not throw cold water on this work, but instead to give a sense of a living science in which may valuable things may be heuristically defined and used, but which nonetheless are not fully formed from a mathematical perspective.

3.2.2 A Formal Mathematical Presentation of the Heuristic Description of the Path Integral

Returning to a mathematical description of the heuristic description of the path integral, using Feynman's notation, the preceding thought experiments that describe the sum of the quantum amplitudes may be more precisely stated as follows,

$$K(2,1) = \sum_{(\cdot)\,=\,\text{all paths}} \frac{1}{A} e^{\frac{i}{\hbar} S[(\cdot)]}, \tag{3.4}$$

where A is the normalization constant in question and $K(2,1)$ is the quantum probability amplitude[2] associated with a particle transitioning from state 1 to state 2. The probability $P(2,1)$ is then given by $|K(2,1)|^2$. Feynman interprets the integral of the action present in the preceding equation (3.4) to be well described by a Riemann sum and so discretizes or slices $S[(\cdot)]$ using the Riemann or midpoint rule type quadrature formula.

Using this primitive Riemann-type discretization gives an action that may described as

$$S = \sum_{j=0}^{M-1} \frac{\tau}{2} \Big(\mathcal{L}\Big[\Delta \dot{q}^{(j+1)}, q^{(j)}\Big] + \mathcal{L}\Big[\Delta \dot{q}^{(j+1)}, q^{(j+1)}\Big] \Big), \tag{3.5}$$

where

$$\tau = \frac{it}{M} \tag{3.6}$$

and

$$\Delta \dot{q}^{(j+1)} = \frac{(q^{(j+1)} - q^{(j)})}{\tau}. \tag{3.7}$$

---

[2]This is the notation used in Feynman and Hibbs [60] and used here for convenience and for review purposes as it is still used occasionally, particularly for teaching purposes.

Putting these definitions together gives the final synthesis of the discretized action as

$$S = \sum_{j=0}^{M-1} \tau \frac{m}{2} \left(\frac{x^{(j+1)} - x^{(j)}}{\tau^2} + V(x^{(j+1)}) \right). \tag{3.8}$$

Inserting this expression into the previously defined framework gives a form for calculating the transition amplitude that may be discretized in the following fashion,

$$K(2,1) = \lim_{\tau \to 0} \frac{1}{A} \int \cdots \int e^{\frac{i}{\hbar} S[(2,1)]} \prod_{j=0}^{M-1} \frac{dx_j}{A}, \tag{3.9}$$

where $A = (\frac{2\pi i \hbar \tau}{m})^{1/2}$ for the Lagrangian given by eqn. (3.2). Taking the limit of an infinite number of slices or sweeping everything under the rug if one prefers to be mathematically correct gives the functional form of the path integral as

$$K(2,1) = \int_{\text{State 1}}^{\text{State 2}} \mathcal{D}[x] e^{\frac{i}{\hbar} S[2,1]}. \tag{3.10}$$

3.3   Connecting the Path Integral to the Schrödinger Equation

The N-particle Schrödinger equation may be expressed as,

$$i\hbar \frac{\partial \Psi(X,t)}{\partial t} = \hat{H} \Psi(X,t), \tag{3.11}$$

where

$$\hat{H} = \hat{T} + \hat{V} = \sum_{j=1}^{N} \frac{\hat{P}^2}{2m_j} + \hat{V}, \tag{3.12}$$

and expressing the operators given by eqn. (3.12) in a position basis set yields,

$$\sum_{j=1}^{N} \frac{-\hbar^2}{2m_j} \nabla_j^2 + V(X,t). \tag{3.13}$$

This equation may be put in a form so that it is comparable to the path integral by solving the time-dependent part as follows,

$$i\hbar \frac{\partial \psi}{\partial t} = \hat{H}\psi \rightarrow |\psi(t)\rangle = e^{\frac{it}{\hbar}\hat{H}} |\psi(t=0)\rangle. \tag{3.14}$$

The factor, $e^{\frac{it}{\hbar}\hat{H}}$, is the operator form of the propagator, $K(2,1)$, and may be considered to time-evolve from the initial state of the system given here as $|\psi(t=0)\rangle$ at $t = 0$ to the final state of the system in question, $|\psi(t)\rangle$, where the time of the final state is given by an arbitrary t. Clearly, if the propagator $K(2,1)$ is

thought of as a kernel of an integral, the evolution of a quantum state forward to a new time and position may be expressed in a manner similar to eqn. (3.14). The initial state of the system given here as $|\psi(t=0)\rangle$ at $t = 0$ to the final state of the system in question, $|\psi(t)\rangle$, where the time of the final state is given by an arbitrary t. Clearly, if the propagator $K(2,1)$ is thought of as a kernel of an integral, and hence the K, that evolves a quantum state forward to a new a time and position then it may be expressed in a similar fashion to eqn. (3.14) as

$$\psi(x_2, t_2) = \int_{-\infty}^{\infty} dx_1 K(x_2, x_1, t_2 - t_1)\psi(x_1, t_1) \tag{3.15}$$

Using the ansatz suggested by Dirac and given by eqn.(3.3) to propagate the initial state in eqn. (3.15) forward an arbitrarily short-time,τ, produces,

$$\psi(x_2, t_1 + \tau) = \int_{-\infty}^{\infty} dx_1 \frac{1}{A} e^{\frac{i}{\hbar}\tau(\frac{m}{2}\frac{(x^{(2)} - x^{(1)})^2}{\tau^2} - V(x^{(2)}))}\psi(x_1, t_1), \tag{3.16}$$

where A is a yet underived normalizing constant. Taking advantage of the arbitrarily short-time of evolution described by τ, it may be assumed that the only paths that will contribute to the path integral are arbitrarily close to the starting position x_1, and hence, x_2 may be made arbitrarily close by η to x_1, so that $x_1 = x_2 - \eta$. Substituting this relation into the ansatz given by eqn. (3.16) yields

$$\psi(x_1 + \eta, t_1 + \tau) = \int_{-\infty}^{\infty} d\eta \frac{1}{A} e^{\frac{i}{\hbar}\tau(\frac{m}{2}\frac{\eta^2}{\tau^2} + V(x^{(2)}))}\psi(x_1, t_1) \tag{3.17}$$

If this equation (3.17) is then expanded in a power series about τ, then a discretized form of the Schrödinger equation may be recovered and the normalization constant found,

$$\psi(x_1 + \eta, t_1 + \tau) + \tau\frac{\partial}{\partial t}\psi(x_1 + \eta, t_1 + \tau) = \int_{-\infty}^{\infty} \frac{1}{A} e^{\frac{i}{\hbar}\tau(\frac{m}{2}\frac{\eta^2}{\tau^2})} \times \left(1 - \frac{i\tau}{\hbar}V(x_2)\right)$$
$$\times \left(\psi(x_1 + \eta, t_1 + \tau) + \tau\frac{\partial}{\partial x_1} + \frac{1}{2}\eta^2\frac{\partial^2}{\partial x_1^2}\psi(x_1 + \eta, t_1 + \tau)\right) d\eta. \tag{3.18}$$

If the right- and left-hand sides of eqn. (3.18) are compared and the various orders of τ matched, then the following relations are found. The zeroeth order equation furnishes the normalization constant A as

$$\frac{1}{A}\int_{-\infty}^{\infty} d\eta \frac{1}{A} e^{\frac{i}{\hbar}\tau(\frac{m}{2}\frac{\eta^2}{\tau^2})} = 1 \implies A = (\frac{2\pi i\hbar\tau}{m})^{1/2}. \tag{3.19}$$

The first order equation yields the relations that ultimately determine the Schrödinger equation as

$$\psi + \tau\frac{\partial\psi}{\partial t} = \psi - \frac{i\tau}{\hbar}V\psi - \frac{\hbar i\tau}{2m}\frac{\partial^2\psi}{\partial x^2}. \tag{3.20}$$

49

Rearranging this expression and canceling out the various τ's gives the time-dependent Schrödinger equation,

$$i\hbar\frac{\partial\psi}{\partial t} = -\frac{\hbar^2}{2m}\frac{\partial^2\psi}{\partial x^2} + V(x)\psi, \tag{3.21}$$

as is expected, since with a little thought it is clear that these manipulations are undoing the formal manipulations that lead from the time-dependent Schrödinger equation to the quantum propagator in operator form.

3.4   The Significance of the Path Integral

After performing these various mathematical maneuvers one may think, "That this is quite nice and all, but what can be gained from all of these inexact mathematical niceties?" It is important to recognize that with this formulation one may completely sidestep the Schrödinger equation meaning that while it is necessarily equivalent to that older form of quantum mechanics, it is independent of it like Heisenberg's matrix mechanics. This means that in principle all of the measurable quantities associated with the quantum mechanical wave equation may be derived in a way completely independent from that formulation without using wavefunctions. For instance, time correlation functions may be expressed in a fashion completely independent from having to calculate the underlying wavefunctions, which represent the time evolution the operator(s) of interest's underlying state(s). In the context of both the computation and the conceptualization of the underlying physics, this path integral formulation frees the practitioner of the art from having to think about wavefunctions to thinking directly about the time propagation of observables of interest. Thus, this methodological change opens up new possibilities for arriving at approximations and answers to physical problems.

Before continuing, it is worth considering why the path integral is such a powerful formalism: Time and time again what makes the path integral such a versatile and relatively simple quantum mechanical object from both an analytical and computational perspective is the iterative use of propagating a state of interest a short-time using a moderately accurate approximate propagator. That is if one has an approximate propagator kernel, $K_{App}(2, 1, \tau)$ where 1 and 2 are meant to indicate that this approximate kernel propagates a state from 1 to 2 over a short-time τ then a propagation from over a much longer time t may be made by letting $\tau = \frac{t}{M}$ and propagating the initial state of the system forward by applying K_{App} M times so that

$$|2\rangle = K_{App}(2, 1, t)|1\rangle \approx \int_{-\infty}^{\infty}\cdots\int_{-\infty}^{\infty} dx^M \prod_{j=1}^{M} K_{App}(x_{j+1}, x_j, \tau)|1\rangle. \tag{3.22}$$

Thematically, this result encapsulates the power of the path integral approach. Namely, that a very poor approximation to the quantum propagator may be leveraged to obtain a very accurate approximation to a much longer time propagation if enough short-time approximations are integrated over. While based upon the heuristic arguments given so far, it probably quite unclear to the reader how good this approach may be, and in truth when Feynman first published his derivation of the path integral it was probably unclear whether or not finite approximations to the path integral would ever be useful outside of a few toy cases. Fortunately, work in the later part of the 1950's cleared up much of this uncertainty and showed that the path integral may be identified with what are referred to as split-operator approaches in applied mathematics via the Lie-Trotter theorem. Moreover, this approach describes in asymptotic fashion roughly how many time slices are required to approximate the propagation for a given length of time.

As is always important for new approaches, toy problems are are critical to understanding the flexibility and naturalness of the path integral formalism. Hence, the sections that follow this one focus on the derivation of the two most critical toy models in path integrals and indeed the whole of non-relativistic quantum mechanics, namely the free particle and the harmonic oscillator.

3.5   The Path Integral for the Free Particle

In the case of the free particle, Feynman began his approximation by quite sensibly assuming that the quantum amplitude would more or less follow the trajectory of the classical path from a coordinate $(x_0, 0)$ to (x_M, t) with a classical trajectory $x_{cl}(t) = x_0 + \frac{t}{M}(x_M - x_0)$. This results in a classical action for the free particle being

$$S_{cl}(t) = \frac{m}{2}\left(\frac{(x_M - x_0)}{t}\right)^2,$$ (3.23)

in the classical limit of $\hbar \to 0$. Returning to quantum mechanics, the path integral framework yields

$$K_{FP}(2,1,t) = \int \mathcal{D}[x]e^{\frac{i}{\hbar}\int_0^t dt \frac{m}{2}\dot{x}^2} = \lim_{M\to\infty}\left(\frac{m}{2\pi i\hbar\tau}\right)^{M/2}\int_{-\infty}^{\infty}\cdots\int_{-\infty}^{\infty}dx^M\prod_{j=1}^{M}e^{\frac{i}{\hbar}\tau\frac{m}{2}\left(\frac{x_{(j+1)}-x_{(j)}}{\tau^2}\right)}.$$ (3.24)

Integrating the right-hand side of eqn. (3.24) yields the expected propagator for the free particle,

$$K_{FP}(x_M, x_0, t) = \left(\frac{m}{2\pi i\hbar t}\right)^{1/2}e^{\frac{i}{\hbar}\frac{m}{2}\frac{(x_M - x_0)^2}{t}},$$ (3.25)

which is just the substitution of the classical free particle action into Dirac's quantum mechanical action functional. Initially, it may seem strange that a classical quantity, in this case the free particle's action, may

be directly substituted into a quantum mechanical functional without any further modification to account for quantum effects. Nonetheless, for exactly solvable potentials, it is often the case that by expanding or incorporating the dominant classical paths of the underlying potential of interest excellent approximations for various propagators may be arrived. This insight is among the many methods that quantum mechanics is approximated from a semiclassical perspective.

The free particle propagator is in essence a case of repeated Gaussian integration, wherein an integration over some variable results in the same rescaled integral. This effect is generally referred to as the the semigroup property of the propagator and must appear for any exact propagator as can be seen by the following mathematical argument,

$$K(3, 1, t_2 + t_1)|1\rangle = \int_{-\infty}^{\infty} dx_2 K(3, 2, t_2) K(2, 1, t_1)|1\rangle. \tag{3.26}$$

Since K must have the same form at any time or state, when an intervening state is integrated out from two exact propagators the resulting propagator must be exactly the same as the two prior propagators, excepting a rescaling by an appropriate factor. This odd but seemingly useless property is, in fact, very important for designing efficient numerical sampling techniques for the integration of approximations to these functions since the a potential perturbed form of the free particle propagator is in effect Feynman's path integral formulation. The semigroup property associated with the free particle portion of this approximate propagator may then be used to relatively quickly find acceptable samples for numerical integration techniques. This will be covered in detail in the chapter on computational approaches to path integrals.

3.6   The Path Integral for the Harmonic Oscillator

3.6.1   Introduction

Like the free particle, the harmonic oscillator is another classical toy potential within physics and quantum mechanics in particular. The Schrödinger equation which determines it in a single dimensional setting is given by

$$i\hbar \frac{\partial \psi}{\partial t} = -\frac{\hbar^2}{2m} \frac{\partial^2 \psi}{\partial x^2} + \frac{m}{2} \omega x^2 \psi \tag{3.27}$$

where ω is the frequency of oscillation. The quantum Hamiltonian of this potential is then necessarily given by

$$\hat{H} = \frac{\hat{p}^2}{2m} + \frac{m}{2} \omega \hat{x}^2, \tag{3.28}$$

and the classical Lagrangian by

$$\mathcal{L} = \frac{m}{2}\dot{x}^2 + \frac{m}{2}\omega x^2. \tag{3.29}$$

However, unlike the prior presentation for the free particle, this presentation for the harmonic oscillator will first show how the harmonic oscillator propagator may be derived using classical path techniques and fluctuation terms. Afterwards, that same harmonic oscillator propagator will be manipulated and deconstructed in order to find the underlying eigenfunctions of the associated harmonic oscillator.

3.6.2 Deriving the Propagator of the Harmonic Oscillator Using the Classical Path and Fluctuation Terms

First, the path integral for the harmonic oscillator may be described as follows where $\mathcal{A}$ is used indicate the action of the system in question and that it is being used in a "looser" fashion than previously presented. As an aside, it should be noted that the derivation of the harmonic oscillator propagator which follows descends from that given by H. Kleinert in his truly massive tome on path integrals [67].

The propagator for the harmonic oscillator is given in the following functional form as

$$\langle x_2, t_2 | e^{\frac{it}{\hbar}\hat{H}_{osc}} | x_1, t_1 \rangle = \int \mathcal{D}[x] \int \frac{\mathcal{D}[p]}{2\pi} e^{\frac{i}{\hbar}\mathcal{A}[p,x]},$$

$$= \int \mathcal{D}[x] e^{\frac{i}{\hbar}\mathcal{A}[\dot{x},x]} \tag{3.30}$$

where the action expressed in terms of momentum, p, and position, x, is

$$\mathcal{A}[p,x] = \int_{t_1}^{t_2} dt \left(p\dot{x} - \frac{p^2}{2m} - \frac{m\omega^2}{2}x^2 \right), \tag{3.31}$$

and the action in terms of of velocity $\dot{x}$ and position, x, is

$$\mathcal{A}[\dot{x},x] = \int_{t_1}^{t_2} dt \frac{m}{2} \left(\dot{x}^2 - \omega^2 x^2 \right). \tag{3.32}$$

Following from the path formalism of Feynman's approach to the path integral, the propagator of the harmonic oscillator may be expressed as in terms of quantum fluctuations around the classical paths of the harmonic as oscillator as

$$\mathcal{A}_{fl} = \int_{t_1}^{t_2} dt \frac{m}{2} \left((\delta\dot{x})^2 - \omega^2 (\delta x)_{cl}^2 \right), \tag{3.33}$$

where the classical paths of the harmonic oscillator are defined in terms of the classical action as

$$\mathcal{A}_{cl} = \int_{t_1}^{t_2} dt \frac{m}{2} \left(\dot{x}_{cl}^2 - \omega^2 x_{cl}^2 \right). \tag{3.34}$$

Applying the following boundary conditions,

$$\delta x(t_1) = \delta x(t_2) = 0, \tag{3.35}$$

to the fluctuations at times t_1 and t_2. Thus there is no term that mixes the classical path coordinates with the fluctuation terms and consequently the path integral expression for the quantum propagator of the harmonic oscillator may be rewritten as a product of terms due to the classical path and the fluctuation terms as

$$\langle x_2, t_2 | e^{\frac{it}{\hbar} \hat{H}_{osc}} | x_1, t_1 \rangle = \int \mathcal{D}[x] e^{\frac{i}{\hbar} \mathcal{A}[x]}$$

$$= e^{\frac{i}{\hbar} \mathcal{A}_{cl}} F_\omega(t_2 - t_1). \tag{3.36}$$

The classical trajectory may then be solved to give

$$x_{cl}(t) = \frac{x_2 \sin(\omega(t - t_1)) + x_1 \sin(\omega(t_2 - t))}{\sin(\omega(t_2 - t_1))}, \tag{3.37}$$

where it is assumed that $\omega(t_2 - t_1) \neq n\pi, n \in \mathbb{Z}$.

The classical action requires some algebraic manipulation to re-express it in terms of the boundary conditions as,

$$\mathcal{A}_{cl} = \int_{t_1}^{t_2} dt \frac{m}{2} (x_{cl} \ddot{x}_{cl} - \omega^2 x_{cl}) + \frac{m}{2} x_{cl} \dot{x}_{cl} |_{t_1}^{t_2}$$

$$= \frac{m}{2} x_{cl} \dot{x}_{cl} |_{t_1}^{t_2}, \tag{3.38}$$

where the integrand term cancels because it defines the equation of motion minus itself, leaving the boundary term as the answer. Taking the time derivative of eqn. (3.37) and solving for the boundary times gives the

following expressions,

$$\dot{x}_{cl}(t_2) = \frac{\omega}{\sin(\omega(t_2 - t_1))} \left(x_2 - x_1 \cos(\omega(t_2 - t_1)) \right)$$

$$\dot{x}_{cl}(t_1) = \frac{\omega}{\sin(\omega(t_2 - t_1))} \left(x_2 \cos(\omega(t_2 - t_1)) - x_1 \right). \tag{3.39}$$

Substituting these equations into eqn. (3.38) yields an expression for the classical action in terms of the boundary conditions (x_2, t_2) and (x_1, t_1),

$$\frac{m\omega}{\sin(\omega(t_2 - t_1))} \left((x_2^2 + x_1^2) \cos(\omega(t_2 - t_1)) - 2x_2 x_1 \right), \tag{3.40}$$

so that the classical portion of the propagator may be expressed as,

$$e^{\frac{i}{\hbar} \mathcal{A}_{cl}} = e^{\frac{i}{\hbar} \frac{m\omega}{\sin(\omega(t_2 - t_1))} \left((x_2^2 + x_1^2) \cos(\omega(t_2 - t_1)) - 2x_2 x_1 \right)}. \tag{3.41}$$

The fluctuation term is a bit more tricky but may be ultimately be derived in the following fashion. Recalling the fluctuation factor, $F_\omega(t_2 - t_1)$, its N-slice limited form indicated as $F_\omega^N(t_2 - t_1)$ may be expressed via the following expression,

$$F_\omega^N(t_2 - t_1) = \sqrt{\frac{m}{2\pi\hbar i\epsilon}} \prod_{n=1}^{N} \left[\int_{-\infty}^{\infty} d\delta x_n \right] \left(\sqrt{\frac{m}{2\pi\hbar i\epsilon}} \right)^N e^{\frac{i\epsilon}{\hbar} \frac{m}{2} [\sum_{m,m'=1}^{N} \delta_m (\nabla \overline{\nabla} + \omega^2) \delta_{m'}]}, \tag{3.42}$$

where ∇ and $\overline{\nabla}$ indicate the forward and backward difference operators and the $\sum_{m,m'=1}^{N}$ indicates that object being manipulated is a matrix. If this matrix is diagonalized, the following eigenvalues result

$$\Omega_m \overline{\Omega}_m = \frac{2 - 2\cos(\nu_m \epsilon)}{\epsilon^2} - \omega^2, \tag{3.43}$$

and $F_\omega^N(t_2 - t_1)$ may expressed in terms of these eigenvalues as

$$F_\omega^N(t_2 - t_1) = \sqrt{\frac{m}{2\pi\hbar i\epsilon}} \prod_{m=1}^{N} = \frac{1}{\sqrt{\epsilon^2 \Omega_m \overline{\Omega}_m - \epsilon^2 \omega^2}}. \tag{3.44}$$

The following factor is then defined for convenience,

$$\sin(\epsilon \frac{\tilde{\omega}}{2}) = \epsilon \frac{\omega}{2}, \tag{3.45}$$

so that a term in the RHS of eqn. (3.44) may expressed using this expression and then simplified using

various product identities as,

$$\prod_{m=1}^{N} \left(\epsilon^2 \Omega_m \overline{\Omega}_m - \epsilon^2 \omega^2\right) = \prod_{m=1}^{N} \left(\epsilon^2 \Omega_m \overline{\Omega}_m\right) \prod_{m=1}^{N} \left(\frac{\epsilon^2 \Omega_m \overline{\Omega}_m - \epsilon^2 \omega^2}{\epsilon^2 \Omega_m \overline{\Omega}_m}\right)$$
$$= \prod_{m=1}^{N} \left(\epsilon^2 \Omega_m \overline{\Omega}_m\right) \prod_{m=1}^{N} \left(1 - \frac{\sin(\epsilon \frac{\tilde{\omega}}{2})^2}{\sin(\epsilon \frac{m\pi}{2(N+1)})^2}\right)$$
$$= \frac{\sin(\tilde{\omega}(t_2 - t_1))}{\sin(\epsilon \tilde{\omega})}. \tag{3.46}$$

The finite N-slice fluctuation factor may be given as,

$$F_\omega^N(t_2 - t_1) = \sqrt{\frac{m}{2\pi\hbar i\epsilon}} \sqrt{\frac{\sin(\epsilon\tilde{\omega})}{\sin(\tilde{\omega}(t_2 - t_1))}}. \tag{3.47}$$

Finally, taking the continuum limit as $\lim_{N\to\infty}\left(\sin(\epsilon\frac{\tilde{\omega}}{2}) = \epsilon\frac{\omega}{2}\right) = \tilde{\omega} = \omega$, which allows

$$\lim_{N\to\infty} F_\omega^N(t_2 - t_1) = \sqrt{\frac{m}{2\pi i\hbar}} \sqrt{\frac{\sin(\omega)}{\sin(\omega(t_2 - t_1))}}. \tag{3.48}$$

Combining this fluctuation term with that of the classical path term given by eqn. (3.41) yields the expected propagator

$$\langle x_2, t_2| e^{\frac{it}{\hbar}\hat{H}_{osc}} |x_1, t_1\rangle = \sqrt{\frac{m}{2\pi i\hbar}\frac{\sin(\omega)}{\sin(\omega(t_2 - t_1))}} e^{\frac{i}{\hbar}\frac{m\omega}{\sin(\omega(t_2-t_1))}\left((x_2^2+x_1^2)\cos(\omega(t_2-t_1))-2x_2x_1\right)}. \tag{3.49}$$

3.6.3 Extracting the Eigenfunctions of the Harmonic Oscillator from Its Propagator

Now that the propagator of the harmonic oscillator has been derived, it is both enjoyable and instructive to use it perform some mathematical tricks and show that it relates as expected to the underlying wavefunction expression for the quantum propagator. This section follows closely the original presentation on this subject in Feynman and Hibbs [64], which the author enjoyed so much and found so instructive when first learning about path integrals that he felt it important to include it in his thesis.

This presentation begins by changing from a time-dependent description of quantum mechanics to a time-independent one (The methodology for doing so may be found in any reasonable introductory textbook on quantum mechanics.) allows the Schrödinger equation to be presented in terms of the underlying

eigenfunctions of the harmonic oscillator as

$$\hat{H}\phi_n(x) = \left(\frac{\hat{p}^2}{2m} + \frac{k}{2}\omega\hat{x}^2\right)\phi_n(x) = E_n\phi_n(x). \tag{3.50}$$

Solving for this equation yields energy levels given by

$$E_n = \hbar\omega(n + \frac{1}{2}), \; n \in \mathbb{Z}^+, \tag{3.51}$$

where $\omega = \sqrt{\frac{k}{m}}$ and the eigenfunctions given as

$$\phi_n(x) = \frac{1}{(2^n n!)^{1/2}} \left(\frac{m\omega}{\pi\hbar}\right)^{1/4} H_n(x\sqrt{\frac{m\omega}{\hbar}})e^{-\frac{m\omega}{2\hbar}x^2}, \tag{3.52}$$

where $H_n(x)$ are the Hermite polynomials which may be determined via the following generating formula

$$H_n(x) = (-1)^n e^{x^2} \frac{d^n}{dx^n} e^{-x^2}. \tag{3.53}$$

Using the definition of a propagator along with the previously derived harmonic oscillator propagator allows the following statement

$$\langle x_2, t_2 | e^{\frac{it}{\hbar}\hat{H}_{osc}} | x_1, t_1 \rangle = \sum_{n=0}^{\infty} \phi_n^*(x_2)\phi_n(x_1) \, e^{\frac{-it}{\hbar}E_n}$$

$$= \left(\frac{m\omega}{2\pi i\hbar \sin(\omega t)}\right)^{1/2} e^{\frac{im\omega}{2\pi\hbar \sin(\omega t)}((x_2^2+x_1^2)\cos(\omega t)-2x_2x_1)}. \tag{3.54}$$

While using the complex exponential form of the trigonometric functions in eqn. (3.54) allows the propagator to be rewritten as

$$\left(\frac{m\omega}{2\pi i\hbar}\right)^{1/2} \frac{e^{i\omega t/2}}{(1-e^{-2i\omega t})^{1/2}} e^{\frac{im\omega}{2\pi\hbar \sin(\omega t)}((x_2^2+x_1^2)\frac{1+e^{-2i\omega t}}{1-e^{-2i\omega t}} - 2x_2x_1\frac{e^{i\omega t/2}}{1-e^{-2i\omega t}})}. \tag{3.55}$$

The geometric series may then be used to expand the ratio of factors and give the following expression,

$$\left(\frac{m\omega}{2\pi i\hbar}\right)^{1/2} e^{i\omega t/2} \left(1 + \frac{1}{2}e^{-i2\omega t} + \cdots\right) e^{-\frac{m\omega}{2\hbar}(x_2^2+x_1^2)}$$

$$\times \left[1 + \frac{2m\omega}{\hbar}x_2x_1 e^{-i\omega t} + \frac{1}{2}\left(\frac{2m\omega}{\hbar}\right)^2 x_2^2 x_1^2 e^{-i2\omega t} - \frac{m\omega}{\hbar}(x_2 + x_1)e^{-i2\omega t} + \cdots\right]. \tag{3.56}$$

After laboriously grouping the terms of like energy of the form $\phi_n^*(x_2)\phi_n(x_1)e^{-in\omega(t+\frac{1}{2})}$ of eqn. (3.56),

the wavefunctions, as well as the energy levels, may be extracted back out from the propagator. Giving $E_n = \hbar\omega(n + \frac{1}{2})$, $n \in \mathbb{Z}^+$ as expected for the energy levels as well as,

$$\phi_0(x) = \left(\frac{m\omega}{\pi\hbar}\right)^{1/4} e^{-\frac{m\omega}{2\hbar}x^2}, \tag{3.57}$$

for the ground state wavefunction of the harmonic oscillator. Similar groupings may be performed for the excited states.

3.7 The Thermal Density Matrix: An Imaginary-Time Complement to Feynman's Formulation

3.7.1 Overview of Quantum Statistical Mechanics

Within computational physics, lattice methods aside, quantum statistical mechanics is the major application of the path integral due to the numerical stability of the integrands that this methodology yields. While so far, the presentation in this chapter has focused upon the real-time or time-dependent quantum mechanical applications of the Feynman path integral, in a computational setting these methods are in fact of limited or of highly specialized importance/interest due to the oscillatory effects of the complex factor present in the real-time phase factor, $|\psi(t)\rangle = e^{\frac{it}{\hbar}\hat{H}}|\psi\rangle \sim e^{\frac{i}{\hbar}S[x,t]}$. Applying standard Monte Carlo numerical integration techniques to integrate the high-dimensional integrands that would be generated by the Feynman path integral results in a statistical error that becomes exponentially worse with each added dimension of integration. This fact has resulted in this field being considered from a computational perspective to be quite outside the mainstream or as a starting point for semiclassical approaches which typically yield much better behaved integrands.

That said, when exploring quantum statistical mechanics it is quite common to come across the quantum Boltzmann operator $e^{-\beta\hat{H}}$ which yields the equilibrium Boltzmann distribution and hence the weighting for for quantum systems. Moreover, this operator shares its mathematical form with the Heisenberg time-evolution operator $e^{-\frac{it}{\hbar}\hat{H}}$ and has thus far been indirectly the subject of this chapter. While clearly related to Heisenberg's operator, the Boltzmann operator may in fact be found by analytically continuing in the real time coordinate t to an imaginary time $t \to i\tau$ such that $\frac{i\tau}{\hbar} = -\beta$. This simple analytical trick allows all of the reasoning used by Feynman to initially derive quantum propagators to be applied to quantum Boltzmann factors, although it is arguable that the heuristic arguments underlying Feynman's manipulations are lost in the transition from real- to imaginary-time. Fortunately, what is lost in heuristic is gained in mathematical

rigor as techniques such as Feynman-Kac integrals and split-operator methods become applicable.

To state it succinctly, the trace over the Boltzmann operator defines the quantum canonical partition function $Z(\beta)$ of quantum statistical mechanics. This quantity may be variously defined as follows

$$Z(\beta) = \sum_i d(i) e^{-\beta E_i} = \int dx \, \langle x | e^{-\beta \hat{H}} | x \rangle, \tag{3.58}$$

where the middle expression of eqn. (3.58) is a summation over energy where the Boltzmann factor, $e^{-\beta E_i}$, of each energy state is weighted by its degeneracy, d_i. To make a fuller identification with the Feynman path integral, the Dirac ansatz for the Boltzmann operator may be stated as follows

$$\int dx \langle x | e^{-\beta \hat{H}} | x \rangle = \sum_{\text{Closed Paths}} e^{-i \int_0^{-it} d\tau \, \mathcal{L}[\dot{q}(\tau), q(\tau)]}. \tag{3.59}$$

Continuing on, while the partition function is typically regarded as the function of central interest in statistical mechanics due to its direct relationship to the free energy F as $Z(\beta) = e^{-\beta F}$, in truth, what makes it useful from an experimental and hence ultimately scientific viewpoint is that it can be used to calculate average macroscopic quantities of interest using the following expression,

$$\langle A(\beta) \rangle = \frac{\int dx \, \langle x | \hat{A} \, e^{-\beta \hat{H}} | x \rangle}{Z(\beta)}. \tag{3.60}$$

Once an average value for some expectation value $\hat{A}$, such as average magnetization of a material or average energy of a system or even heat capacity of a system, is found it may be corroborated with experiment.

3.7.2 Quantum Statistical Mechanics via the Bloch Equation

The previous subsection has focused on presenting quantum statistical mechanics in its usual framework of counting states, finding partition functions, and calculating expectation values. However, another approach links the thermal density matrix or the quantum observable matrix element defined by the Boltzmann operator to a Schrödinger-like equation called the Bloch equation. This should not come as a surprise to the reader since the quantum propagator may be (and has been) derived in exactly the same fashion using formal manipulations of the Schrödinger equation. The Bloch equation is defined as,

$$-\frac{\partial \rho(x', x; \beta)}{\partial \beta} = \hat{H} \, \rho(x', x; \beta) \rightarrow \rho(x', x; \beta) = \langle x' | e^{-\beta \hat{H}} | x \rangle, \tag{3.61}$$

where this expression ought to look much like an analytically continued Schrödinger equation to the reader with the following boundary conditions for boltzmannon particles (particles without quantum exchange effects),

$$\rho(x', x; 0) = \delta(x' - x), \tag{3.62}$$

and the following boundary conditions

$$\rho(x', x; 0)_{B/F} = \sum_{\mathcal{P}} (\pm 1)^{\mathcal{P}} \delta(\mathcal{P}x' - x), \tag{3.63}$$

for bosons and fermions, both types of quantum particles, the later of which will be covered extensively in this thesis.

Since the matrix element which is the solution to the Bloch equation is an expectation value for the Schrödinger equation it may be expressed via eigenfunction just like any other average quantity as

$$\rho(x', x; \beta) = \sum_i \psi_i^*(x') e^{-\beta E_i} \psi_i(x). \tag{3.64}$$

This expression is a fundamental relation for the thermal density matrix and provides a convenient way to prove assertions that are often difficult to show in other frameworks.

3.7.3 Connecting the Thermal Density Matrix to the Path Integral

So far, a great deal of background for statistical mechanics has been covered, however, the reader may wonder how this relates to path integrals. While it is clear and has been previously alluded to that the thermal density matrix shares a form with quantum propagator, its direct connection may still seem elusive. It is the purpose of this subsection to concretely demonstrate how the Boltzmann operator may be expressed in a path integral expression using an alternant split-operator approach to the path integral that is actually the standard formalism within the computational physics/chemical physics communities.

First, consider the Boltzmann operator $e^{-\beta \hat{H}}$. Using the Lie-Trotter theorem, it may be split and reformulated in an approximate form so that calculations may be performed as follows

$$\begin{aligned} e^{-\beta \hat{H}} &\approx \left(e^{-\beta \frac{\hat{T}}{n}} e^{-\beta \frac{\hat{V}}{n}} \right)^n \approx \left(e^{-\beta \frac{\hat{T}}{2n}} e^{-\beta \frac{\hat{V}}{n}} e^{-\beta \frac{\hat{T}}{2n}} \right)^n \\ &= \left(e^{-\beta \frac{\hat{T}}{n}} e^{-\beta \frac{\hat{V}}{n}} \right)^n + O\left(\frac{1}{n} \right) \\ &= \left(e^{-\beta \frac{\hat{T}}{2n}} e^{-\beta \frac{\hat{V}}{n}} e^{-\beta \frac{\hat{T}}{2n}} \right)^n + O\left(\frac{1}{n^2} \right). \end{aligned} \tag{3.65}$$

At first sight, these operations may seem abstruse and possibly unnecessary; however, they are required because a direct evaluation of the Boltzmann operator would require the solution of the Schrödinger equation for the Hamiltonian of interest. Instead, $\hat{H} = \hat{T} + \hat{V}$ may be split, so that only the individual exponential operator functions, $e^{-\beta \hat{T}}$ and $e^{-\beta \hat{V}}$, need be considered. Repeatedly splitting the Boltzmann operator using the formalism given by eqn. (3.65) develops the direct connection to the path integral framework so that,

$$Z(\beta) = Tr(e^{-\beta \hat{H}}) \approx Tr(\prod_{j=1}^{n} e^{-\beta \frac{\hat{T}}{n}} e^{-\beta \frac{\hat{V}}{n}}). \tag{3.66}$$

Inserting complete sets of position and momentum states in front of the kinetic energy operators, $\hat{T}$, and potential energy operators, $\hat{V}$, and operating on those states with those exponential operators yields,

$$Z(\beta) = Tr(e^{-\beta \hat{H}}) \approx Tr(\prod_{j=1}^{n} \int dp_j dx_j e^{-\beta \frac{\hat{T}}{n}} |p_j\rangle \langle p_j| e^{-\beta \frac{\hat{V}}{n}} |x_j\rangle \langle x_j|), \tag{3.67}$$

where after some rearrangement of terms, these individual matrix elements may be evaluated as follows,

$$\begin{aligned}
\langle y|e^{-\beta \hat{T}} e^{-\beta \hat{V}}|x\rangle &= \int dp \, \langle y|e^{-\beta \hat{T}}|p\rangle \langle p|e^{-\beta \hat{V}}|x\rangle \\
&= \int dp \, \langle y|p\rangle \langle p|x\rangle e^{-\beta \frac{p^2}{2m}} e^{-\beta V(\{x\})} \\
&= \int dp \, e^{ip(y-x)} e^{-\beta \frac{p^2}{2m}} e^{-\beta V(\{x\})} \\
&= \left(\frac{m}{2\pi\beta}\right)^{\frac{d}{2}} e^{-\frac{m(y-x)^2}{2\beta}} e^{-\beta V(\{x\})}.
\end{aligned} \tag{3.68}$$

So that, after the momentum states are integrated out and the resulting functions that describe the underlying matrix elements may be reinserted into the split-operator path integral framework given by eqn. (3.66) to yield the final path integral expression for the thermal density matrix,

$$Z(\beta) \approx \left(\frac{m}{2\pi\beta}\right)^{\frac{dn}{2}} \int dx^n \prod_{j=0}^{n-1} e^{-\frac{mn(x^{(j+1)}-x^{(j)})^2}{2\beta}} e^{-\frac{\beta}{n} V(\{x^{(j)}\})}. \tag{3.69}$$

3.7.4 An Exact Solution for the Partition Function of the Harmonic Oscillator

As a final exercise for the thermal density matrix, the partition function as well as the average energy, $\langle E \rangle$, for the harmonic oscillator will be found as it is a ubiquitous test problem within this field. First, recall that

the Hamiltonian of the harmonic oscillator is given by following operator expression

$$\hat{H} = \frac{\hat{p}^2}{2m} + \frac{k}{2}\hat{x}^2. \tag{3.70}$$

Solving for the energy levels of the harmonic oscillator via the time-independent Schrödinger equation, $\hat{H}\phi_n(x) = E_n\phi_n(x)$, yields the following relations

$$E_n = \hbar\omega(n + \frac{1}{2}), \ n \in \mathbb{Z}^0, \tag{3.71}$$

where $\omega = \sqrt{\frac{k}{m}}$. Consequently, the partition function, $Z(\beta)$, may be described as

$$Z(\beta) = Tr(e^{-\beta\hat{H}_{osc}}) = \int dx\langle x|e^{-\beta\hat{H}_{osc}}|x\rangle = \sum_{n=0}^{\infty} e^{-\beta(\hbar\omega(n+\frac{1}{2}))}. \tag{3.72}$$

While all of the various forms for $Z(\beta)$ given in eqn. (3.72)are soluble, by far the easiest method is summing the series given by the far RHS of the equation (In fact, it is given as a problem in the introductory undergraduate thermal physics course here at the University of Illinois). By using the geometric series, it may be shown that,

$$Z(\beta) = \sum_{n=0}^{\infty} e^{-\beta(\hbar\omega(n+\frac{1}{2}))} = \frac{e^{-\frac{\beta\hbar\omega}{2}}}{e^{-\beta\hbar\omega} - 1}, \tag{3.73}$$

and then by applying the definition,

$$-\frac{\partial\,ln(Z(\beta))}{\partial\beta} = \langle E\rangle, \tag{3.74}$$

of average energy to the partition function for the harmonic oscillator gives

$$\langle E\rangle = \frac{\hbar\omega}{2}\frac{1 + e^{-\beta\hbar\omega}}{e^{-\beta\hbar\omega} - 1}. \tag{3.75}$$

This average energy for a single particle in a one-dimensional harmonic oscillator then becomes a convenient test case for various simulations.

3.8 The Lie-Trotter Discretization of $e^{t(\hat{T}+\hat{V})}$

3.8.1 Overview of the Lie-Trotter Theorem

Previously in this chapter, the path integral has been presented in a fashion meant to make explicit connections between the Lagrangian-Action approach of classical mechanics and sum over paths approach to

determining the real- (and imaginary-) time propagators of quantum mechanics. The path integral was presented in this fashion to give a sense both historic and current to how many researchers coming from the physical sciences approach this methodology. That said, from a mathematical standpoint the path integral as a literal sum-over-paths has never been shown to be mathematically well founded for real-time calculations (the case is different for imaginary time) and reading between the lines of various statements he made concerning mathematics and physics seems to have been a source of consternation for R.P. Feynman [64, 65]. Consequently, this section seeks to present an approach to the path integral, which while not technically a sum-over-paths approach, is nonetheless mathematically solid, and moreover, as will be shown in the subsequent chapter on computational approaches to the path integral allows one to explain why Feynman's arguments yield correct answers. Within the applied mathematics, these techniques are referred to as "split-operator methods"; here, they will be referred to as Lie-Trotter-type formulas.

At its most fundamental level, Lie-Trotter-type formulas concern the relationship between an exponential function of a sum of non-commuting operators and the individual exponential functions of those same operators, and more importantly, how well products of those individual exponential functions of a single operator may approximate the initial exponential function of a sum of non-commuting operators. Typically, the goal of research into Lie-Trotter-type formulas is to make as high of an order approximation to the initial exponential operator function as possible while using as few as individual operator functions as possible in the approximating product in order to limit the number of variables ultimately used in the approximation. Moreover, it is often a goal to structure these approximations in ways to preserve desirable symmetries and properties like hermiticity as doing so often has useful error limiting consequences. The following presentation of a proof of the standard and symmetric Lie-Trotter theorems will closely follow the proofs presented in M. Suzuki's book on path integration techniques [68].

3.8.2   Proof of the Standard Lie-Trotter Theorem

To apply Lie-Trotter-type formulas to the approximation of a quantum mechanical propagator $e^{t(\hat{T}+\hat{V})}$ or as will be subsequently used $e^{t(\hat{A}+\hat{B})}$, where t here is some time, real or imaginary, and $[\hat{A}, \hat{B}] \neq 0$. It is the non-commuting nature of the underlying operators $\hat{A}$ and $\hat{B}$ that makes finding these approximations beguiling and challenging problems. In general, the Lie-Trotter theorem may be simply stated as follows,

$$e^{t(\hat{A}+\hat{B})} = \lim_{m \to \infty} \left(e^{\frac{t}{m}\hat{A}} e^{\frac{t}{m}\hat{B}} \right)^m. \tag{3.76}$$

Although in truth in any computational application this identity will be truncated at some finite m and so it is useful to see how the error decays asymptotically as a function of the number of replicas

$$e^{t(\hat{A}_1+\hat{A}_2+...+\hat{A}_n)} = \left(e^{\frac{t}{m}(\hat{A}_1+\hat{A}_2+...+\hat{A}_n)}\right)^m$$

$$= \left(e^{\frac{t}{m}\hat{A}_1}e^{\frac{t}{m}\hat{A}_2}\cdots e^{\frac{t}{m}\hat{A}_n} + O(\frac{t^2}{m^2})\right)^m$$

$$= \left(e^{\frac{t}{m}\hat{A}_1}e^{\frac{t}{m}\hat{A}_2}\cdots e^{\frac{t}{m}\hat{A}_n}\right)^m + O\left(\frac{t^2}{m}\right). \tag{3.77}$$

Proving these statements, however, are quite challenging and based on the many theses and papers concerning path integration that use these methods that the author has perused seldom understood or appreciated by the computational physics/chemical physics communities. Consequently, the explanations that are meant to fill in that gap while providing proofs of Lie-Trotter-type theorems in succinct and as accessible a way as possible.

First, some basics are required. A matrix norm for an operator $\hat{A}$ or $\hat{B}$ in some sense measures the "size" of an operator just as a ruler measures the length of a line. Typically, we equip our matrix operator norms with the following properties by definition:

1. $||\hat{A}|| \geq 0$

2. $||x\hat{A}|| = |x|\,||\hat{A}||$

3. $||\hat{A} + \hat{B}|| \leq ||\hat{A}|| + ||\hat{B}||$

4. $||\hat{A}\hat{B}|| \leq ||\hat{A}|| \cdot ||\hat{B}||$

5. $||1|| = 1$. $\tag{3.78}$

Examples of a norm for a matrix are maximal absolute eigenvalue of a Hermitian matrix,$|\lambda_{max}|$ or the maximal columns sum of a matrix $||\hat{A}|| = max_i \sum_j |a_{ij}|$. Next, for the purpose of convenience, two dummy expressions p and q are defined as

$$p = e^{\frac{t}{m}(\hat{A}_1+\hat{A}_2+...+\hat{A}_n)}, \tag{3.79}$$

and as

$$q = e^{\frac{t}{m}\hat{A}_1}e^{\frac{t}{m}\hat{A}_2}\cdots e^{\frac{t}{m}\hat{A}_n}. \tag{3.80}$$

Next these expressions are constructed for p and q so as to measure the mth order difference between them using the binomial theorem, the triangle inequality, and the Taylor series expansion for the exponential function,

$$||p^m - q^m|| \leq ||p - q|| \left(||p||^{m-1} + ||p||^{m-2}||q|| + \cdots + ||q||^{m-1} \right)$$

$$\leq ||m|| \, e^{\frac{(m-1)|t|}{m}(||\hat{A}_1|| + ||\hat{A}_2|| + \cdots + ||\hat{A}_n||)}. \tag{3.81}$$

A similar line of reasoning gives gives rise to the following inequality,

$$||p - q|| \leq 2 \left(e^{\frac{|t|}{m}(||\hat{A}_1|| + ||\hat{A}_2|| + \cdots + ||\hat{A}_n||)} - \left(1 + \frac{|t|}{m}(||\hat{A}_1|| + ||\hat{A}_2|| + \cdots + ||\hat{A}_n||)\right) \right)$$

$$\leq \left(\frac{|t|}{m}(||\hat{A}_1|| + ||\hat{A}_2|| + \cdots + ||\hat{A}_n||) \right)^2 \left(e^{\frac{|t|}{m}(||\hat{A}_1|| + ||\hat{A}_2|| + \cdots + ||\hat{A}_n||)} \right). \tag{3.82}$$

Consolidating these inequalities down, simplifying, and replacing our expressions for p and q back into the expressions allows for,

$$||e^{t(\hat{A}_1 + \hat{A}_2 + \ldots + \hat{A}_n)} - (e^{\frac{t}{m}\hat{A}_1} e^{\frac{t}{m}\hat{A}_2} \cdots e^{\frac{t}{m}\hat{A}_n})^m|| \leq \frac{|t|^2}{m} \left(\sum_{j=1}^n ||\hat{A}_j|| \right)^2 \left(e^{|t| \sum_{j=1}^n ||\hat{A}_j||} \right), \tag{3.83}$$

which implies both the convergence of the Lie-Trotter theorem in the $\lim_{m \to \infty}$ as well as the first order $O(\frac{1}{m})$ convergence of this primitive form of the theorem.

3.8.3 Advantages of Conserving Hermiticity in the Proof of a Lie-Trotter-Type Theorem

Fortunately, tighter bounds for Lie-Trotter-type theorems may be found when a discretization is made in a way that is mindful to preserve the underlying Hermiticity of the exponential operator. Let us begin by defining the symmetrized product formula,

$$S(t) = e^{\frac{t}{2m}\hat{A}_1} e^{\frac{t}{2m}\hat{A}_2} \cdots e^{\frac{t}{2m}\hat{A}_{n-1}} e^{\frac{t}{m}\hat{A}_n} e^{\frac{t}{2m}\hat{A}_{n-1}} \cdots e^{\frac{t}{2m}\hat{A}_2} e^{\frac{t}{2m}\hat{A}_1}. \tag{3.84}$$

As a teaser, note that this formula has a second order convergence which means that far fewer product terms are required to gain the same level of accuracy as the initial Lie-Trotter formula i.e.,

$$e^{\frac{t}{m}(\hat{A}_1+\hat{A}_2+...+\hat{A}_n)} = S(t) + O(t^2). \tag{3.85}$$

In order to prove this, it is convenient to re-frame $S(t)$ in the form of an exactly equivalent exponential operator function,

$$S(t) = e^{t(\hat{A}_1+\hat{A}_2+...+\hat{A}_n)+t^2 R_2+t^3 R_3+...}, \tag{3.86}$$

where the terms R_j refers to the various commutators that are multiplied by t^j,

$$S(-t) = e^{-t(\hat{A}_1+\hat{A}_2+...+\hat{A}_n)+t^2 R_2-t^3 R_3+...}. \tag{3.87}$$

Taking advantage of the special structure of an approximate symmetrized operator is easy to show that if the parity of t is reversed and the resulting operator multiplied as follows,

$$S(t)S(-t) = S(-t)S(t) = 1, \tag{3.88}$$

so that the identity may be used to argue that even-ordered commutator terms with the exception of 1 must vanish like so,

$$S(t)S(-t) = e^{2(t^2 R_2+t^4 R_2+t^6 R_6+...)} = 1. \tag{3.89}$$

This line of reasoning leads quite naturally to the following argument,

$$e^{t(\hat{A}_1+\hat{A}_2+...+\hat{A}_n)} = \left(S(t/m) + O(t^3/m^3)\right)^m$$

$$= \left(S(t/m)^m + m \cdot O(t^3/m^3)\right)$$

$$= \left(S(t/m)^m + O(t^3/m^2)\right), \tag{3.90}$$

which proves that a symmetrized Lie-Trotter-type product approximation converges to the initial starting exponential operator function as $O(t^3/m^2)$, which is much faster than the primitive Lie-Trotter formula would predict.

3.9 The Effects of Identical Particles in Path Integration

Within quantum mechanics, there are two types of indistinguishable quantum particles, bosons and fermions. When spin is suppressed for clarity, in the wavefunction formalism, this indistinguishability is manifested as,

$$\Phi(X) = \hat{\mathcal{G}}_{F/B}\Psi(X)$$
$$= \frac{1}{N!}\sum_j (\mp 1)^P_{F/B}\hat{P}_j\psi(x_1,\ldots,x_u,\ldots,x_v,\ldots,x_N), \qquad (3.91)$$

where $\Phi(X)$ denotes the total (anti-)symmetrized wavefunction, $\hat{\mathcal{G}}_{F/B}$, the (anti-)symmetrization operator (F and B denoting fermionic or bosonic respectively), and $\Psi(X)$ the multi-particle boltzmannon wavefunction.

The process of (anti-)symmetrization proceeds as follows,

$$\hat{P}_{u\leftrightarrow v}\psi(x_1,\ldots,x_u,\ldots,x_v,\ldots,x_N)$$
$$=\psi(x_1,\ldots,x_v,\ldots,x_u,\ldots,x_N), \qquad (3.92)$$

where the coordinates that define the position of a single particle state and hence its identity in the sense of "being" are permuted with those of another particle, so that their individual existences become blurred and intimately interconnected. In the bosonic case, the exchange of the particle coordinates is always associated with multiplying of the resultant new resultant wavefunction by a 1 so that the new collective wavefunction for an N identical bosonic system is just the average $\Phi(X)_B = \frac{1}{N!}\sum_j (1)^P\hat{P}_j\psi(x_1,\ldots,x_u,\ldots,x_v,\ldots,x_N)$ of the $N!$ permutation resultant wavefunctions.

For fermions, this formula is different. In the fermionic case, the exchange of the particle coordinates is always associated with multiplying of the resultant new resultant wavefunction by a -1 so that the new collective wavefunction for an N identical fermionic system is just the average,

$$\Phi(X)_F = \frac{1}{N!}\sum_j (-1)^P\hat{P}_j\psi(x_1,\ldots,x_u,\ldots,x_v,\ldots,x_N), \qquad (3.93)$$

of the $N!$ permutation resultant wavefunctions.

Within the path integral framework, the necessity of the (anti-)symmetrization process is no different from that of the wavefunction formalism and proceeds in a similar fashion except that in this framework instead of permuting coordinates, one permutes and averages over the permutations of paths so that within

the standard framework a propagator may be expressed as,

$$\langle X_2, t_2 | e^{\frac{it}{\hbar}\hat{H}} | X_1, t_1 \rangle = \frac{1}{N!} \sum_P (\mp 1)^P \rangle \int_{x(t_2}^{\hat{P}x(t_2)} \mathcal{D}[X(t_2)] \mathcal{D}[X(t_1)] e^{\frac{i}{\hbar} \int_0^t dt \frac{m}{2} \dot{x}^2}, \tag{3.94}$$

for a fermionic/bosonic quantum system and as,

$$Z(\beta) = \mathrm{Tr}\left(\langle X | \hat{\mathcal{G}}_{\mathrm{F/B}} e^{-\beta\hat{H}} | X \rangle \right) = \frac{1}{N!} \sum_P (\mp 1)^P \rangle \int_{x(t_2}^{\hat{P}x(t_2)} \mathcal{D}[X(t_2)] \mathcal{D}[X(t_1)] e^{\frac{i}{\hbar} \int_0^\beta d\tau \frac{m}{2} \dot{x}^2}, \tag{3.95}$$

for the partition function $Z(\beta)$ of a fermionic/bosonic quantum statistical mechanical system.

Chapter 4

Path Integral Monte Carlo as a Computational Framework

4.1 Introduction

From a computational standpoint, the imaginary-time path integral provides a robust, arbitrarily exact framework for accurately predicting measurable properties of (nearly) real systems. The ability of path integral methods to attain arbitrary exactness arises from the Lie-Trotter discretization formalism which allows for a discretization error which may be made as small as desired by increasing the number of discretizations. As a result of these properties, these path integral methods have been of considerable interest to the computational physics/chemical physics communities over the past 30-40 years for calculating quantum statistical mechanical quantities. That said there are also considerable drawbacks and open problems within imaginary-time path integration techniques. In particular, sign problems in which the density in question has negative regions which scale with system size bedevil this and other related methodologies for fermionic and magnetic systems and restrict the practical utility of path integral type simulations to static or non-time dependent quantities.

Typically, the mathematical parts and approach to the computational path integral are divided into 3 underlying parts: the action of the path integral, the numerical methodology used to evaluate the path integral, and the estimators used to determine the physical quantities of interest. The action of the approximate path integral in its most basic form is the function associated with $\ln(\rho_{\mathrm{app}}(\mathrm{x}))$, where $\rho_{app}(x)$ is the approximate density matrix. This function dictates a great deal about how numerical methodology will be applied to $\rho_{app}(x)$. For instance, the harmonic spring-like structure associated with the kinetic energy term suggests a natural isomorphism between the thermal density matrix and a ring-polymer, an observation which has inspired many connections between these quantum simulations and their coarse-grained soft matter polymer counterparts [69, 70].

Selecting a numerical methodology for evaluating the expectation values associated with the thermal density matrix can be both the easiest and most difficult decision made for the numerical evaluation of the path integral. It is easy in the sense that the high-dimensional nature of the computational path integral

necessitates the usage of Monte Carlo integration or molecular dynamics since these methods are more or less the only practical ones available for integrating such a high-dimensional integrand. However, choosing from among the available Monte Carlo methodologies can be challenging as it is important to find a Monte Carlo methodology which achieves ergodicity relatively quickly, while minimizing the amount of work required to perform the samples in question, while minimizing the correlation between samples as much as possible.

Often the selection of an appropriate methodology is highly dependent upon the underlying probability distribution to be sampled from as well as the information available to define that distribution. Within the context of path integration, a standard approach for the sampling algorithm is the bisection method, which successively constructs a Brownian bridge in a hierarchical fashion such that the coarsest levels are constructed and accepted or rejected first and then the lower levels are constructed and rejected or accepted down to the lowest level. This is a highly successful method as it both samples the kinetic energy terms of boltzmannon particles exactly and has the capacity to reject unlikely samples at a high level and thus avoid performing the unnecessary computations associated with the lower levels of the Brownian paths.

Estimators are the functions evaluated using the time series generated by the simulation to estimate the values of the associated expectation values of interest. In many cases, they are fairly straightforward to derive.This is particularly true for expectation values which are diagonal in the underlying basis set of the density matrix i.e. they are easily expressible in terms of the coordinates of the simulated density matrix.

The derivation of estimators becomes more challenging, however, when the underlying quantities of interest are not diagonal in the basis set of the path integral simulation. This is particularly true for thermodynamic quantities such as the average energy of a system, its heat capacity, its entropy, or most seriously its free energy. Free energy calculations comprise an entire subfield of computational methods unto themselves. In this thesis, the only off-diagonal estimators that will be considered are estimators used to assess the average energy of the quantum system under investigation.

Finally, quantum mechanics requires that the computational practitioner pay attention not only to the direct simulation of the path integral, but to the boundary conditions which arise from the underlying quantum statistics as well. In the final section of this chapter, a brief review of bosonic sampling methods for path integrals will be given. This review will then directly lead into the related and still very challenging methodology associated fermionic path integral systems. In particular, the sampling strategy of Takahashi and Imada [71] for one-dimensional systems will be reviewed and finally, the fixed node fermionic PIMC sampling method due to Ceperley [72–74], which is used in this thesis, will be reviewed.

4.2 The Practical Consequences of the Structure of the Path Integral

First, recall the underlying approximate form of the imaginary-time path integral or thermal density matrix

$$Z(\beta) \approx \left(\frac{m}{2\pi\beta}\right)^{\frac{dM}{2}} \int dx^M \prod_{j=0}^{M-1} e^{-\frac{mM(x^{(j+1)}-x^{(j)})^2}{2\beta}} e^{-\frac{\beta}{M}V(\{x^{(j)}\})} \tag{4.1}$$

where eqn. (4.1) defines a path integral for a one-dimensional single particle systems, d is the dimensionality, m is the mass of the particle, M is the number of slices, and the $x^{(j)}$ variables define the position coordinates of the jth slice. As has already been argued and demonstrated in the preceding chapter, arbitrarily increasing the number of slices, M, yields a high-dimensional integral that becomes an asymptotically better approximation as $O(\frac{1}{M^2})$ to the thermal density matrix.

After a visual inspection of the argument in the exponential present in eqn. (4.1)'s integrand and some thought, it is apparent that the path integral may be considered as being like the simulation of a ring polymer, where each of the comprising monomers of that polymer are subject to the external potential given by $V(\{x^{(j)}\})$. While at first thought this description may seem like a pleasant if not terribly important, this isomorphism may is, in fact, quite useful as it suggests physical consequences for the underlying wave-like nature of the particles being studied.

In effect, the dimensionlessness of a quantum point particle is replaced by a ring polymer or necklace like object which describes the extent of the quantum delocalization of that particle due to its wave-like nature of the ring polymer standing in for that quantum particle's thermal wavelength. This description results is a unique situation for the practitioner of quantum mechanics as it is unusual in the field to get a classical-like object which describes a quantum system in way that it accessible to intuition.

Because this ring polymer is a classical-like object, it has been studied extensively using the techniques and tools of both classical mechanics and classical statistical mechanics. In particular, the development of a quantitative and qualitative understanding of the extent of the delocalization of the quantum particle as a function of temperature has been of great interest to practitioners of the art. To this effect various means to describe this phenomena although only the most basic will be presented here and follows the presentation in [62].

Among the most obvious quantities to calculate to describe the motion of a ring polymer is its radius of gyration which is defined as follows

$$R_g = \frac{1}{M}\sum_{j=1}^{M}(x_j - \overline{x})^2 \tag{4.2}$$

where the mean position of a monomer $\bar{x}$ is calculated as

$$\bar{x} = \frac{1}{M} \sum_{j=1}^{M} x_j. \tag{4.3}$$

R_g may be physically interpreted in the standard mechanical fashion such that as R_g gets larger the average amount of space occupied by the ring polymer grows and hence the quantum particle is more delocalized. As R_g gets smaller, the ring polymer begins to collapse in upon itself and thus turn into a classical-like particle where quantum effects are minimal. The free particle case in the infinite slice limit $M \to \infty$ may be calculated exactly as

$$R_g = \frac{\beta \hbar^2}{12m} = \frac{\pi}{6} \lambda^2 \tag{4.4}$$

where λ is the thermal wavelength of the quantum system [62].

Having an exact result allows for a more detailed analysis of the underlying system as a function of temperature. Clearly, as $\beta \to 0$ or conversely $m \to \infty$, $R_g \to 0$, the particle described the ring polymer becomes more classical as expected since its thermal wavelength, λ, which can be thought of as a stand-in for its quantum nature, goes to 0. This analysis becomes far more difficult in the presence of a potential as this term acts as a limit on how far the polymer may spread and is dependent upon temperature in a complex way.

If one neglects the classical entropic term of the ring polymer one may derive the following heuristic for the number of slices to be used in a simulation. In essence, since there are two opposing forces present in a ring polymer in a potential: the potential itself which will tend to attract beads to its lower energy wells and the harmonic oscillator chain of the ring polymer itself which causes the polymer to tend to contract upon itself. A ring polymer is in equilibrium when the average value of these two competing forces are balanced. Consequently, this line of reasoning may be used to estimate about how many beads are necessary for simulating a given system. If too few beads or slices are used, the ring polymer will tend towards the classical limit since the harmonic chain connecting the beads will be too strong to allow the necklace to fully feel the effects of the external potential. However, if more beads than are necessary for a given level of desired accuracy are added to the ring polymer then the sampling of the finer details of the potential which those beads allow are completely unnecessary. Thus, in order to have the most important simulation possible, it is important to consider the trade-offs between slice number and desired accuracy. A general rule of thumb has been derived to give a convenient lower bound for these issues and may be summarized as follows,

$$M >> \frac{\beta \hbar^2}{m\ell}, \tag{4.5}$$

where ℓ is the length scale of the potential of interest. This result suggests that to get a simulation of reasonable accuracy the number of slices ought to be much larger than $\frac{\beta\hbar^2}{m\ell}$. While this rule of thumb ignores issues like bosonic and fermionic exchange as well a effects due to intermolecular potentials, it, nonetheless, is a good starting heuristic, so that the practitioner is not blindly guessing his/her slice number M.

4.3 Path Integral Actions

Path integral actions are defined as,

$$\ln(\rho_{\mathrm{app}}(\mathrm{x})), \tag{4.6}$$

where $\rho_{app}(x)$ is the approximate density matrix. A simple action for the Lie-Trotter expression where the split operators are the kinetic energy operator and the potential energy operator may be given succinctly as

$$\mathcal{S}(T) = \mathcal{S}(K) + \mathcal{S}(V) \tag{4.7}$$

where

$$\mathcal{S}(K) = ln\left(\frac{m}{2\pi\beta}\right)^{\frac{dM}{2}} - \sum_{j=0}^{M-1} \frac{mM(x^{(j+1)} - x^{(j)})^2}{2\beta} \tag{4.8}$$

and

$$\mathcal{S}(V) = -\frac{\beta}{M} \sum_{j=0}^{M-1} V(x^{(j)}) \tag{4.9}$$

which has been chosen since the study of more exotic actions, excepting fermionic permutation effects, are not used.

4.3.1 Pair-Product Action and Propagator

While the study of alternative actions is major area of methodological research within the PIMC community, typically with the intent to devise an approximate path integral which converges faster with fewer time slices or has some other computationally convenient property, perhaps the most venerable and certainly the most used of these alternant actions is the pair-product approximation. In this discretization a pair-wise interacting potential given by,

$$V(R) = \sum_{i<j} v(r_i - r_j), \tag{4.10}$$

73

is integrated as the potential term of the Feynman-Kacs path integral. As related in [75], the integrated pair energy along a random walk is give as,

$$x_{ij} = e^{-\int_0^\tau dt\, v(r_{ij}(t))}, \tag{4.11}$$

where $r_{ij}(t)$ is the random walk variable which describes the interaction between particles i and j. This means that x_{ij} may be interpreted itself as a random variable drawn from some distribution described by the Feynman-Kac formula for a pair interaction. The x_{ij} may then be used to describe the exact Feynman-Kac formula for the potential given by eqn. (5.1) as,

$$e^{-\beta U} = \langle \prod_{i<j} x_{ij} \rangle, \tag{4.12}$$

which is the pair interaction potential part of the imaginary-time Feynman propagator.

Using this result it is not difficult to make a qualitative argument for why the pair-product propagator is an effective approximation for the path integral: While all particles do interact the vast majority of the interactions may be considered to be dominated by a single pairwise interaction for each particle which means that each of the individual x_{ij} may be assumed to be statistically independent of each other, which is an excellent assumption in low density regimes where 3-body, 4-body, and n-body interactions are extremely rare events. Thus, the approximation becomes

$$e^{-\beta U} \approx \prod_{i<j} \langle x_{ij} \rangle, \tag{4.13}$$

which means that the pairwise potential given by eqn (5.1) may be replaced with the individual pairwise actions of the system with negligible consequence. Moreover, because this approximation amounts to little more than a slight alteration of the operator-splitting the Hamiltonian in the sense of the Lie-Trotter-Suzuki theorem one maintains the exact approximability of the path integral.

This leaves the question of how one actually calculates the pair product approximation. In most applications, one takes advantage of the interaction typically being that of a central potential and uses the squaring framework of Klemm and Storer [75, 76] to numerically determine the action of the pair-interaction system. In this thesis, however, this numerical framework will not be used and instead an exact pair interaction pair propagator and action will be derived in a subsequent chapter.

4.4 Introduction to Monte Carlo Methods

In numerical analysis, Monte Carlo methods comprise approaches to numerical problems which seek to take advantage of random phenomena and produce answers to those numerical problems within some statistical error. The easiest form of Monte Carlo method to understand is typically considered to be naive Monte Carlo integration. In this naive approach, the goal is to numerically evaluate the following integral

$$I = \int_0^1 \cdots \int_0^1 dx^N f(x). \tag{4.14}$$

If a random vector X_j is drawn from the N-dimensional unit probability measure defined by dx^N then the test integral may be evaluated as

$$I \approx \frac{1}{M} \sum_{j=1}^M f(X_j), \tag{4.15}$$

such that the standard deviation is calculated as

$$\sigma = \sqrt{\frac{1}{M-1} \sum_{j=1}^M (f_j - \langle f \rangle)^2} = \sqrt{\frac{\langle f^2 \rangle - \langle f \rangle^2}{M-1}} \tag{4.16}$$

and which is used as the standard error for Monte Carlo methods. Thus, an integral integrated in the fashion described may be written as

$$\mathcal{A}(I) = I_{Ans} \pm \sigma, \tag{4.17}$$

so that each mean evaluated as in eqn.(4.15) has statistical error bars defined by the standard deviation as $\pm \sigma$.

So far, Monte Carlo numerical integration has been considered as sampling from a uniform probability density, $\mu(dx)$. While theoretically, this method is an extremely agreeable one as it is easy analyze and its quality of convergence depends only upon the quality of the underlying pseudorandom points, in practice, it is very slow to converge as most points sampled from it are in areas that don't contribute much to the hypervolume of the multivariate integrand under consideration. Consequently, it is of great importance to sample from a distribution that closely mirrors the integrand under consideration. For all but the simplest distributions such as the Gaussian distribution, this sampling is easier said than done.

Consequently, instead of directly drawing random samples from a given distribution, a Markov chain model is setup to simulate an arbitrary distribution. Developing this methodology was the groundbreaking work of Metropolis et. al. [77] for statistical mechanical partition functions and arbitrary probability distributions. Hastings [78] generalized the arguments concerning the construction of the underlying Markov

chains to more general cases than those considered by Metropolis et. al. Before continuing, it is important to consider just what exactly are the consequences of such a simulation and how it changes the integrand of interest. In particular, if $X_j \in \mu(\rho(x)dx)$ then

$$I_{app} = \frac{1}{N} \sum_{j=1}^{N} f(X_j) \approx \frac{\int f(x)\mu(\rho(x)dx)}{\int \mu(\rho(x)dx)} \tag{4.18}$$

so that if X_j are drawn from such a distribution $\mu(\rho(x)dx)$ then the resulting integrand is normalized by the normalization constant associatied with that same distribution.

To simulate such a distribution, a Markov chain system is implemented so in the infinite limit it reaches equilibrium and thus any transition, forward or backward, between two states denoted by s and s' are of equal likelihood,

$$\pi(s)T(s \rightarrow s')A(s \rightarrow s') = \pi(s')T(s' \rightarrow s)A(s' \rightarrow s). \tag{4.19}$$

To explain, in this simulation $\pi(s)$ is the probability integrand of interest in state s and associated with $\rho(x)$ in eqn. (4.18), $T(s \rightarrow s')$ is the transition probability associated with the probability distribution the random number from which the transition probability is drawn. In this thesis, it will be a Gaussian probability distribution with an appropriate variance as needed for all presented formulas. Finally the acceptance probability, $A(s \rightarrow s')$, is the probability associated with the acceptance of the suggested move. Re-arranging the previous equation yields the more manageable expression,

$$A(s \rightarrow s') = min \left[1, \frac{\pi(s')T(s' \rightarrow s)}{\pi(s)T(s \rightarrow s')} \right], \tag{4.20}$$

where the given expression is accepted if a random number drawn from a uniform probability distribution is less than the quantity defined as above. Running this algorithm for a sufficiently long time, which may be analyzed using autocorrelation methods, yields an ergodic behavior of the states throughout a given probability state space and thus guarantees after a sufficiently long run which may be gauged using autocorrelation functions for the states involved that the expected probability distribution is being drawn from.

4.5 Monte Carlo Methods Specialized to the Path Integral

4.5.1 Metropolis Monte Carlo PIMC: Bead-by-Bead Sampling

Bead-by-bead sampling performs Metropolis importance sampling on the thermal density matrix given by eqn. (4.1) whereby for each Monte Carlo step a single variable is displaced and either accepted or rejected in an attempt to sample from the following distribution,

$$\mu(x) = \frac{1}{Z(\beta)} \prod_{j=0}^{M-1} e^{-\frac{mM(x^{(j+1)} - x^{(j)})^2}{2\beta}} e^{-\frac{\beta}{M} V(\{x^{(j)}\})}. \tag{4.21}$$

In essence, this method samples a ring polymer in the fashion after Metropolis et. al. Unfortunately, it is quite slow to converge and in fact has an autocorrelation time which diverges quadratically as a function of the number of polymer beads which effectively limits the applicability of this method to very small necklaces. A greater overview of this topic will be be given in the following subsection.

4.5.2 Bisection Sampling

Bisection Sampling Overview and Background

The critical slowdown of associated with the Metropolis algorithm has been recognized as a problem for PIMC since at least the 1980's. This slowdown occurs because moving a path integral simulation a single bead at a time is an incredibly slow way for the ring polymer to diffuse through path space in its totality. In effect, this slowdown prevents Metropolis-type sampling from being applicable to approximate path integrals for systems larger than a single quantum particle depending upon underlying potential. As a consequence of the rather early recognition of this problems, a great deal of work on this problem was performed in this field from approximately the mid-1980's to mid-1990's at which time Ceperley's bisection algorithm [75] became the gold standard for the field, and arguably, has yet to be superseded. Nonetheless, it is important to give context and a brief description of other methods in this field before describing the inspiration and derivation of the bisection algorithm.

Among the major efforts in path integrals not discussed extensively in this thesis, but which require mentioning are path integral molecular dynamics techniques. These methods actively seek to simulate the path integral ring polymer as a real polymer under the confines of the simulated potential. While a direct application of the molecular dynamics methods go back to the early 1980's with the work of Chandler and Wolynes [79]. More modern and efficient approaches based upon the movement of the centroid of ring polymer (CMD) are due to Voth and his co-workers [80–82]. These methods have even been extended into

real-time situations using a heuristic formalism begun by Craig and Manolopoulos [83–86] and extended and reviewed by Miller, Markland, and Habershon [87]. Other methods such as the W-cycle multgrid method have attempted to model the diffusion of the path integrals' ring polymers using methods from numerical stochastic differential equations [88]. And still others, have attempted to model the paths being summed over using the Fourier path decomposition approach originally developed by Feynman, but since generalized to wavelet methods by Doll et. al [60, 89]. These methods have been fully generalized by Bond et. al. to describe the full decomposition of path spaces in a non-basis set dependent way.

As has already been alluded to in the introduction to this chapter, the bisection method is widely regarded as the best importance sampling method for PIMC. The essential goal of the bisection method is to improve upon the quadratic divergence with slice and particle number of the Metropolis algorithm's autocorrelation times for the Lie-Trotter path integral by sampling larger sections of the polymer ring and updating more variables per accepted move. That the critical slowdown of the Metropolis algorithm has been recognized as a problem for PIMC since at least the 1980's is not in doubt.

Due to the recognition of this problem, the first steps towards constructing a workable solution were taken by Sprik, Klein, and Chandler [90] in developing the staging algorithm, an approach that contains many of the seeds of the bisection method, although it lacks that the bisection method's polish. In the staging method, among the key concerns addressed by the staging method was the inefficiency of only moving a single variable per move of the Monte Carlo Markov chain as in the Metropolis algorithm. The method operates by first performing a variable change upon the segment of the path integral targeted for movement, so that the kinetic energy terms become uncoupled harmonic oscillators. Next these uncoupled oscillators are sampled exactly and the relevant potential terms evaluated and Metropolis-type acceptance/rejection methods are applied to the move. If the movements are accepted the ring polymers positions are updated, the estimators evaluated and recorded and the process repeated.

While the staging algorithm is able to move many particles at once, it is somewhat difficult to implement due to the consequences of the required coordinate change and moreover, it wastes a lot of effort calculating many variable changes that will ultimately be rejected. Consequently, a method which is able to avoid these unnecessary movements while retaining the efficiency of the multivariable movement as the exact sampling of kinetic energy term was highly desirable by the late 1980's. The bisection sampling algorithm addresses all of these concerns and has arguably not been improved upon since its publication.

The bisection sampling algorithm was developed by David Ceperley at the University of Illinois at Urbana-Champaign in 1994 [75] and its derivation begins by recognizing that the multivariate kinetic energy term, the free particle action, is both easy to sample and applicable at coarser or higher levels of an approximate

density matrix due to the semigroup nature of an exact propagator. Typically, there are two equivalent ways to approach the derivation of this algorithm which while similar give insight to the various modes of thought taken by practitioners when constructing these sorts of methods: The first is to view this algorithm as approximating the propagator via a hierarchy of levels such that a finer and finer level to the approximation is derived with algorithm stopping and moving onto to another configuration if any of those levels are rejected. The second approach is to view this method as creating a Levy construction of a Brownian path which, while similar to the first viewpoint, potentially opens up other mathematical possibilities for improving the method. In this method, the Brownian path is taken by the free particle is successively bisected so that the details of the free particle path is successively calculated. The potential term then enters consideration as the perturbation to the Brownian path such that these proposed paths are "pinned" by this potential and either accepted or rejected according to the standard Metropolis Monte Carlo acceptance function framework.

An astute reader may be wondering what makes this method so powerful. In truth it is the accretion of little things in a computationally efficient structure that makes this method appealing. First and foremost, like the staging algorithm, it is able to move large sections of the ring polymer chain at a time. Unlike the staging method, however, this is accomplished while minimizing the actual amount of computation necessary to complete the task. Specifically, only Gaussian random variables are required, which are easy and fast to compute using the Box-Mueller algorithm and any number of standard random number generators. This leaves only the potential function as the difficult or computationally intensive function that needs to be calculated and the number of computations of this difficult potential function is minimized by accepting or rejecting the proposed moves in a hierarchical fashion so that only the most likely paths ever need to be fully calculated.

Bisection Sampling Implementation

After giving the rationale for the bisection method in the preceding sub-subsection, this sub-subsection presents the actual derivation/implementation of the bisection method. It's equation flow will closely follow the presentation given by K. Esler's thesis [61] as it is the opinion of the author that this presentation is difficult to improve upon in terms of clarity of explanation. The construction and implementation of the bisection method begins by randomly selecting a $N = 2^L + 1$-slice segment of the path integral density where L describes the numbers level of the bisection method and then exactly samples from the level of the moment's kinetic energy term and rejects or accepts that sample based on acceptance function for that level. The transition to the next finer level begins by taking advantage of the semigroup property of the kinetic energy propagator so that the acceptance function can be considered as only a ratio of the potential energy

terms.

To calculate the transition probability of the forward and reverse moves respectively, the following expressions are considered which defines the transition of a free particle from a 3-slice segment of a kinetic energy defined by the collective coordinate variables r_0, r_1, and r_2 with $\bar{r} \equiv \frac{1}{2}(r_0 + r_2)$,

$$T(r_1 \to r_1') = (2\pi\sigma)^{-\frac{3}{2}} e^{-\frac{(r_1'-)^2}{2\sigma^2}}, \tag{4.22}$$

and

$$T(r_1' \to r_1) = (2\pi\sigma)^{-\frac{3}{2}} e^{-\frac{(r_1-\bar{r})^2}{2\sigma^2}}. \tag{4.23}$$

The forward transition can then be sampled using any standard library Gaussian random variable routine with the mean $\bar{r}$ and the variance σ^2 to find the new variable r_1'. The decision to accept or reject this new variable may then be described via the acceptance function,

$$A(r_1 \to r_1') = min\left[1,\ R(r_1, r_1')\right], \tag{4.24}$$

- where $R(r_1, r_1')$ is described using the Markov Chain transition probability equation,

$$\pi(r_1)T(r_1 \to r_1')A(r_1 \to r_1') = \pi(r_1')T(r_1' \to r_1)r_1(s' \to r_1), \tag{4.25}$$

so that when rearranged the preceding expression yields,

$$R(r_1, r_1') = \frac{\pi(r_1')T(r_1' \to r_1)}{\pi(r_1)T(r_1 \to r_1')}. \tag{4.26}$$

Working out $R(r_1, r_1')$ for a single level of the bisection method yields,

$$R(r_1, r_1') = \frac{T(r_1' \to r_1)}{T(r_1 \to r_1')} e^{-\Delta(\mathcal{KE})} e^{-\Delta(\mathcal{V})}$$

$$= \frac{e^{-\frac{(r_1-\bar{r})^2}{2\sigma^2}} e^{-\frac{M(r_1'-\bar{r})^2}{2\lambda\beta}}}{e^{-\frac{(r_1'-\bar{r})^2}{2\sigma^2}} e^{-\frac{M(r_1-\bar{r})^2}{2\lambda\beta}}} e^{-\Delta(\mathcal{V})}, \tag{4.27}$$

where the $\Delta(\mathcal{KE})$ is defined as

$$
\begin{aligned}
\Delta(\mathcal{KE}) &= [(r_1' - r_0)^2 + (r_1' - r_2)^2 - (r_1 - r_0)^2 - (r_1 - r_2)^2] \\
&= [(r_1')^2 - 2r_1' \cdot \bar{r} - (r_1^2 - r_1 \cdot \bar{r})] \\
&= [(r_1' - \bar{r})^2 + (r_1 - \bar{r})^2]
\end{aligned}
\tag{4.28}
$$

and

$$
\sigma^2 = 2^L \lambda \frac{\beta}{M}.
\tag{4.29}
$$

The acceptance function is then applied to each level of the bisected path integral for the reasons given in the preceding sub-subsection.

4.5.3 The Displace Move

While the bisection sampling method is very effective for importance sampling along a contiguous stretch of time slices, its relatively low acceptance ratio for large numbers of slices prevents the ring polymer of the path integral from diffusing effectively through space [75]. Consequently, a rigid displacement movement is often beneficial. In this displacement move, the ring polymer is translated in its entirety with a single random, rigid movement defined by a random vector. To define this rigid movement, a random vector with a Gaussian distribution is drawn with a σ chosen to ensure a sufficiently high/low acceptance rate. The thesis of Ken Esler [61] recommends an acceptance rate of 0.2.

4.6 Estimators

Estimators are essential for performing a PIMC calculation as they computationally define the quantities to be measured. They are the functions evaluated and averaged over for the probability distribution of the approximate thermal density matrix to estimate the expectation value of a Monte Carlo-type simulation. While in many simulations, it is quite easy to express the quantity of interest in terms of the chosen basis of the simulation, which is typically the position basis for PIMC. Nonetheless, many quantities, such as the total energy of the system under investigation, are not well expressed by the basis set used to represent the approximate thermal density matrix.

4.7 Estimators Diagonal in the Underlying Basis Set

4.7.1 Standard Diagonal Estimators

Before showing how a diagonal estimator is applied, first a brief review of the expression for expectation value,

$$\langle A \rangle = \frac{1}{Z(\beta)} Tr(\hat{A}\rho) = \frac{\int dx\, \langle x|\hat{A}\rho|x\rangle}{Z(\beta)}, \tag{4.30}$$

where ρ is the Boltzmann operator or the approximate Boltzmann operator. If the expectation value's operator $\hat{A}$ is diagonal in the basis set x then the preceding equation may be expressed as

$$\langle A \rangle = \frac{1}{Z(\beta)} Tr(\hat{A}\rho) = \frac{\int dx\, A(x)\rho(x)}{Z(\beta)}. \tag{4.31}$$

where $A(x)$ and hence the estimator in question is just a function of the basis set x.

4.7.2 Pair Correlation Functions

Pair correlation functions are used to describe the probability as a function of distance of two particles. In effect, they may be used to calculate the average spherically symmetric structure around a given particle type and thus may be used to describe pairing interactions as well as the shell-like structures which appear in liquid systems. The pair correlation function is defined as follows [36],

$$g_{\alpha,\gamma}(r_1, r_2) = \frac{1}{n_\alpha(r_1)n_\gamma(r_2)}\langle \sum_{i\in\alpha, j\in\gamma} \delta(r_i - r_1)\delta(r_j - r_2)\rangle, \tag{4.32}$$

where α and γ are used to describe the different species of interest and $n_\alpha(r_1)$ and $n_\gamma(r_2)$ describe the particle densities of their respective species.

For a periodic system or conversely a unit cell of a bulk, homogeneous system a translationally invariant form may derived which is given as

$$g_{\alpha,\gamma}(r) = \frac{1}{n_\alpha n_\gamma}\langle \sum_{i\in\alpha, j\in\gamma} \delta(r_i - r_j - r)\rangle. \tag{4.33}$$

This form yields a much simpler protocol for calculation since one needs to only to create a binned histogram of the interparticle distances and then normalize with the particle number of the given species n_α and n_γ to give the pair correlation or in this case, radial distribution function.

4.8 Off-Diagonal Estimators or Estimators Not Diagonal in the Underlying Basis Set

For estimators not diagonal in the underlying basis set, the situation is quite different as a means must be found to indirectly find functions that may act as their estimators in a non-diagonal basis set (It will be presumed in the following discussion that the position coordinates are the diagonal basis set of the system under study). Often it is the case that these non-diagonal estimators are for fundamental thermodynamic quantities such as total and kinetic energy or in the most complicated of cases free energy. In these cases there are generally two approaches available.

4.8.1 Energy

For total energy, it may be expressed in terms of an operation upon auxiliary variable in this case the inverse temperature, β, so that

$$\langle E \rangle = -\frac{\partial ln(Z)}{\partial \beta} = -\frac{1}{Z}\frac{\partial Z}{\partial \beta} \tag{4.34}$$

and the estimator becomes,

$$\langle E \rangle \approx \frac{1}{M}\sum_{i=1}^{M} -\frac{\partial \rho(X_i)_{App}}{\partial \beta}, \; X_i \in \frac{\rho(X_i)_{App}}{Z}, \tag{4.35}$$

where $Z \approx \int dX \rho(X)_{App}$.

When these operations are applied to the actual path integral formalism, the resultant estimator may vary quite widely depending upon the precise condition of the variable coordinates in use when the derivative with respect to β is applied. The classical, primitive estimator [69] is given by the following

$$\langle E \rangle_T = \frac{1}{M}\langle\sum_{i=1}^{M}\left(\frac{dN}{2\tau} - \frac{(X_i - X_{i-1})^2}{4\lambda\tau^2} + \frac{dU^i}{d\tau}\right)\rangle. \tag{4.36}$$

If one associates the mass derivative of the partition function with the kinetic energy estimator, one derives the following,

$$\langle K \rangle_T = \frac{m}{\beta Z}\frac{\partial Z}{\partial m} = \frac{1}{M}\langle\sum_{i=1}^{M}\left(\frac{dN}{2\tau} - \frac{(X_i - X_{i-1})^2}{4\lambda\tau^2}\right)\rangle. \tag{4.37}$$

And, thus finds that the average potential energy may described as,

$$\langle E \rangle_T - \langle K \rangle_T = \langle V \rangle_T = \frac{1}{M}\langle\sum_{i=1}^{M}\left(\frac{dU^i}{d\tau}\right)\rangle. \tag{4.38}$$

While this primitive derivation is relatively straightforward, it was the subject of considerable concern in the 1980's because of its perceived computational inefficiency which arises from the subtraction in the kinetic and total energy terms upon the variance of the estimator which makes the variance of the estimator decay as $O(\tau^{-1})$ as opposed to the preferable convergence $O(\tau^{-2})$ seen in the approximate density matrix [75,91–95].

Within the literature, there is a slight divergence between the condensed matter and chemical physics/physical chemistry communities in terms of what is termed a virial estimator [75,93–96]. Within the chemistry community, the virial estimator is typically refers to an estimator that is applied to all space and is derived by using a variable substitution [91–93,95,97] and scaling argument whereas within the physics literature the boundary conditions are more general but typically assumed to be periodic boundary conditions unless otherwise stated and derived using both the early work of Berne et. al. [91] and later conditions detailed in by Ceperley [75,94]

Beginning with the chemist's interpretation of the virial estimator, recall that the basic functional form of the approximate path integral is given by,

$$Z(\beta) \approx \left(\frac{m}{2\pi\beta}\right)^{\frac{dM}{2}} \int dx^M \prod_{j=0}^{M-1} e^{-\frac{mM(x^{(j+1)}-x^{(j)})^2}{2\beta}} e^{-\frac{\beta}{M}V(\{x^{(j)}\})}. \tag{4.39}$$

Now, allowing that $x^{(j)}$ may be substituted as $x^{(j)} \to q^{(j)}\sqrt{(\beta)}$, applying the definition given in eqn. (4.38), and then backsubstituting $q^{(j)}\sqrt{(\beta)} \to x^{(j)}$ yields the estimator,

$$\langle E \rangle_T = \frac{1}{M}\langle \sum_{i=1}^{M} \frac{dU^i}{d\tau} + \frac{R_i}{2} \cdot \frac{\partial^2 U^i}{\partial\tau\partial R_i}\rangle. \tag{4.40}$$

The physicists' version of the virial estimator which is subject to periodic boundary requires a more detailed derivation given explicityly in [75]. It may be succinctly stated as,

$$\langle E \rangle_T = \frac{1}{M}\langle \frac{3N}{2L\tau} - \frac{1}{4L\tau^2\lambda}(R_{L+i} - R_i)(R_{i+1} - R_i) + \frac{\partial U^i}{\partial\tau} + \frac{\nabla_i(U^{i+1} + U^i)}{4L\tau} \sum_{j=-L+1}^{L-1}\rangle. \tag{4.41}$$

4.8.2 Specific Heat

Heat capacity or specific heat at a constant volume,

$$C_v = \langle \frac{\partial E}{\partial T}\rangle|_\Omega = -\beta^2 \frac{\partial E}{\partial\beta}|_\Omega, \tag{4.42}$$

which measures the change of the energy containment as function, may be approached in a similar fashion. As for its parent estimator, energy, it may be derived in the fashion of a straight forward application of eqn.

(4.42) to an approximate density matrix or it may derived using a virial type transformation. That said, it is perhaps easiest and most effective to construct it as a fluctuation estimator as

$$C_v = \beta^2 \langle (\mathcal{H} - \bar{E})^2 \rangle \tag{4.43}$$

$$= \beta^2 \langle (E_{i,i+L} - \bar{E})(E_{j,j+K} - \bar{E}) \rangle, \tag{4.44}$$

where the preceding equation has been derived by taking the τ derivative at 2 different time slices and the $E_{i,i+L}$ notation refers to the energy calculated using a preceding energy estimator for time slices from i to $i + L$. Typically one performs many such calculations with varying intervals and then averages over them to get a final estimate.

4.8.3 Free Energy

In the case of free energy the situation is considerably more complex, and is often regarded as an almost entirely different area of study with its own techniques and jargon. Nonetheless, it is approachable within the computational path integral framework as well using methods known in the statistics community as Ogata's method [98] and within the computational chemistry and physics communities as thermodynamic integration [99].

While the introduction of this method to this thesis would be too long of detour, in essence, this method work by multiplying the integration variables of the probability density of interest by a dummy parameter and taking a derivative with respect to that parameter and then integrating over that parameter while sampling from the probability distribution of interest. The resultant estimator yields $ln(Z(\beta))$ which can be used to calculate the normalizing constant $Z(\beta)$ as well as the free energy $-\frac{1}{\beta}ln(Z(\beta))$.

Given the direct challenges typically associated with the calculation of the free energy a simplified estimate may be made for it using only information gleaned from the $\langle E(\beta) \rangle$. Using the thermodynamic relationship $\langle E(\beta) \rangle = \frac{\partial \beta F}{\partial \beta}$ as well as a quadrature procedure, the free energy may be calculated using the relation,

$$\beta_2 F(\beta_2) - \beta_1 F(\beta_1) = \int_{\beta_1}^{\beta_2} d\beta E(\beta), \tag{4.45}$$

which allows the calculation of the free energy at arbitrary temperatures since $F(T \to 0) \to E(T = 0)$.

4.8.4 Pressure

The pressure estimator like estimators for total energy and heat capacity has both a standard and virial form. The definition of pressure is defined by the statistical mechanical relationship as,

$$P = \frac{1}{\beta Z}\frac{\partial Z}{\partial \Omega}|_\beta. \tag{4.46}$$

When this relation is applied to the approximate density matrix this results in the following

$$P = \frac{1}{3\tau\Omega}\langle 3N - \frac{(R_i - R_{i-1})^2}{2\lambda\tau} - 2R_i\nabla_i U\rangle \tag{4.47}$$

which is averaged over the path variables. When the virial theorem is applied to a pair potential, the pressure estimator may be expressed as,

$$P = \frac{1}{3\Omega}\langle 2K - \sum_{i<j} r_{ij}\frac{\partial v(r_{ij})}{\partial r}\rangle, \tag{4.48}$$

where K is the estimator for the kinetic energy. The order of convergence as well as the statistical error will necessarily depend upon the choice of kinetic energy estimator used in the preceding expression.

4.8.5 Superfluid Density

Following [75, 100], the superfluid density, ρ_s of an N-particle system may be cursorily defined as the linear superfluidic response to a rotation via a fractional density term. From more detailed and experimentally oriented view it may be considered from the following thought experiment [100]: Consider a system enclosed and rotating with an angular frequency, ω, between two cylindrical shells. The internal shell has a radius of R; the external shell has a radius of $R + d$. If $d/R << 1$, the system may be considered to be in box defined by two planes with a depth of d and periodic in a single direction moving at that same direction at a velocity $v = \omega R$. The density operator, $\rho' = e^{-\beta H'}$, where

$$H' = \sum_i \frac{(p_i - m\mathbf{v})^2}{2m} + V, \tag{4.49}$$

for this system in the rest frame can then be used to calculate the superfluid fraction. Returning to the lab frame, which may be done because the $m\mathbf{v}$ term in eqn. (4.49) amounts to nothing more than a scalar operator, allows $\rho' = \rho_v$.

The response of the system to the moving boundary may then be captured by the normal component of

the fluid as

$$\frac{\rho_N}{\rho} N m \mathbf{v} = \langle \mathbf{P_v} \rangle = \frac{\mathbf{Tr}[\mathbf{P}\rho_{\mathbf{v}}]}{\mathbf{Tr}[\rho_{\mathbf{v}}]}$$

$$= \frac{\partial}{\beta \partial \mathbf{v}} \ln(Tr[\rho_v]) + N m \mathbf{v}$$

$$= -\frac{\partial F_v}{\partial \mathbf{v}} + N m \mathbf{v}, \tag{4.50}$$

where F_v is the free energy of the system defined by eqn. (4.49). Ultimately, eqn. (4.50) may be expressed in terms of the superfluid fraction [100] as,

$$\frac{\rho_S}{\rho} = \frac{\partial(F_v/N)}{\partial(mv^2/2)}, \tag{4.51}$$

which is arrived at by considering that the superfluid density is that fraction of the density of the fluid that does not rotate or couple via friction with the cylinder.

Taking the finite difference of the second line of eqn. (4.51) results in a power series expansion as

$$\frac{\Delta F_v}{N} = \frac{mv^2}{2} \frac{\rho_s}{\rho} + O(v^4) \tag{4.52}$$

$\Delta F_v = 0$, i.e. a free energy change due to uniform boundary motion, when no superfluid is present and thus as $v \to 0$, ρ_S is linearly related to the change in the system's free energy.

Typically, the approach utilized in [75, 100] descend from methods to calculate ρ_v and ΔF_v in systems defined by periodic boundary conditions. In particular, ΔF_v may be calculated as

$$e^{-\beta \Delta F_v} = \langle e^{i(m\hbar)\mathbf{v} \cdot \mathbf{WL}} \rangle, \tag{4.53}$$

where L is the box dimension, and $\mathbf{W}$, which is essentially a running tally of the number of times the paths wind around the systems starting from a location R_i and ending at the periodic image $R_{\mathcal{P}i}$.

For a standard superfluid like helium-4, the superfluid fraction may be expressed as,

$$\frac{\rho_s}{\rho} = \frac{\mathbf{W^2}}{2\lambda \beta N}. \tag{4.54}$$

In the case of unpolarized paired particles of like charges the superfluid fraction becomes [52]

$$\frac{\rho_s}{\rho} = \frac{(\mathbf{W_\uparrow} + \mathbf{W_\downarrow})^2}{2\lambda \beta N}. \tag{4.55}$$

4.8.6 Momentum Distribution

The momentum distribution is defined as the single particle density presented in momentum space which is given by,

$$n_k(k, \beta) = \left(\frac{1}{2\pi}\right)^3 \int dx e^{-k \cdot x} n(x, \beta). \tag{4.56}$$

The single particle density matrix is then given by

$$n(x, \beta) = \int dX \rho(x_1, \cdots, x_i, \cdots, x_N) \rho(x_1, \cdots, x_i + x, \cdots, x_N), \tag{4.57}$$

where X subsumes all of the labeled values x_j.

4.9 Path Integral Simulations with Quantum Statistics

Accurately simulating quantities defined by quantum mechanics requires that the particle statistics of the underlying particles be incorporated into the simulation as well. For our purposes quantum particles come in 2 flavors: fermions and bosons; anyons are beyond the scope of this thesis.

While the exact details and reasons for these different particle types have been covered in a previous chapter, their particle exchange imposes significant and at least in the case of fermions daunting challenges for their simulation. Recall that bosons or fermions are indistinguishable particles and thus are subject to exchange of identical particles as follows,

$$\rho_{B/F}(\mathbf{R}, \mathbf{R}'; \beta) = \frac{1}{\mathbf{N}!} \sum_{\mathcal{P}} (\pm_{\mathbf{B/F}} \mathbf{1})^{\mathcal{P}} \rho_{\mathbf{D}}(\mathcal{P}\mathbf{R}, \mathbf{R}'; \beta), \tag{4.58}$$

where $\mathcal{P}$ indicates a permutation and the B/F subscript delineates whether or not the interpretation in question is bosonic or fermionic.

4.9.1 Path Integral Bosonic Sampling Methods

Clearly from eqn. (4.58), a bosonic system may be described as a summation over the $N!$ permutations, where all of the subterms $\rho_D(\mathcal{P}\mathbf{R}, \mathbf{R}'; \beta)$ have an equivalent weighting of $+1$. While bosonic systems present no intrinsic challenges from a positivity standpoint, they do present challenges from the viewpoint of strictly calculating the permutation sum. In fact, from just the standpoint of calculating the permutation sum of the free particle the problem is NP-Hard because permutation sum can be represented as an arbitrary permanent of a matrix with strictly positive elements which is a known NP-Complete/NP-Hard problem

[101]. Fortunately, calculating a permanent may be done approximately in probabilistic polynomial time [102] and this is exactly the approach taken in simulating path integrals.

Within PIMC, the particle exchange of bosons in a simulation is achieved by randomly sampling the permutation space which results in an algorithm which randomly samples the various possible connections among the N-particle bosonic paths. Since this permutation algorithm takes a Monte Carlo approach just like the various moves for the path integral it is easy to incorporate into overall Monte Carlo integration algorithm.

In the permutation moves algorithm, the permutations themselves are represented by a single vector of length N, where N is the number of identical bosonic particles [61] where the vector scalar at each index i is the particle to which the particle i permutes; an identity entry is just represented by i at index i. Since any particle may be exchanged with another at any time slice, the join or the slice after which a permutation has occurred is stored as metadata.

The bisection algorithm is incorporated into the permutation algorithm by selecting a range of 2^L slices. Then, at each level a permutation move involving typically 2-4 (or more) particles is proposed. Initially for convenience, the following notation for a transition element is defined as

$$t_{ab} \equiv \frac{e^{-\frac{(r_b' - r_a)^2}{2^{l+1}\tau\lambda}}}{e^{-\frac{(r_a' - r_a)^2}{2^{l+1}\tau\lambda}}}. \tag{4.59}$$

For the permutation of a pair of particles a and b, the transition probability is constructed as follows,

$$\mathcal{T}(\mathcal{R} \rightarrow \mathcal{P}_{ab}\mathcal{R}) = K t_{ab} t_{ab} = K \frac{e^{-\frac{(r_b' - r_a)^2}{2^{l+1}\tau\lambda}}}{e^{-\frac{(r_a' - r_a)^2}{2^{l+1}\tau\lambda}}} \frac{e^{-\frac{(r_a' - r_b)^2}{2^{l+1}\tau\lambda}}}{e^{-\frac{(r_b' - r_b)^2}{2^{l+1}\tau\lambda}}} \tag{4.60}$$

where a and b are the denote the positions the 2 particles in question on one slice and a' and b' denote the positions those same particles respectively on another slice; K is the normalization constant. The symmetry of the transition probability for both the forward and reverse transition of free particle transitions is clear and thus $\mathcal{T}(\mathcal{R} \rightarrow \mathcal{P}_{ab}\mathcal{R}) = \mathcal{T}(\mathcal{P}_{ab}\mathcal{R} \rightarrow \mathcal{R})^{-1}$. In this particular case the permutation transition may be sampled exactly without rejection.

When simulations are performed only permutations up to a certain depth are allowed due to computational constraints since the number of permutations grows as roughly N^p, where N is the number of particles and p is the depth of permutations Building up higher order permutations is relatively easy and may be represented as $K t_{ab} t_{bc} t_{ca}$ for a 3 particle permutation, $K t_{ab} t_{bc} t_{cd} t_{da}$ for a 4 particle permutation, $K t_{ab} t_{bc} t_{cd} t_{de} t_{ea}$ for a 5 particle permutation, and so on for more particles. K, the normalization constant

for may then be derived to be for varying depths as follows: For a depth of 2-particle permutations, it is

$$K = \sum_a [t_{aa} + \sum_b t_{ab} t_{ba}]. \tag{4.61}$$

For a depth of 3-particle permutations, it is

$$K = \sum_a [t_{aa} + \sum_b t_{ab} [t_{ba} + \sum_c t_{bc} t_{ca}]], \tag{4.62}$$

and for a depth of 4-particle permutations, it is

$$K = \sum_a [t_{aa} + \sum_b t_{ab} [t_{ba} + \sum_c t_{bc} [t_{ca} + \sum_d t_{cd} t_{da}]]]. \tag{4.63}$$

This trend may be continued for higher permutation depths as well. Typically though, only fourth or fifth order depths are utilized in simulations since the aforementioned scaling N^p applies for the permutation table size. If higher order permutations are needed, a probability cutoff ϵ may be applied in the table construction so that unlikely permutations are discarded and not tabulated.

After the table is constructed, a permutation may sampled from it by randomly selecting a number γ from a uniform distribution and then constructing the associated cumulative distribution function by first labeling each of the permutations i and then defining the cumulative distribution function of those permutations as,

$$c_j = \sum_{i<j} p_i \tag{4.64}$$

where p_i is probability of a specific permutation i. Once the permutation is found such that $c_{j-1} < \gamma \leq c_j$, this permutation j is selected as the trial permutation. The backward probability transition for it is calculated by constructing a similar table and it is accepted or rejected based on those merits. Afterwards a bisection move is applied, another permutation is attempted for the next level down the bisection and this process is repeated until the entire move is accepted or rejected.

4.9.2 Path Integral Fermionic Sampling Methods

Over the past 30 years, computational path integral Monte Carlo methods (PIMC) have found widespread application and success in the simulation of quantum statistical mechanics of many-body phenomena, partic-ularly for bosonic and high-temperature systems [75]. Unfortunately, the application of PIMC to fermionic systems has been hindered by the notorious "sign problem," which arises from the sign changes associated

with the antisymmetrization of the approximate many-body density matrix. The sign problem poses a great difficulty for the Monte Carlo integration methods typically used to evaluate the resulting high-dimensional integrals. The near-cancellation of roughly equal positive and negative contributions of the integrand results in a statistical variance increasing exponentially with the number of variables being integrated for a fixed number of function evaluations [103].

During the last decade, Troyer and Wiese [104] showed that the evaluation of an expectation value of a general function with a sign-problem is NP-Hard, and thus likely to be intractable, by reducing a NP-Complete Ising spin glass problem to a form with the sign problem. While at first this result may seem unfortunate since many interesting phenomena such as Fermi-Dirac condensates in optical lattices or superconductivity arise from interacting fermionic systems, the sheer generality of their result leaves open the possibility that most fermionic systems may not be subject to this curse since the extent of the space of fermionic problems that are not NP-Hard is unknown. Methods such as the density matrix renormalization group [14] and 1-D fermionic PIMC [105] already suggest that the set of non-NP-Hard fermionic problems is quite large. Moreover, the trace of the density matrix which defines the quantum partition function and more importantly its integrand are both strictly positive which suggests that the sign-problem is not necessarily inherent to fermionic systems and is quite possibly an artifact of approximations from a computational and theoretical standpoint.

Due to the inherent difficulty caused by the aforementioned fermionic-sign problem, published work on the sign-problem within the context of path integrals is relatively scant in comparison to other methodological developments like improved sampling. This is particularly true in relation to other Monte Carlo approaches like diffusion Monte Carlo. Often, both within the field of path integral simulations and outside of it as well, approaches towards dealing with the fermionic-sign problem seek to ameliorate the effects of oscillation in Monte Carlo simulations as in [72, 106, 107] rather than tackling the problem from the head. In particular, special cases based on potentials or boundary conditions are often developed, particularly within lattice systems. Other approaches involve using uncontrolled approximations to simulating fermionic systems. In this thesis, one approach from each type will be considered. In order these approaches are: the one-dimensional of Takahashi and Imada and the fixed node approximation due to Ceperley.

4.10 Approaches to Fermionic PIMC

4.10.1 The Approach of Takahashi and Imada to Fermionic PIMC

A standard approach to the fermionic density matrix path integral is developed with the aid of the Trotter formalism. To review, the typical Hamiltonian used in imaginary-time PIMC is

$$\hat{H} = \sum_k \frac{\hat{P}_k^2}{2m} + \hat{V}\{x_k\} = \hat{T} + \hat{V}, \tag{4.65}$$

where $\hat{P}$ is the momentum operator of a particle with mass m, $\hat{V}$ is the operator denoting an N-particle, interaction potential. The fermionic canonical partition function is then defined as

$$Z = \int dX \, \langle X_\mathcal{A} | e^{-\beta \hat{H}} | X_\mathcal{A} \rangle, \tag{4.66}$$

where $X_\mathcal{A}$ denotes an antisymmetrized position ket. Using the Trotter formula, the Boltzmann operator $e^{-\beta \hat{H}}$ is expressed as

$$e^{-\beta \hat{H}} = \lim_{M \to \infty} \left(e^{-\beta \frac{\hat{T}}{M}} e^{-\beta \frac{\hat{V}}{M}} \right)^M. \tag{4.67}$$

For subsequent convenience, the antisymmetrized N-free particle propagator ρ without normalization is defined as

$$\rho\left(g; X^{(j+1)} | X^{(j)}\right)$$
$$= \det \begin{vmatrix} e^{-g(x_1^{(j+1)} - x_1^{(j)})^2} & \cdots & e^{-g(x_1^{(j+1)} - x_N^{(j)})^2} \\ \vdots & \ddots & \vdots \\ e^{-g(x_N^{(j+1)} - x_1^{(j)})^2} & \cdots & e^{-g(x_N^{(j+1)} - x_N^{(j)})^2} \end{vmatrix}, \tag{4.68}$$

where g is a constant containing all relevant non-positional information, and $X^{(j)}$ collectively denotes $x_1^{(j)}, \cdots, x_N^{(j)}$. Limiting eqn. (4.67) to a finite number M slices and inserting and integrating out, when possible, complete sets of antisymmetrized position and momentum states, given $X^{(M)} = X^{(0)}$, yields an approximate canonical partition function Z due to Takahashi and Imada (TI) [71]. Each individual slice is then given as

$$\rho_{TI}^{(j)}\left(X^{(j+1)} | X^{(j)}\right) = \frac{1}{N!} \left(\frac{mM}{2\pi\beta\hbar^2}\right)^{\frac{dN}{2}} \times$$
$$\rho\left(\frac{mJ}{2\beta}; X^{(j+1)} | X^{(j)}\right) e^{-\frac{\beta}{2M}(V(\{x_i^{(j)}\}) + V(\{x_i^{(j+1)}\}))}, \tag{4.69}$$

with d denoting the spatial dimensionality of the system and the approximate partition function is given by

$$Z \approx \int dX^M \prod_{j=0}^{M-1} \rho_{TI}^{(j)} \left(X^{(j+1)} | X^{(j)} \right). \tag{4.70}$$

While this approach to the fermionic path integral results in a strictly positive representation of the path integral for one-dimensional systems, it quickly breaks down when applied to systems with dimensions higher than 1 due to the reappearance of the sign problem manifested by the non-negative regions present in the antisymmetrically permuted approximate fermionic propagator.

4.10.2 The Fixed-Node Approach

Another approach to fermionic PIMC, as well as the one that will be used in this thesis, was first proposed by Ceperley in [74] which yields a strictly positive integrand at the expense of being an uncontrolled approximation. The methodology is developed by first observing that flux of positive and negative paths through the nodal boundaries separating negative and positive regions of the integrand must be equal at the nodes because they cancel and hence there is a node. Since the nodes are already zero, an infinite potential may be imposed at the exact nodal surface without changing the underlying integral. Since negative paths (odd permutations) must cross the nodal surface at some point, they may be discarded. Thus, only positively signed, even permutations are required for this method. This results in an evaluation of the density matrix that may be symbolically defined as [72],

$$\rho_F(\mathbf{R}_\beta, \mathbf{R}_*; \beta) = \int d\mathbf{R_0} \rho_{\mathbf{F}}(\mathbf{R_0}, \mathbf{R}_*; \mathbf{0}) \oint_{\mathbf{R_0} \to \mathbf{R}_\beta \in \mathbf{\Gamma}(\mathbf{R}_*)} d\mathbf{R_r} e^{-\mathbf{S}[\mathbf{R_t}]}, \tag{4.71}$$

where S_t is the system action, R_0 is the starting location of the paths, R_* is the reference point or slice of the path, and $\mathbf{R}_\beta \in \mathbf{\Gamma}(\mathbf{R}_*)$ denotes the nodal surface obeyed by the reference point R_*. In the rare occasions in which one has the exact nodal surface, this method is exact. To perform a simulation all one needs to do is restrict the paths via the reference slice to that nodal surface, perform even permutations upon the paths, and then calculate expectation values taking care to use the reference slice.

Unfortunately, one rarely has the exact nodal surfaces available unless the problem being explored has already been solved. In practice, an approximation to the nodal surface is often made. Since it is known that for a system which is not in a magnetic field, that density matrix a system at a high enough temperature becomes like that of the ideal gas, the nodes of the free particle density matrrix are often used in simulation [36, 61, 72].

Low and intermediate temperatures are more challenging. For very low temperatures often the nodal

surface defined by the ground state wavefunction is used, but a rigorous interpolation to the intermediate temperature region is still lacking [36].

Consequently, when actual simulations are performed within this framework, inexact nodal surfaces are imposed from the few exactly solved problems that are available such as the free particle, the harmonic oscillator or from BCS theory [73, 74]. As a result of these approximations, the analysis and interpretation of the results calculated with this method can be difficult without an understanding of a related experiment or a calculation of the same quantity using a different albeit more expensive method. Despite these drawbacks, this technique presents one of the few potentially systematically improvable approaches to calculating temperature dependent quantities with for general systems with fermionic statistics.

Chapter 5

Pair Propagators in PIMC and the Delta Function Pair Potential and Propagator

5.1 The Pair Potential in Path Integral Monte Carlo and the Underlying Motivation for Applying It to the Delta Function Pair Potential

Within PIMC and related methods, pair interactions, and their actions and propagators are useful because the potentials of most physical systems within a chemical and condensed matter context may be described in *ab initio* terms as being the sum of single particles' interactions with external fields and with each other in a pairwise fashion. For those interested in simulating bulk systems such as liquid helium or hydrogen or a bulk gas either in the presence of a nonexistent or negligible external field such as gravity, the potential may be described in its entirety as a summation of pair interactions for an N-particle system [75] as,

$$V(R) = \sum_{j<i}^{N(N-1)/2} v(|\mathbf{r}_i - \mathbf{r}_j|). \tag{5.1}$$

When the Lie-Trotter discretization is applied to this pairwise sum as described in section (4.3.1), the pair propagator may be derived.

In the specific case of a fermionic unitary gas the pair propagator is expected to be extremely effective since the physical behavior of the unitary gas is dominated by two particle interactions. However, in some of the simulations of unitary gases [52], it has been unclear how well the unitary regime has been reached due to the usage of a short range pair potential such as the modified Pöschl-Teller potential, which necessarily has non s-wave terms. Consequently an improved pair propagator will be developed in this chapter, which strips a short-range pair product propagator down to its essence by including that only the terms that define the unitary regime, the δ-function pair interaction. Being defined by a distribution, this interaction is most easily simulated via a pair propagator term as it cannot be simulated via a simple potential.

5.2 Introduction: Unitarity and Potentials

The unitary limit is reached when the range of attractive pair interactions between fermionic species become zero-range. This interaction effect results in the dominance of the s-wave scattering interaction between the attractive short-range pair interactions of the fermionic particles [12]. In the unitary regime, the aforementioned fermionic system has been so diluted that the average spacing amongst the particles is much larger than the range of interaction, or conversely, the scattering length, ζ, is much larger than the interparticle spacing. Being located in this dilute spatial regime results in the bifermionic system having only a single effective length scale, which within the literature is typically described by one of two values: the previously described scattering length, ζ, of the underlying interaction potential or by the density n of the system itself [12]. The presence of only a single length scale has been the source of considerable difficulty in probing the unitary limit from an analytic standpoint due to the lack of an appropriately small parameter to use within the framework of perturbation theory. That said this not to paint situation as entirely bad asthe single length scale has also been a source of strength due to the applicability of scaling arguments [12]. Nonetheless, due to the theoretical difficulties presented by unitarity, the unitary regime is thus a uniquely well-suited for investigation by computational techniques

As has already been covered in an introductory chapter, when the system in question is manipulated to an appropriate density and interaction strength as is achievable naturally in some nuclear many-body systems and via optical lattice methods in atomic and optical physics [1, 12, 108], the interactions between classes of fermions between any short-range potentials may be tuned to be in the unitary regime. Because the unitary regime is dominated by s-wave scattering between pair interactions and a single length scale, which for this chapter's purpose's shall be set to the scattering length a_s, all possible short-range potentials effectively become a zero-range, hard wall interaction. This statement may be justified by the following derivation: First, consider the Schrödinger equation of two bodies of mass m's finite range potential $V(|\mathbf{r}|)$ [34],

$$\left[-\frac{1}{2}\nabla^2 + \hat{V}\right]\psi(\mathbf{r}) = E\psi(\mathbf{r}), \ |\mathbf{r}| < r_c$$
$$\left[-\frac{1}{2}\nabla^2 + 0\right]\psi(\mathbf{r}) = E\psi(\mathbf{r}), \ |\mathbf{r}| > r_c, \tag{5.2}$$

where the various physical constants involved have been set to 1 for convenience and r_c denotes the finite range of the pair potential. Setting $E = k^2/2$ and rearranging the the outer range portion of eqn. (5.2)

results in the Helmholtz equation,

$$\left[-\frac{1}{2}\nabla^2 + k^2 \right] \psi(\mathbf{r}) = 0, \ |\mathbf{r}| > r_c$$

(5.3)

which may be solved in terms of spherical harmonics, $Y_{lm}(\theta, \psi)$, and spherical Bessel functions, $j_l(kr)$, as,

$$\psi(\mathbf{r}) = \sum_{l=0}^{\infty} \sum_{m=-l}^{l} A_{lm}[j_l(kr) - \tan(\eta_l)\eta_l(kr)]Y_{lm}(\theta, \psi),$$

(5.4)

where $\eta_l = \frac{j_l(kr_c)}{\eta_l(kr_c)}$ is the phase shift constant caused by the reflection of the particle off of the boundary at r_c caused by the boundary conditions $\psi(r_c) = 0$.

Utilizing an intuitive approach to the justification of this pseudopotential, since the unitary system being studied is defined as being a dilute one of necessarily low energy, this implies that the preceding equation (5.4) must effectively be considered in the dual limits: $k \to 0$ and $r_c \to 0$. The condition $k \to 0$ follows from the energy being low since as $E \to 0$ by definition $k \to 0$. Subsequently, this causes only the lowest s-wave interaction to matter. The condition $r_c \to 0$ results from the dilute conditions present in a unitary system since if one considers the system to be continuously rescaled the attractive short-range potential rapidly becomes δ-function-like and zero-range because the particles are very far away from each other so that the rescaled length of the inner core effectively becomes 0. Ultimately, this analysis implies that the two-body potential interaction under consideration becomes governed by a pseudopotential in the unitary limit due to the effective infinity of the δ function term which arises from the rescaled residual short-range potential.

From a mathematical standpoint, this pseudopotential has been previously studied and justified in a more general form in [34] and may be derived by considering the lowest order term associated with the constant A_{00},

$$\psi((r)) \overset{l \to 0}{=} A_{00}[j_0(kr) - \tan(\eta_0)\eta_0(kr)]Y_{00}(\theta, \psi)$$
$$= \frac{A_{00}}{\sqrt{4\pi}} \left[\frac{\sin(kr)}{kr} + \tan(\eta_0 \frac{\cos(kr)}{kr}) \right].$$

(5.5)

If the preceding equation is then studied in the same limit as before where $r \to 0$, $\frac{\sin(kr)}{kr} \to 1$ and $\frac{\cos(kr)}{kr} \to \infty$, it may be considered that the term $\tan(\eta_0 \frac{\cos(kr)}{kr})$ dominates the wavefunction, $\psi(\mathbf{r})$.

This approach corresponds to the extension of the range of validity of the outer function expression (5.5) to the entirety of r i.e. to $r < r_c$ as well as to $r > r_c$. Moreover, when since the preceding solution is valid

within this inner region $r < r_c$ for the Helmholtz equation, the inner Helmholtz equation may be extended using the relation $\nabla^2(1/r) = -4\pi\delta(\mathbf{r})$ and re-written as,

$$\left[\nabla^2 + k^2\right]\psi(\mathbf{r}) = -4\pi\frac{A_{00}}{\sqrt{4\pi}}\frac{\tan(\eta_0)}{k}\delta(\mathbf{r}). \tag{5.6}$$

Taking advantage of the limiting value [34],

$$\frac{A_{00}}{\sqrt{4\pi}} = \frac{\partial}{\partial r}[r\psi(\mathbf{r})]|_{r=0} \tag{5.7}$$

results in the following expression

$$\left[\nabla^2 + k^2\right]\psi(\mathbf{r}) = -4\pi\frac{\tan(\eta_0)}{k}\delta(\mathbf{r})\frac{\partial}{\partial r}[r\psi(\mathbf{r})], \tag{5.8}$$

which may then be re-arranged to yield the idealized the *infinitesimally* short ranged, s-wave, pseudopotential pair interaction Schrödinger equation as,

$$\left[\nabla^2 + 4\pi\frac{\tan(\eta_0)}{k}\delta(\mathbf{r})\frac{\partial}{\partial r}[r\psi(\mathbf{r})]\right]\psi(\mathbf{r}) = E\psi(\mathbf{r}). \tag{5.9}$$

Restoring the materials constants to this Schrödinger equation then yields the potential

$$[-\frac{\hbar^2}{2\mu}\nabla^2 + U(\mathbf{r}) - E]\psi(\mathbf{r}) = 0$$
$$U(\mathbf{r}) = \frac{2\pi\hbar^2 a_s}{\mu}\delta(|\mathbf{r}|)\frac{\partial}{\partial|r|}|r| \tag{5.10}$$

where μ is the reduced mass since the assumption in this derivation is that a pair transformation has already been applied to the equation. The mass, m, may be replaced with μ for a δ field interaction and a_s, the screening length, results from the absorption of various constants associated with η_0. Using the pseudopotential given in eqn. (5.10) for the pair interaction term present in unitary Fermi gas simulations allows one to strip this model system down to its bare essentials as one is solely simulating the interaction term relevant to the unitary gas, and consequently, one does not have to be concerned by higher order effects.

5.3 Derivation of the Pair Propagator with the Delta Pair Interaction

Following the derivation of the δ-function pair interaction pseudopotential, eqn. (5.10) from a general short-range pair interaction applicable to the unitary regime, the derivation of that pseudopotential's pair propagator will be considered. The plan of attack is as follows: First, the Wick-rotated or imaginary time Schrödinger equation for the pair interaction will be considered. A coordinate transformation will be performed to separate out the center of mass coordinate (the translational degrees of freedom) from the pair interaction potential. The center of mass term will be solved as a free particle propagator and the relative coordinates integral equation for the Green function or propagator will be solved using the Laplace transform method for the solution of that integral equation.

5.3.1 The Wick-Rotated or Imaginary Time Schrödinger Equation for the Delta Pair Interaction and Center of Mass Coordinate Transformation

The imaginary time Schrödinger equation for the δ-pair potential is given by

$$-\hbar\frac{\partial\psi}{\partial\tau} = \left[-\frac{\hbar^2}{2m}\nabla^2\mathbf{r}_1 - \frac{\hbar^2}{2m}\nabla^2\mathbf{r}_2 + \frac{2\pi\hbar^2 a_s}{\mu}\delta(|\mathbf{r}_1 - \mathbf{r}_2|)\frac{\partial}{\partial|\mathbf{r}_1 - \mathbf{r}_2|}|\mathbf{r}_1 - \mathbf{r}_2|\right]\psi \qquad (5.11)$$

By performing a center of mass transformation upon eqn. (5.11) three of the six coordinates may be separated out. Beginning with the coordinate transformation, the derivatives, which are given in dummy cartesian coordinates, and the gradient, which is given in vector form,

$$\mathbf{r} = r_1 - r_2, \, R = \frac{m_1 r_1 + m_2 r_2}{m_1 + m_2} \qquad (5.12)$$

$$\frac{d}{dr_1} = \frac{\partial r}{\partial r_1}\frac{\partial}{\partial r} + \frac{\partial R}{\partial r_1}\frac{\partial}{\partial R} \qquad (5.13)$$

$$\frac{d}{dr_2} = \frac{\partial r}{\partial r_2}\frac{\partial}{\partial r} + \frac{\partial R}{\partial r_2}\frac{\partial}{\partial R} \qquad (5.14)$$

$$\frac{\hbar^2}{2m}\nabla^2_{\mathbf{r}_1} + \frac{\hbar^2}{2m}\nabla^2_{\mathbf{r}_2} = \frac{\hbar^2}{2M}\nabla^2_{\mathbf{R}} + \frac{\hbar^2}{2\mu}\nabla^2_{\mathbf{r}} \qquad (5.15)$$

yields the following equation when substituted into eqn. (5.11) relationship in terms of the gradient operators,

$$\hbar\frac{\partial\Psi}{\partial\tau} = \left[-\frac{\hbar^2}{2M}\nabla^2_{\mathbf{R}} - \frac{\hbar^2}{2\mu}\nabla^2_{\mathbf{r}} + \frac{2\pi\hbar^2 a_s}{\mu}\delta(|\mathbf{r}|)\frac{\partial}{\partial|r|}|r|\right]\Psi, \qquad (5.16)$$

where $\Psi = \phi(\mathbf{R})\psi(\mathbf{r})$, μ is the reduced mass, $\frac{m_1 m_2}{m_1 + m_2}$, and M is the total mass of the two particle system. As eqn. (5.16) is separable in terms of the coordinates given by $\mathbf{R}$ and $\mathbf{r}$ then leads naturally to

$$\hbar \frac{\partial \phi}{\partial \tau} = \left[-\frac{\hbar^2}{2M} \nabla_{\mathbf{R}}^2 \right] \phi \tag{5.17}$$

and the familiar equation derived in the prior section

$$\hbar \frac{\partial \psi}{\partial \tau} = \left[\nabla_{\mathbf{R}}^2 - \frac{\hbar^2}{2\mu} \nabla_{\mathbf{r}}^2 + \frac{2\pi \hbar^2 a_s}{\mu} \delta(|\mathbf{r}|) \frac{\partial}{\partial |r|} |r| \right] \psi \tag{5.18}$$

Because eqn. (5.17) is just the Schrödinger equation for the free particle, this expression may be solved exactly and, when implemented as propagator or action in code, may be sampled exactly as well. This leaves the propagator/action for eqn. (5.18) to be solved for, which may be handled using standard Green function techniques.

5.4 Green Function Propagator Derivation for the Delta-Pair Pseudopotential

The Green function formalism for the Schrödinger equation may be expressed by recalling the formal definition for the propagator $\hat{K}(\tau)$ with the initial condition $\hat{K}(0) = 1$ as,

$$\hat{K}(\tau) = e^{-\tau \hat{H}} \tag{5.19}$$

Since this is a propagator, it by definition propagates a state vector from one state to another in imaginary time, which is symbolically written as,

$$\hat{K}(\tau)|\psi(0)\rangle = e^{-\tau \hat{H}}|\psi(0)\rangle = |\psi(\tau)\rangle \tag{5.20}$$

The Bloch equation may be recovered from the propagator by taking the derivative with respect to τ,

$$\frac{\partial}{\partial \tau}|\psi(\tau)\rangle = \frac{\partial}{\partial \tau} e^{-\tau \hat{H}}|\psi(0)\rangle = -\hat{H} e^{-\tau \hat{H}}|\psi(0)\rangle = -\hat{H}|\psi(\tau)\rangle$$

$$\Rightarrow \left(\frac{\partial}{\partial \tau} + \hat{H} \right) |\psi(\tau)\rangle = \left(\frac{\partial}{\partial \tau} + \hat{H} \right) \hat{K}(\tau) = 0 \tag{5.21}$$

Putting the propagator into a coordinate representation, $\hat{K}(\tau) \to K(\mathbf{r}, \mathbf{r}'; \tau) = \langle \mathbf{r} | \hat{K}(\tau) | \mathbf{r}' \rangle$, allows the initial condition to be expressed as $K(\mathbf{r}, \mathbf{r}'; 0) = \delta(\mathbf{r} - \mathbf{r}')$, which may substituted back into the differential equation given by eqn. (5.21). Having now defined the notation, the Hamiltonian $\hat{H}$ and propagator $\hat{K}$ may be subdivided into the free particle and other components which will be used to derive the actual expression for the propagator,

$$\hat{H} = \hat{H}_0 + \hat{V} \tag{5.22}$$

$$\hat{K} = \hat{K}_0 + \Delta\hat{K}. \tag{5.23}$$

Using the preceding expressions, an integral equation may be derived that will allow for the full solution of the δ-pair propagator. Beginning with

$$
\begin{aligned}
\delta(\mathbf{r} - \mathbf{r}') &= \left(\frac{\partial}{\partial \tau} + \hat{H} \right) \hat{K}(\mathbf{r}, \mathbf{r}'; \tau) \\
&= \left(\frac{\partial}{\partial \tau} + \hat{H}_0 + \hat{V} \right) \left(\hat{K}_0 + \Delta\hat{K} \right) \\
&= \left(\frac{\partial}{\partial \tau} + \hat{H}_0 \right) \hat{K}_0 + \hat{V}\hat{K}_0 + \left(\frac{\partial}{\partial \tau} + \hat{H} \right) \Delta\hat{K} \\
&= \delta(\mathbf{r} - \mathbf{r}') + \hat{V}\hat{K}_0 + \left(\frac{\partial}{\partial \tau} + \hat{H} \right) \Delta\hat{K},
\end{aligned}
\tag{5.24}
$$

and thus,

$$\left(\frac{\partial}{\partial \tau} + \hat{H} \right) \Delta\hat{K} = -\hat{V}\hat{K}_0 \Rightarrow$$

$$\left(\frac{\partial}{\partial \tau} + \hat{H} \right) \Delta\hat{K} - \hat{V}\Delta\hat{K} = -\hat{V}\hat{K}_0 - \hat{V}\Delta\hat{K}$$

$$\left(\frac{\partial}{\partial \tau} + \hat{H}_0 \right) \Delta\hat{K} = -\hat{V}\hat{K}, \tag{5.25}$$

which in a coordinate representation becomes

$$\left(\frac{\partial}{\partial \tau} + \hat{H}_0 \right) \Delta\hat{K} = -V(\mathbf{r})K(\mathbf{r}, \mathbf{r}'; \tau)$$

$$\tag{5.26}$$

which results in the following derivation,

$$\left(\frac{\partial}{\partial \tau} + \hat{H}_0\right) \Delta K = -V(\mathbf{r})K(\mathbf{r}, \mathbf{r}'; \tau)$$

$$= -\int d^D\mathbf{r}'' \int_0^\tau dt'' \delta(\tau - t'')\delta(\mathbf{r} - \mathbf{r}'')V(\mathbf{r}'')K(\mathbf{r}'', \mathbf{r}'; t'')$$

$$= -\int d^D\mathbf{r}'' \int_0^\tau dt'' \left(\frac{\partial}{\partial \tau} + \hat{H}_0\right) K_0(\mathbf{r}, \mathbf{r}''; \tau - t'')V(\mathbf{r}'')K(\mathbf{r}'', \mathbf{r}'; t''), \tag{5.27}$$

and concludes in an integral equation as,

$$\Delta K(\mathbf{r}, \mathbf{r}'; \tau) = -\int d^D\mathbf{r}'' \int_0^\tau dt'' \left(\frac{\partial}{\partial \tau} + \hat{H}_0\right) K_0(\mathbf{r}, \mathbf{r}''; \tau - t'')V(\mathbf{r}'')K(\mathbf{r}'', \mathbf{r}'; t'') \tag{5.28}$$

which may be re-written as an integral equation related variously to second-order Fredholm and Volterra integral equations as,

$$K(\mathbf{r}, \mathbf{r}'; \tau) = K_0(\mathbf{r}, \mathbf{r}'; \tau) - \int d^D\mathbf{r}'' \int_0^\tau dt'' \left(\frac{\partial}{\partial \tau} + \hat{H}_0\right) K_0(\mathbf{r}, \mathbf{r}''; \tau - t'')V(\mathbf{r}'')K(\mathbf{r}'', \mathbf{r}'; t''). \tag{5.29}$$

Eqn. (5.29) may be solved [109–111] by first integrating out the spatial coordinates $\mathbf{r}''$ and then applying the Laplace transform to the imaginary time variable τ.

Since the δ-function of the studied pseudopotential may be integrated exactly within the coordinate framework of eqn. (5.29), the regularization of the potential is not required in this case and so it becomes,

$$V(\mathbf{r}) = \frac{2\pi\hbar^2 a_s}{\mu}\delta(|\mathbf{r}|)\frac{\partial}{\partial|r|}|r| \to a_3\delta(\mathbf{r}), \tag{5.30}$$

where a_3 is a constant introduced to simplify calculations.

Introducing the potential from eqn. (5.30) to the integral eqn. (5.29) and integrating over $\mathbf{r}''$ yields,

$$K(\mathbf{r}, \mathbf{r}'; \tau) = K_0(\mathbf{r}, \mathbf{r}'; \tau) - \int d^D\mathbf{r}'' \int_0^\tau dt'' \left(\frac{\partial}{\partial \tau} + \hat{H}_0\right) K_0(\mathbf{r}, \mathbf{r}''; \tau - t'')a_3\delta(\mathbf{r}'')K(\mathbf{r}'', \mathbf{r}'; t'') \tag{5.31}$$

$$= K_0(\mathbf{r}, \mathbf{r}'; \tau) - a_3 \int_0^\tau dt'' \left(\frac{\partial}{\partial \tau} + \hat{H}_0\right) K_0(\mathbf{r}, 0; \tau - t'')K(0, \mathbf{r}'; t'') \tag{5.32}$$

Applying the Laplace transform to eqn.(5.32),

$$\mathcal{L}[K(\mathbf{r}, \mathbf{r}'; \tau)] = \mathcal{L}\left[K_0(\mathbf{r}, \mathbf{r}'; \tau) - a_3 \int_0^\tau dt'' K_0(\mathbf{r}, 0; \tau - t'')K(0, \mathbf{r}'; t'')\right] \Rightarrow$$

$$L(\mathbf{r}, \mathbf{r}'; s) = L_0(\mathbf{r}, \mathbf{r}'; s) - a_3 L_0(\mathbf{r}, 0; s)L(0, \mathbf{r}'; s), \tag{5.33}$$

where L signifies the Laplace transformed term, allows an algebraic equation to appear, which may be solved for by setting $\mathbf{r} = 0$ so that

$$L(0, \mathbf{r}'; s) = L_0(0, \mathbf{r}'; s) - a_3 L_0(0, 0; s) L(0, \mathbf{r}'; s) \rightarrow$$

$$L(0, \mathbf{r}'; s) + a_3 L_0(0, 0; s) L(0, \mathbf{r}'; s) = L_0(0, \mathbf{r}'; s) \rightarrow$$

$$L(0, \mathbf{r}'; s) = \frac{L_0(0, \mathbf{r}'; s)}{1 + a_3 L_0(0, 0; s)}. \tag{5.34}$$

Substituting eqn. (5.34) back into eqn. (5.33) yields

$$L(\mathbf{r}, \mathbf{r}'; s) = L_0(\mathbf{r}, \mathbf{r}'; s) - a_3 \frac{L_0(\mathbf{r}, 0; s) L_0(0, \mathbf{r}'; s)}{1 + a_3 L_0(0, 0; s)}. \tag{5.35}$$

Finding the inverse Laplace transform on eqn (5.35) has its main source of difficulty in the term,

$$a_3 \frac{L_0(\mathbf{r}, 0; s) L_0(0, \mathbf{r}'; s)}{1 + a_3 L_0(0, 0; s)}. \tag{5.36}$$

Fortunately, a solution is known and may be found by preceding as follows: First, the Laplace transforms which comprise all of the substituent terms of eqn. (5.36) are known [112] and given by the following,

$$L_0(0, 0; s) = \mathcal{L}\left[\frac{1}{(2\pi\tau)^{3/2}}\right] = -\frac{\sqrt{2s}}{2\pi} \tag{5.37}$$

$$L_0(\mathbf{r}, \mathbf{r}'; s) = \mathcal{L}\left[\frac{1}{(2\pi\tau)^{3/2}} e^{-\frac{|\mathbf{r}-\mathbf{r}'|^2}{2\tau}}\right] = \frac{1}{2\pi|\mathbf{r} - \mathbf{r}'|} e^{-|\mathbf{r}-\mathbf{r}'|\sqrt{2s}}. \tag{5.38}$$

Substituting (5.37) and (5.38) into eqn. (5.36) results in the following expression,

$$\Delta L(\mathbf{r}, \mathbf{r}'; s) = a_3 \frac{\frac{1}{2\pi|\mathbf{r}|} e^{-|\mathbf{r}|\sqrt{2s}} \frac{1}{2\pi|\mathbf{r}'|} e^{-|\mathbf{r}'|\sqrt{2s}}}{1 - a_3 \frac{\sqrt{2s}}{2\pi}}. \tag{5.39}$$

This expression may then be inverted by using the following inverse Laplace transform relation also known as the Bromwich integral from [112, 113],

$$\frac{a}{2} \oint \frac{ds}{2\pi i} \frac{e^{s\tau}}{\sqrt{s}} \frac{e^{-q\sqrt{2s}}}{\sqrt{s} - \frac{a}{\sqrt{2}}} = \frac{a}{2} e^{-aq + \frac{\tau a^2}{2}} erfc(\frac{q - \tau a}{\sqrt{2\tau}}), \tag{5.40}$$

where a and q are arbitrary constants and s and τ have same meaning as previously defined for the Laplace transform. The expression given by eqn. (5.39) may be converted into a form suitable for the inverse

transform relation (5.40) by taking advantage of the following derivative relationship [112],

$$
\begin{aligned}
\Delta L(\mathbf{r},\mathbf{r}';s) &= a_3 \frac{\frac{1}{2\pi|\mathbf{r}|}e^{-|\mathbf{r}|\sqrt{2s}}\frac{1}{2\pi|\mathbf{r}'|}e^{-|\mathbf{r}'|\sqrt{2s}}}{1-a_3\frac{\sqrt{2s}}{2\pi}} \\
&= \frac{1}{2\sqrt{2}\pi|\mathbf{r}||\mathbf{r}'|}\frac{e^{-(|\mathbf{r}|+|\mathbf{r}'|)\sqrt{2s}}}{\sqrt{s}+\frac{\sqrt{2}\pi}{a_3}} \\
&= -\frac{1}{4\pi|\mathbf{r}||\mathbf{r}'|}\frac{\partial}{\partial|\mathbf{r}|}\left(\frac{1}{\sqrt{s}}\frac{e^{-(|\mathbf{r}|+|\mathbf{r}'|)\sqrt{2s}}}{\sqrt{s}+\frac{\sqrt{2}\pi}{a_3}}\right).
\end{aligned}
\tag{5.41}
$$

Setting $q=(|\mathbf{r}|+|\mathbf{r}'|)$ and $a_3=-\frac{2\pi}{a}$ in eqns. (5.40) and (5.41) results in the following series of expressions,

$$
\Delta K(\mathbf{r},\mathbf{r}';s) = -\frac{1}{4\pi|\mathbf{r}||\mathbf{r}'|}\frac{\partial}{\partial|\mathbf{r}|}\oint\frac{ds}{2\pi i}\frac{e^{s\tau}}{\sqrt{s}}\left(\frac{e^{-(|\mathbf{r}|+|\mathbf{r}'|)\sqrt{2s}}}{\sqrt{s}+\frac{\sqrt{2}\pi}{a_3}}\right)
\tag{5.42}
$$

$$
= -\frac{1}{4\pi|\mathbf{r}||\mathbf{r}'|}\frac{\partial}{\partial|\mathbf{r}|}e^{\frac{2\pi(|\mathbf{r}|+|\mathbf{r}'|)}{a_3}+\frac{2\pi^2\tau}{a_3^2}}\operatorname{erfc}\left(\frac{(|\mathbf{r}|+|\mathbf{r}'|)+\frac{2\pi\tau}{a_3}}{2\tau}\right)
\tag{5.43}
$$

$$
= \frac{\tau}{|\mathbf{r}||\mathbf{r}'|}\frac{1}{(2\pi\tau)^{3/2}}e^{-\frac{(|\mathbf{r}|+|\mathbf{r}'|)^2}{2\tau}} - \frac{1}{2a_3|\mathbf{r}||\mathbf{r}'|}e^{\frac{2\pi(|\mathbf{r}|+|\mathbf{r}'|)}{a_3}+\frac{2\pi^2\tau}{a_3^2}}\operatorname{erfc}\left(\frac{(|\mathbf{r}|+|\mathbf{r}'|)+\frac{2\pi\tau}{a_3}}{2\tau}\right).
\tag{5.44}
$$

Substituting (5.44) into (5.29) yields,

$$
K(\mathbf{r},\mathbf{r}';\tau) = \frac{e^{-\frac{|\mathbf{r}-\mathbf{r}'|^2}{2\tau}}}{(2\pi\tau)^{3/2}} + \left(\frac{\tau}{|\mathbf{r}||\mathbf{r}'|}\right)\frac{e^{-\frac{(|\mathbf{r}|+|\mathbf{r}'|)^2}{2\tau}}}{(2\pi\tau)^{3/2}}
$$

$$
- \frac{1}{2a_3|\mathbf{r}||\mathbf{r}'|}e^{\frac{2\pi(|\mathbf{r}|+|\mathbf{r}'|)}{a_3}+\frac{2\pi^2\tau}{a_3^2}}\operatorname{erfc}\left[\frac{|\mathbf{r}|+|\mathbf{r}'|+\frac{2\pi\tau}{a_3}}{\sqrt{2\tau}}\right]
\tag{5.45}
$$

and restoring the various materials and physical constants results in the following expression for the reduced mass portion of the central potential propagator for the δ-function pair potential,

$$
K(\mathbf{r},\mathbf{r}';\tau) = \left(\frac{\mu}{2\pi\hbar\tau}\right)^{3/2}e^{-\frac{\mu|\mathbf{r}-\mathbf{r}'|^2}{2\hbar\tau}} + \left(\frac{\tau\hbar}{\mu|\mathbf{r}||\mathbf{r}'|}\right)\left(\frac{\mu}{2\pi\hbar\tau}\right)^{3/2}e^{-\mu\frac{(|\mathbf{r}|+|\mathbf{r}'|)^2}{2\hbar\tau}}
$$

$$
+ \frac{\mu}{4\pi\hbar^2 a_s|\mathbf{r}||\mathbf{r}'|}e^{-\frac{\mu}{a_s\hbar}(|\mathbf{r}|+|\mathbf{r}'|)+\frac{\mu\tau}{2\hbar^3 a_s^2}}\operatorname{erfc}\left[\sqrt{\frac{\mu}{2\hbar\tau}}\left(|\mathbf{r}|+|\mathbf{r}'|+\frac{\tau}{a_s\hbar}\right)\right].
\tag{5.46}
$$

5.5 Computational Implementation and Verification of the Delta Pair Propagator

Despite the exact derivation of the pair propagator for the δ-function pair pseudopotential in the previous section, a few challenges still remain concerning its computational implementation as well as checking the correctness of that implementation. This section is intended to address these final computational concerns for this pair propagator and to present their effective solution. In the first subsection, difficulties concerning the computational implementation of the special function definition of the δ-pair propagator will be addressed and a suitable, computationally tractable implementation will be presented. In the final subsection, a method to computationally check this expression will be presented and derived using the radial pair correlation function for the delta-function pair propagator. A simulated radial pair correlation function for a two particle system will then be compared to the exact calculated value and found to be correct to within a normalization constant.

5.5.1 Delta Pair Propagator and Action for Implementation

When eqns. (5.45) and (5.46) or more specifically their actions are implemented using the standard pair potential headers of the PIMC++ source code [1], a certain amount of modification must be made to this propagator and its associated action. First, the total propagator, $K(\mathbf{r}, \mathbf{r}'; \tau)$, is divided through by the reduced mass free particle propagator term, $\left(\frac{\mu}{2\pi\hbar\tau}\right)^{3/2} e^{-\frac{\mu|\mathbf{r}-\mathbf{r}'|^2}{2\hbar\tau}}$, and its corollary for the free particle propagator with suppressed materials constants since the free particle portion represents that which is sampled exactly.

---

[1] PIMC++ is an open source path integral Monte Carlo simulations package used for simulations in this thesis and developed by the Ceperley group.

To present the described as an equation, first the suppressed constants form is presented as

$$K(\mathbf{r}, \mathbf{r}'; \tau) = \frac{e^{-\frac{|\mathbf{r}-\mathbf{r}'|^2}{2\tau}}}{(2\pi\tau)^{3/2}} + \left(\frac{\tau}{|\mathbf{r}||\mathbf{r}'|}\right)\frac{e^{-\frac{(|\mathbf{r}|+|\mathbf{r}'|)^2}{2\tau}}}{(2\pi\tau)^{3/2}} - \frac{1}{2a_3|\mathbf{r}||\mathbf{r}'|}e^{\frac{2\pi(|\mathbf{r}|+|\mathbf{r}'|)}{a_3}+\frac{2\pi^2\tau}{a_3^2}}\,\text{erfc}\left[\frac{|\mathbf{r}|+|\mathbf{r}'|+\frac{2\pi\tau}{a_3}}{\sqrt{2\tau}}\right] \qquad (5.47)$$

$$= \frac{e^{-\frac{|\mathbf{r}-\mathbf{r}'|^2}{2\tau}}}{(2\pi\tau)^{3/2}} + \left(\frac{\tau}{|\mathbf{r}||\mathbf{r}'|}\right)\frac{e^{-\frac{(|\mathbf{r}|+|\mathbf{r}'|)^2}{2\tau}}}{(2\pi\tau)^{3/2}}\left[1 - \frac{\sqrt{2\pi^3\tau}}{a_3}e^{\frac{(-r|+-r'|+\frac{2\pi\tau}{a_3})^2}{2\tau}}\,\text{erfc}\left[\frac{|\mathbf{r}|+|\mathbf{r}'|+\frac{2\pi\tau}{a_3}}{\sqrt{2\tau}}\right]\right] \qquad (5.48)$$

$$= \frac{e^{-\frac{|\mathbf{r}-\mathbf{r}'|^2}{2\tau}}}{(2\pi\tau)^{3/2}}\left(1 + \left(\frac{\tau}{|\mathbf{r}||\mathbf{r}'|}\right)\frac{e^{-\frac{(|\mathbf{r}|+|\mathbf{r}'|)^2-|\mathbf{r}-\mathbf{r}'|^2}{2\tau}}}{(2\pi\tau)^{3/2}}\left[1 - \frac{\sqrt{2\pi^3\tau}}{a_3}e^{\frac{(-r|+-r'|+\frac{2\pi\tau}{a_3})^2}{2\tau}}\,\text{erfc}\left[\frac{|\mathbf{r}|+|\mathbf{r}'|+\frac{2\pi\tau}{a_3}}{\sqrt{2\tau}}\right]\right]\right)$$

$$(5.49)$$

and after division by the appropriate K_0 becomes

$$\rho_\delta(\mathbf{r}, \mathbf{r}'; \tau) = 1 + \left(\frac{\tau}{|\mathbf{r}||\mathbf{r}'|}\right)\frac{e^{-\frac{(|\mathbf{r}|+|\mathbf{r}'|)^2-|\mathbf{r}-\mathbf{r}'|^2}{2\tau}}}{(2\pi\tau)^{3/2}}\left[1 - \frac{\sqrt{2\pi^3\tau}}{a_3}e^{\frac{(-r|+-r'|+\frac{2\pi\tau}{a_3})^2}{2\tau}}\,\text{erfc}\left[\frac{|\mathbf{r}|+|\mathbf{r}'|+\frac{2\pi\tau}{a_3}}{\sqrt{2\tau}}\right]\right], \qquad (5.50)$$

where ρ_δ is the chosen notation for this reduced δ-pair propagator.

Followed, by the form with full materials constants

$$K(\mathbf{r},\mathbf{r}';\tau) = \left(\frac{\mu}{2\pi\hbar\tau}\right)^{3/2} e^{-\frac{\mu|\mathbf{r}-\mathbf{r}'|^2}{2\hbar\tau}} + \left(\frac{\tau\hbar}{\mu|\mathbf{r}||\mathbf{r}'|}\right) \left(\frac{\mu}{2\pi\hbar\tau}\right)^{3/2} e^{-\mu\frac{(|\mathbf{r}|+|\mathbf{r}'|)^2}{2\hbar\tau}}$$

$$+ \frac{\mu}{4\pi\hbar^2 a_s|\mathbf{r}||\mathbf{r}'|} e^{-\frac{\mu}{a_s\hbar}(|\mathbf{r}|+|\mathbf{r}'|)+\frac{\mu\tau}{2\hbar^3 a_s^2}} \operatorname{erfc}\left[\sqrt{\frac{\mu}{2\hbar\tau}}\left(|\mathbf{r}|+|\mathbf{r}'|+\frac{\tau}{a_s\hbar}\right)\right] \qquad (5.51)$$

$$= \left(\frac{\mu}{2\pi\hbar\tau}\right)^{3/2} e^{-\frac{\mu|\mathbf{r}-\mathbf{r}'|^2}{2\hbar\tau}} + \left(\frac{\tau\hbar}{\mu|\mathbf{r}||\mathbf{r}'|}\right) \left(\frac{\mu}{2\pi\hbar\tau}\right)^{3/2} e^{-\mu\frac{(|\mathbf{r}|+|\mathbf{r}'|)^2}{2\hbar\tau}}$$

$$\cdot \left(1 + \frac{\mu}{4\pi\hbar^2 a_s|\mathbf{r}||\mathbf{r}'|}\left(\frac{\mu}{2\pi\hbar\tau}\right)^{-3/2} e^{-\frac{\mu}{a_s\hbar}(|\mathbf{r}|+|\mathbf{r}'|)+\frac{\mu\tau}{2\hbar^3 a_s^2}+\mu\frac{(|\mathbf{r}|+|\mathbf{r}'|)^2}{2\hbar\tau}} \operatorname{erfc}\left[\sqrt{\frac{\mu}{2\hbar\tau}}\left(|\mathbf{r}|+|\mathbf{r}'|+\frac{\tau}{a_s\hbar}\right)\right]\right)$$

$$(5.52)$$

$$= \left(\frac{\mu}{2\pi\hbar\tau}\right)^{3/2} e^{-\frac{\mu|\mathbf{r}-\mathbf{r}'|^2}{2\hbar\tau}} \left(1 + \left(\frac{\tau\hbar}{\mu|\mathbf{r}||\mathbf{r}'|}\right) e^{-\mu\frac{(|\mathbf{r}|+|\mathbf{r}'|)^2}{2\hbar\tau}+\frac{\mu|\mathbf{r}-\mathbf{r}'|^2}{2\hbar\tau}}\right.$$

$$\left.\cdot \left(1 + \frac{\mu}{4\pi\hbar^2 a_s|\mathbf{r}||\mathbf{r}'|}\left(\frac{\mu}{2\pi\hbar\tau}\right)^{-3/2} e^{-\frac{\mu}{a_s\hbar}(|\mathbf{r}|+|\mathbf{r}'|)+\frac{\mu\tau}{2\hbar^3 a_s^2}+\mu\frac{(|\mathbf{r}|+|\mathbf{r}'|)^2}{2\hbar\tau}} \operatorname{erfc}\left[\sqrt{\frac{\mu}{2\hbar\tau}}\left(|\mathbf{r}|+|\mathbf{r}'|+\frac{\tau}{a_s\hbar}\right)\right]\right)\right)$$

$$(5.53)$$

and after division by the appropriate K_0 becomes

$$K(\mathbf{r},\mathbf{r}';\tau) = \left(\frac{\mu}{2\pi\hbar\tau}\right)^{3/2} e^{-\frac{\mu|\mathbf{r}-\mathbf{r}'|^2}{2\hbar\tau}} + \left(\frac{\tau\hbar}{\mu|\mathbf{r}||\mathbf{r}'|}\right) \left(\frac{\mu}{2\pi\hbar\tau}\right)^{3/2} e^{-\mu\frac{(|\mathbf{r}|+|\mathbf{r}'|)^2}{2\hbar\tau}}$$

$$+ \frac{\mu}{4\pi\hbar^2 a_s|\mathbf{r}||\mathbf{r}'|} e^{-\frac{\mu}{a_s\hbar}(|\mathbf{r}|+|\mathbf{r}'|)+\frac{\mu\tau}{2\hbar^3 a_s^2}} \operatorname{erfc}\left[\sqrt{\frac{\mu}{2\hbar\tau}}\left(|\mathbf{r}|+|\mathbf{r}'|+\frac{\tau}{a_s\hbar}\right)\right]. \qquad (5.54)$$

Finally, to derive the action the $-\log$ is taken of eqn. (5.54). The energy estimator for this propagator is found by taking the β derivative of that same action.

5.5.2 Challenges of the Computational Implementation of the Delta Pair Propagator

Despite all of functions present in ρ_δ being computationally well understood and even standard in the various libraries used for scientific computing such as the GNU Scientific Library (GSL), this equation still presents problems from a computational standpoint. These difficulties originate in the exp-erfc term in which the exponential function frequently becomes large as the erfc function becomes small so that rounding error and stability issues are encountered. This issue may be observed directly by considering the offending term from the suppressed constants ρ_δ (the issue is exactly the same for the ρ_δ with the materials constants),

$$e^{\frac{(|\mathbf{r}|+|\mathbf{r}'|+\frac{2\pi\tau}{a_3})^2}{2\tau}} \operatorname{erfc}\left[\frac{|\mathbf{r}|+|\mathbf{r}'|+\frac{2\pi\tau}{a_3}}{\sqrt{2\tau}}\right]. \tag{5.55}$$

Setting $g = \frac{(|\mathbf{r}|+|\mathbf{r}'|+\frac{2\pi\tau}{a_3})^2}{2\tau}$ and $z = \frac{|\mathbf{r}|+|\mathbf{r}'|+\frac{2\pi\tau}{a_3}}{\sqrt{2\tau}}$, results in the simplified form,

$$e^g \operatorname{erfc} z. \tag{5.56}$$

Consequently, a method to calculate this combined special function of an exponential or exponential-like function multiplied by an erfc function is required. First, recalling that $\operatorname{erfc} x = 1 - \operatorname{erf} x$ allows one take advantage of various expressions for the error function. Ultimately, this insight results in the modification of an algorithm for the error function which allows one to implement the erfc with an algorithm capable of achieving a maximal error $\leq 1.2 \times 10^{-7}$ using an exponential expression [113, 114]. This algorithm is expressed as follows as

$$\operatorname{erfc} x = q \text{ for } x \geq 0$$
$$= 2 - q \text{ for } x \leq 0 \tag{5.57}$$

where,

$$q = t \cdot \exp[-x^2 - 1.26551223 + 1.00002368 \cdot t + 0.37409196 \cdot t^2 + 0.09678419 \cdot t^3$$
$$- 0.18628806 \cdot t^4 + 0.27886807 \cdot t^5 - 1.13520398 \cdot t^6$$
$$+ 1.488515887 \cdot t^7 - 0.82215223 t^8 + 0.17087277 \cdot t^9]$$

$$\text{where } t = \frac{1}{1 + 0.5|x|}. \tag{5.58}$$

When eqn. (5.56) is expressed with this algorithm the $\exp(g)$ term may be combined with exponential portion of q and thus the final algorithm becomes,

$$e^g \, \text{erfc} \, z = q e^g q \text{ for } x \geq 0$$
$$= 2e^g - q e^g \text{ for } x \leq 0 \tag{5.59}$$

where,

$$e^g q = t \cdot \exp[g - x^2 - 1.26551223 + 1.00002368 \cdot t + 0.37409196 \cdot t^2 + 0.09678419 \cdot t^3$$
$$- 0.18628806 \cdot t^4 + 0.27886807 \cdot t^5 - 1.13520398 \cdot t^6$$
$$+ 1.488515887 \cdot t^7 - 0.82215223 t^8 + 0.17087277 \cdot t^9]$$

$$\text{where } t = \frac{1}{1 + 0.5|x|}, \tag{5.60}$$

which may be easily implemented without rounding error or stability issues.

5.5.3 Radial Distribution Function as a Check for a Pair Propagator

Testing the δ-pair or any pair propagator presents some unique challenges due to the multidimensional nature of the propagator. Fortunately, any pair propagator may be used to exactly express it's associated radial distribution function and thus to test a pair propagator in a computational setting with very little additional work, assuming that one's underlying simulation program possesses a well-tested radial/pair distribution simulation capability.

The formalism for this approach was among the first computational methods developed in the physics
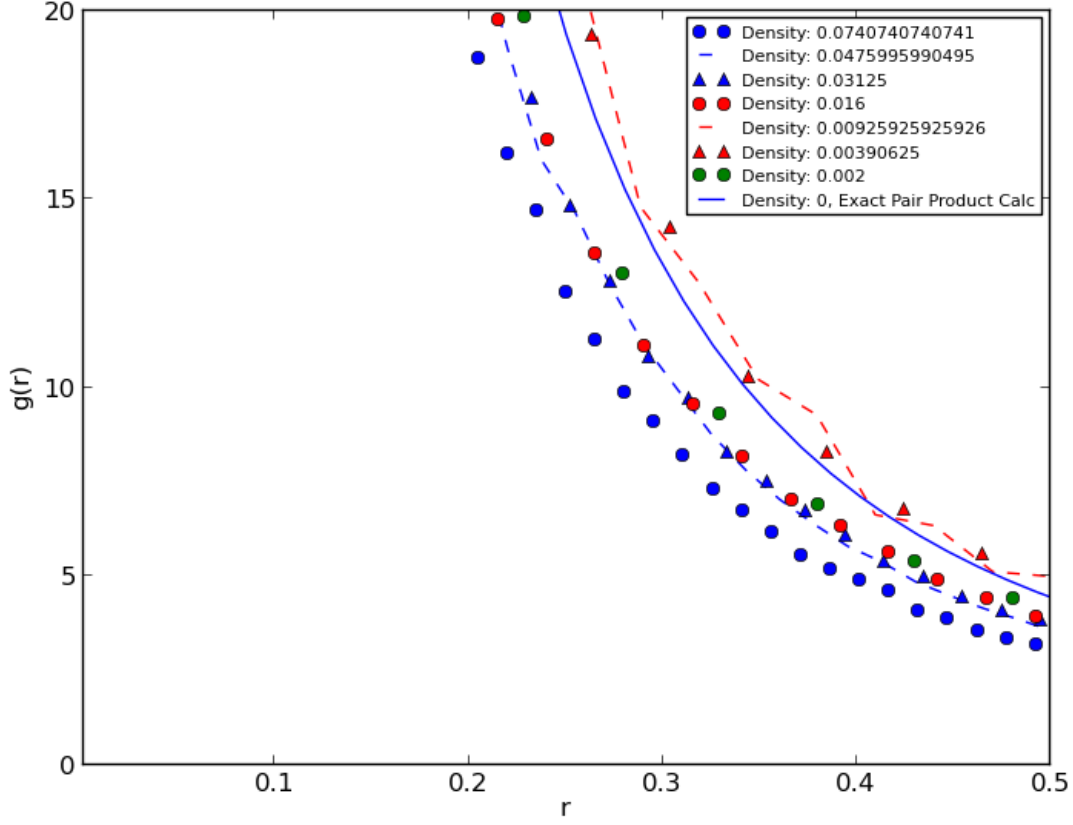
Figure 5.1: The plot of the radial distribution or pair correlation function as a function of density for a δ-pair interaction propagator with a scattering length, $a_s = -100$ intrinsic length units and a $\mu = \frac{1}{2}$ with each particle having a mass of 1, and $T = 2.5\epsilon_0$

community [76, 115, 116]and is presented as follows,

$$g(|\mathbf{x} - \mathbf{y}'|) = \frac{\rho_2(\mathbf{x}, \mathbf{y}, \mathbf{x}, \mathbf{y})}{\rho_1(\mathbf{x}, \mathbf{x})\rho_1(\mathbf{y}, \mathbf{y})}, \tag{5.61}$$

where $\mathbf{x}$ and $\mathbf{y}$ denote the positions of the individual particles, $g(|\mathbf{x} - \mathbf{y}|)$ is the diagonal matrix element two-particle pair correlation or radial distribution function, $\rho_2(\mathbf{x}, \mathbf{y}, \mathbf{x}, \mathbf{y})$ is the diagonal pair propagator, and $\rho_1(\mathbf{x}, \mathbf{x})$ is the diagonal free particle propagator for the particle labeled by $\mathbf{x}$.

Within the context of the pair product transformation, $g(|\mathbf{x} - \mathbf{y}'|)$ may be expressed as the diagonal form of the reduced term denoted in the prior section by $\rho_\delta(\mathbf{r}, \mathbf{r}; \tau)$ because it is just the pair product propagator expressed in terms of the relative coordinates of the underlying particles divided through by the total mass and reduced mass free particle propagator terms, which satisfies the prescription for $g(|\mathbf{x} - \mathbf{y}'|)$ given by eqn.
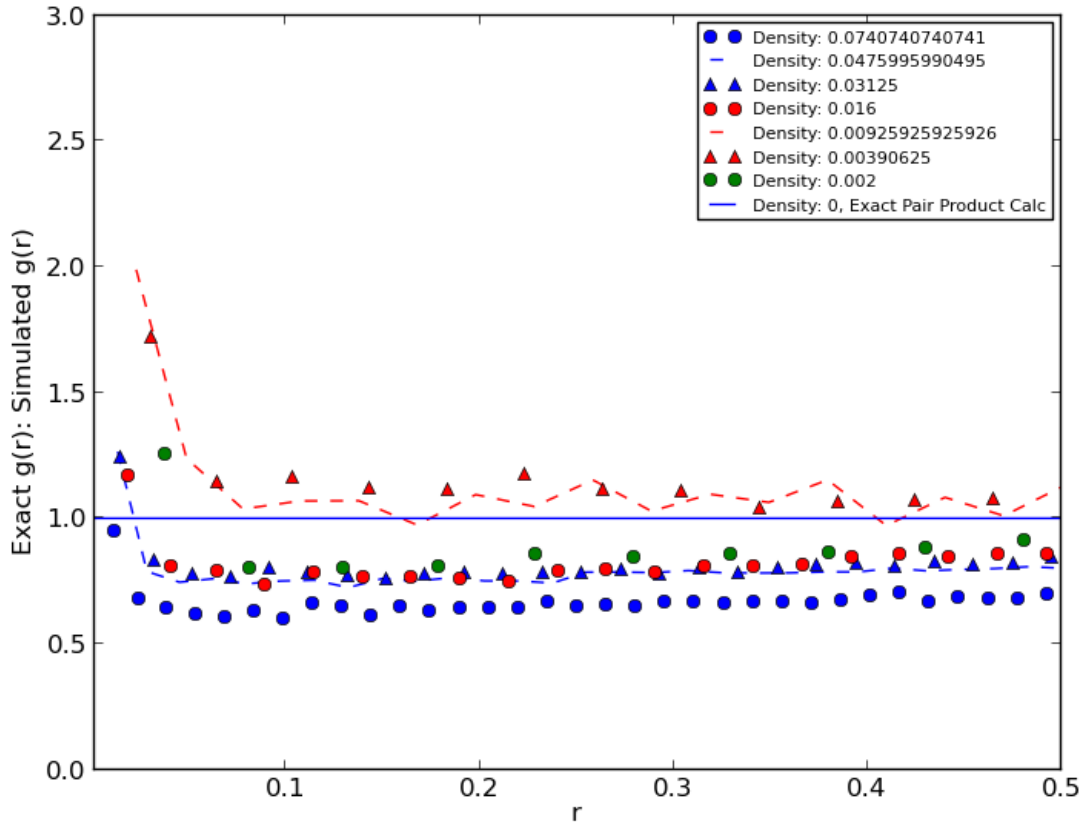
Figure 5.2: The plot of the ratios of simulated radial distribution or pair correlation functions to the exact calculated value as a function of density for a δ-pair interaction propagator with a scattering length, $a_s = -100$ intrinsic length units, a $\mu = \frac{1}{2}$ with each particle having a mass of 1, and $T = 2.5\epsilon_0$. The discrepancy to a ratio of 1 observed in terms of constancy of the approximately flat lines is due to a difference in normalization between the simulated and exact pair correlation functions due to difference in normalization between periodic boundary conditions and all space.

(5.61.

Consequently, a two particle simulation may be run using the previously describe pair propagator code for the δ-pair interaction such that the radial distribution function is observed and the diagonal terms of that same pair propagator code may be used to generate a check. In this type of simulation, the only expected errors would occur variously due either to random noise in the simulation or due to the difference in the implicit normalization constants for the pair propagator in free space and that naturally occurring in the simulation due to the periodic boundary conditions. Thus, one would expect a roughly flat curve when the ratio of the simulated radial distribution function to the exact radial distribution function is plotted. When the δ-pair propagator was implemented in code by the author, this sort of unit testing was performed and

the plots for both the radial distribution functions as well as their ratios are displayed in figs. (5.1) and (5.2) respectively. As can be seen Fig. (5.2), the expected flat lines are observed with a deviation from 1 in terms of the value of the ratios being caused by the aforementioned difference in normalization constants.

5.5.4 The Unitary Propagator or Delta Pair Propagator in the Unitary Limit

The unitary propagator is the delta pair propagator, eqn. 5.51, in the limit of $a_s \to -\infty$, which may be written as

$$K(\mathbf{r}, \mathbf{r}'; \tau) = \left(\frac{\mu}{2\pi\hbar\tau}\right)^{3/2} e^{-\frac{\mu|\mathbf{r}-\mathbf{r}'|^2}{2\hbar\tau}} + \left(\frac{\tau\hbar}{\mu|\mathbf{r}||\mathbf{r}'|}\right) \left(\frac{\mu}{2\pi\hbar\tau}\right)^{3/2} e^{-\mu\frac{(|\mathbf{r}|+|\mathbf{r}'|)^2}{2\hbar\tau}}. \tag{5.62}$$

Dividing the preceding pair propagator through by the free particle term as was done in eqn. (5.50) yields,

$$\rho_U(\mathbf{r}, \mathbf{r}'; \tau) = 1 + \left(\frac{\tau}{|\mathbf{r}||\mathbf{r}'|}\right) \frac{e^{-\frac{(|\mathbf{r}|+|\mathbf{r}'|)^2 - |\mathbf{r}-\mathbf{r}'|^2}{2\tau}}}{(2\pi\tau)^{3/2}}. \tag{5.63}$$

Obtaining convergence with this new unitary propagator becomes difficult due to the hairpin-like divergence of the singular term. If care is not taken in programming this singular term, an unusual error which is present in most current programming languages with limited precision for real numbers occurs. This error is due to a simultaneous underflow error from the exponential part and overflow error from the singular part in the second term of eqn. (5.63) and is very difficult to discover the source of this error in experience of the author as it is an exceedingly rare event which occurs only in specific configurations of the off-diagonal term of the propagator. After its occurrence, however, the error essentially traps the simulation so that it ceases to move.

Fixing this error requires that the singular part be combined with exponential part by re-writing eqn. (5.63) as

$$\rho_U(\mathbf{r}, \mathbf{r}'; \tau) = 1 + e^{-\frac{(|\mathbf{r}|+|\mathbf{r}'|)^2 - |\mathbf{r}-\mathbf{r}'|^2}{2\tau} + \log\left(\frac{\tau}{|\mathbf{r}||\mathbf{r}'|(2\pi\tau)^{3/2}}\right)}. \tag{5.64}$$

The total argument in the exponential term may then be tested for size to prevent subsequent over- or underflow errors. Applying this implementation method to the finite scattering length delta pair propagator may also yield better results for that method as well with regards to scattering length and convergence, but was not attempted in work.
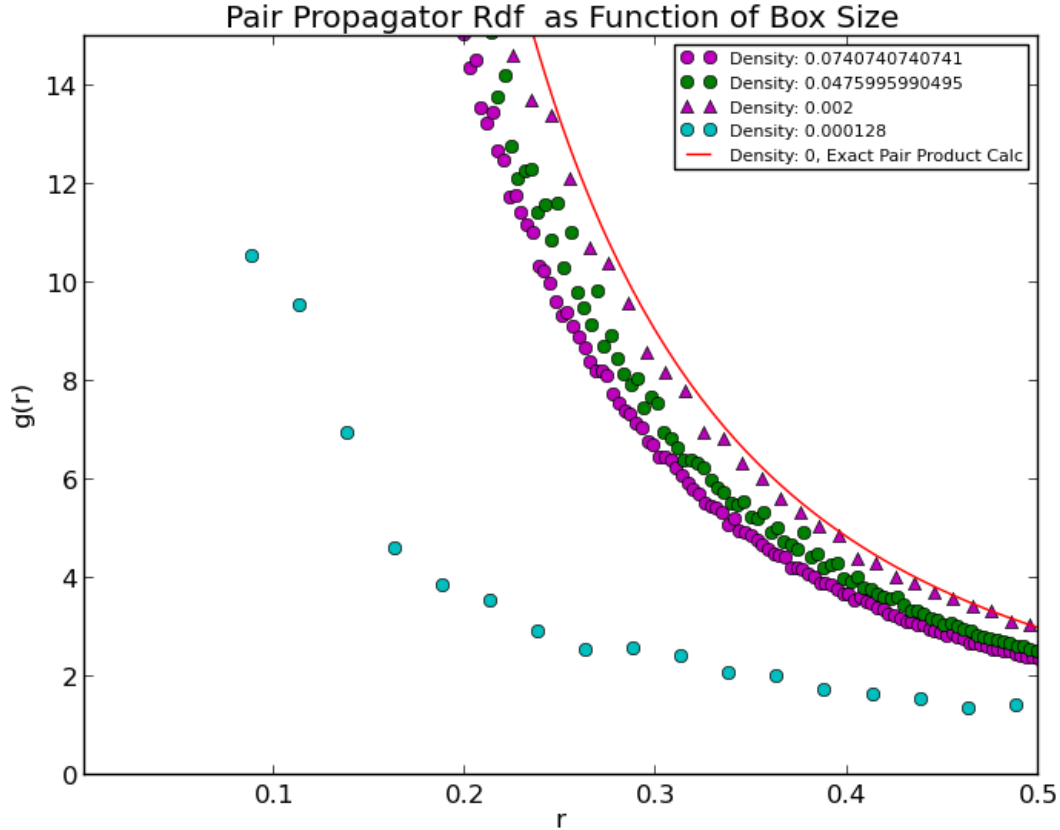
Figure 5.3: The plot of the radial distribution or pair correlation function as a function of density for a δ-pair interaction propagator at unitarity with a $\mu = \frac{1}{2}$ with each particle having a mass of 1, and $T = 2.5\epsilon_0$

5.5.5 Verification of the Delta Pair Propagator in the Unitary Limit using the Radial Distribution Function

Just as in the case of a propagator with a finite scattering length, a simulation of the radial distribution function of a two particle system may be performed with this unitary propagator and compared to the exact pair distribution function for the unitary limit. The procedure, derivation, and justification of this approach is exactly the same as that used is in section (5.5.3) with the exception that the two particle propagator being used is different. Plots for the radial distribution function of the unitary propagator at

113
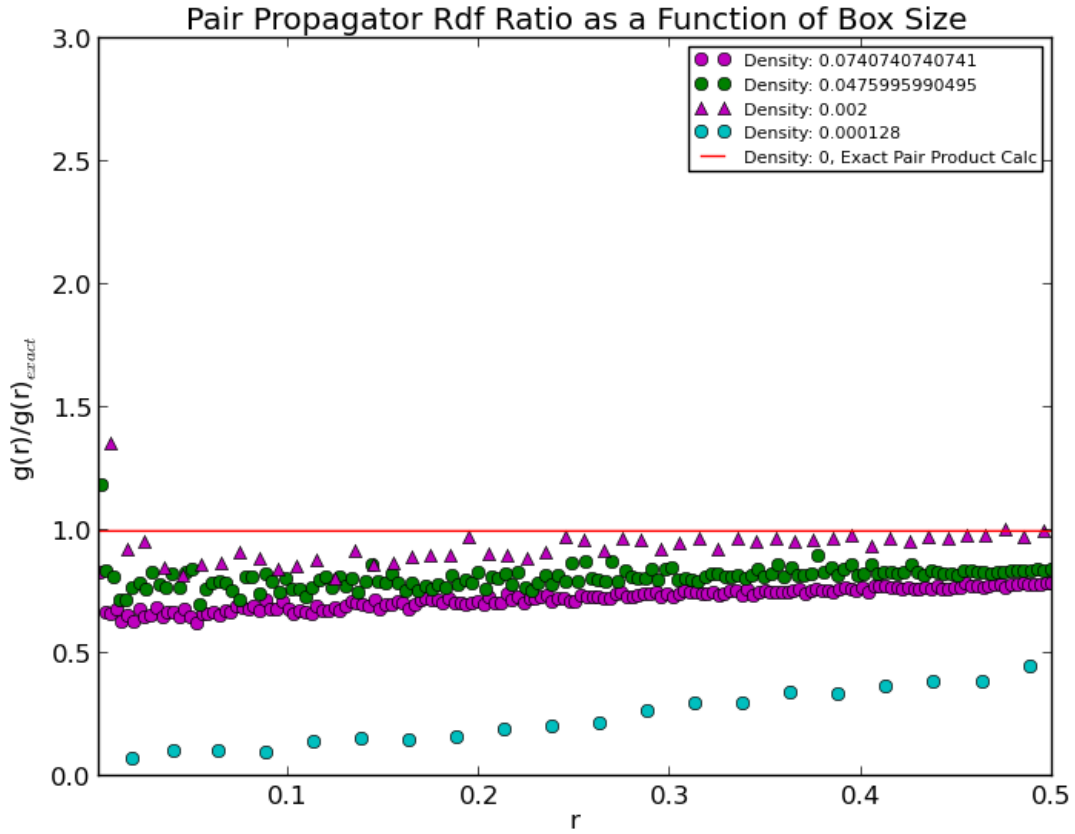
Figure 5.4: The plot of the ratios of simulated radial distribution or pair correlation functions to the exact calculated value as a function of density for a δ-pair interaction propagator at unitarity with a $\mu = \frac{1}{2}$ with each particle having a mass of 1, and $T = 2.5\epsilon_0$. The discrepancy to a ratio of 1 observed in terms of constancy of the approximately flat lines is due to a difference in normalization between the simulated and exact pair correlation functions due to difference in normalization between periodic boundary conditions and all space.

Chapter 6

Simulations of the Unpolarized Fermi Gas at Unitarity

6.1 Overview

The simulations presented in this chapter focus upon systems of dilute, 3-dimensional unitary Fermi gases at the unitary limit calculated with fixed-node path integral Monte Carlo using the nodes of the corresponding fermionic free particle density matrix. The resulting data from these simulations will be presented in the form of plots with commentary on some selected values and their relation to other theoretical results

From a computational standpoint, the system under study is defined using the pair propagators for attractive delta function pseudopotentials at the unitary limit presented in the preceding chapter in the PIMC framework. In particular, a system of 2 species of interacting fermions which do not interact amongst like particles are studied here and are designated here by being considered to be the same particle type in different spin state, spin-up or spin-down with the Hamiltonian for the system in question being given by,

$$\hat{H} = \sum_{i=1}^{N} \frac{\hbar^2}{2m} \nabla_i^2 + \sum_{j=1}^{N} \frac{\hbar^2}{2m} \nabla_j^2 + a_s \sum \delta(\mathbf{r}_{1i} - \mathbf{r}_{2j}), \tag{6.1}$$

in the limit $a_s \to \infty$ and where m is the mass the 2 species considered. In these simulations atomic units are used and all bare masses are set to 1. Simulations are performed for an unpolarized system of 5 spin-up and spin-down particles using the fixed-node path integral Monte Carlo methodology in periodic boundary conditions with a cubic box sized to maintain a 0.238 density from Akkineni et. al. [36, 52] with a discretization of $\tau = 0.00519826$. The energy and temperature units used in this thesis are the intrinsic energy units of this system $\epsilon_0 = \frac{\hbar^2}{mr_0^2}$ where r_0 is an intrinsic length unit also set to 1. The corresponding fermi energy for this system used in Akkineni et. al. [36, 52] is $1\epsilon_F = 1.841\epsilon_0$ and the Fermi gas energy is $1\epsilon_{FG} = \frac{3}{5}\epsilon_F = 1.1046\epsilon_0$.

In the rest of this chapter, the enduring challenges of simulating this system are considered as are some of the workarounds for dealing with these challenges. The total system energy is considered, followed by the radial distribution function, the structure factor, and the superfluid density. Finally, conclusions and future

directions will be considered, which shall conclude this thesis.

6.2   Challenges of the Simulation

The simulation of the system under consideration in this chapter presented many technical challenges from a computational standpoint due to the usage of the novel unitary delta pair propagator. The offending portion of this pair propagator which is treated as a potential is given as follows,

$$\rho_U(\mathbf{r}, \mathbf{r}'; \tau) = 1 + \left(\frac{\tau}{|\mathbf{r}||\mathbf{r}'|}\right) \frac{e^{-\frac{(|\mathbf{r}|+|\mathbf{r}'|)^2 - |\mathbf{r}-\mathbf{r}'|^2}{2\tau}}}{(2\pi\tau)^{3/2}}. \tag{6.2}$$

In looking over, eqn. (6.2) one notices that the second term has an associated singular sub-term. While it can be argued that in some Lie-Trotter type or short-(imaginary)-time discretizations, if a singular term appears that it will be be integrated out in some sense and the sampling will not be adversely effected by it. In this case, however, the exact two-particle propagator has a singular term in it which is conjectured by this author to be a consequence of the pair-interaction being a distribution and not a true function. Consequently for higher particle number propagators defined by the same particle pair interactions, it is not unreasonable to presume that an exact solution for that propagator would feature singularities as well.

These considerations are important since it is empirically observed in simulations with the propagator given by eqn. (5.62) that in some simulations the particles pair up and fall into the singularity in such a way that they are effectively trapped on the timescale of the simulation. This is an effect that was presumably encountered by Pessoa et. al. [53] since while it is not explicitly stated that such an effect occurs, a great deal of effort is expended creating a novel sampling scheme which is designed to swap pairings amongst the interacting particles of the system being studied. A cruder approach than taken by Pessoa et. al. is used in this thesis. Specifically, any simulation whose time series correlation length is greater than 10 time series units is not included in the calculation of any quantities in this thesis. This length was chosen as it empirically divides the simulations as two regimes since the trapped simulations typically have correlation length units of 30 or more intrinsic time series units. This is done so that the large correlations caused by the very tight binding between paired particles are rejected from the calculation. While this may slightly bias the resultant simulations due to failure to include data from regimes of strong binding, in practice it appears to be a reasonable approach as good agreement is found at high temperature between the system in question and prior results from a related system by Akkineni et. al. [36, 52].
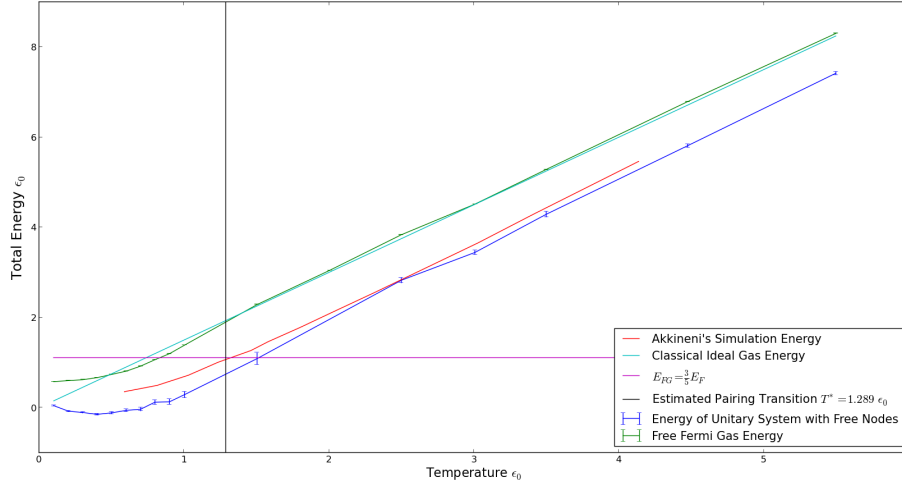
Figure 6.1: The energy per particle is plotted as a function of temperature for the unitary system and compared to a similar calculation performed by Akkineni in [36, 52] for a Pöschl-Teller pair interaction tuned to unitarity and to a free Fermi gas of similar particle number. A classical ideal gas energy is provided for reference as is the theoretical pairing temperature [117] as an energy.

6.3 Energy

The total energy per particle for a free particle fixed node simulation of the system defined by eqn. (6.1) is given in graphical form by Fig. (6.1). It compares quite well particularly at high temperature with simulations performed earlier by Akkineni in [36, 52] for a Pöschl-Teller pair interaction tuned to unitarity and follows quite closely to them for the entire range of his simulation. The total energy per particle at the lowest temperature $T = 0.1\epsilon_0$ is $0.043 \pm 0.013\epsilon_0$ which compares unfavorably with the energy per particle $0.44(1)\epsilon_{FG} = 0.26\epsilon_F = 0.48\epsilon_0$ at $T = 0$ [52]. However, when compared with the range of data from Akkineni, this simulated plot, compares fairly well at high and medium temperatures, only becoming negative or near 0 as temperatures become lower.

It is unclear if this is an indication of a non-ergodic effect in the simulation or caused by a need for a finer discretization. A finer discretization was attempted by the author so that the discretization went from $\tau = 0.00519826$ to $\tau = 0.000519826$. This new discretization unfortunately did not converge after 5 days of simulation and appears to make the particle trapping problem referred to in an early section worse.

The kinetic and potential energy for this unitary system are plotted in Figs. (6.2) and (6.3) respectively. In a visual inspection of Fig. (6.2), it appears that a transition seems to appear at $T = \epsilon_0$ as the kinetic energy of the system appears to plummet. It is unknown if this is due to an issue with the ergodicity of the simulation or due to the system itself; any subsequent exploration of this system ought to explore this as
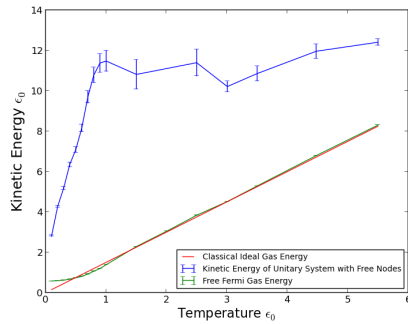
117

Figure 6.2: The kinetic energy per particle is plotted as a function of temperature for the unitary system.
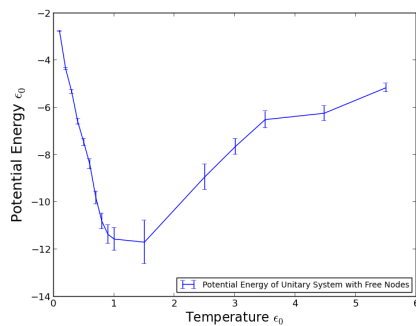

Figure 6.3: The potential energy per particle is plotted as a function of temperature for the unitary system.

interesting physics may be here.

6.4   Radial Distribution Function and Structure Factor

The radial distribution functions produced within this simulation of the unpolarized unitary fermi gas diverges as $\frac{1}{r^2}$ as expected from the exact two-body unitary propagator. Looking at the differences between the high temperature radial distribution plots in Fig. (6.4) and the low temperature radial distribution plots in Fig. (6.5) suggest that a change has occured between the high and low temperature zones, but do not provide a clear indication of any transition.

The structure factors presented in the accompanying plots given by Fig. (6.6) give no indication of any great structural change in k-space at any temperature. The multiple values for each $|k|$ represent individual values for each shell; they should converge in the limit of many runs.
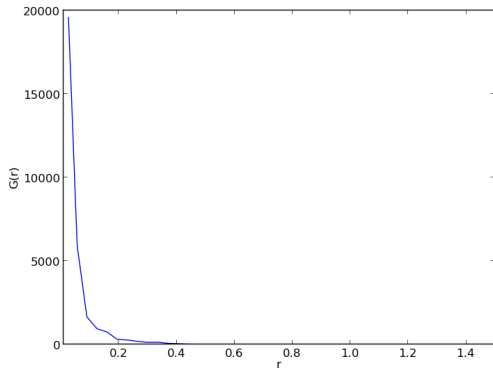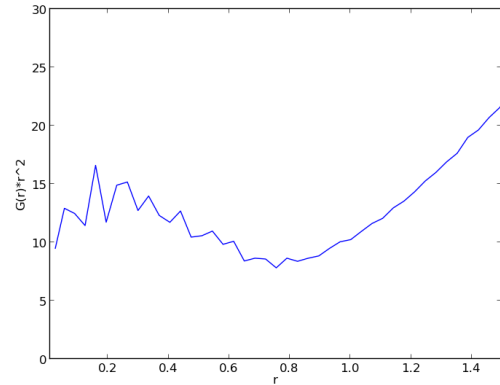
(a) Radial distribution function of spin-up and spin-down particles at $T = 4.5\epsilon_0$
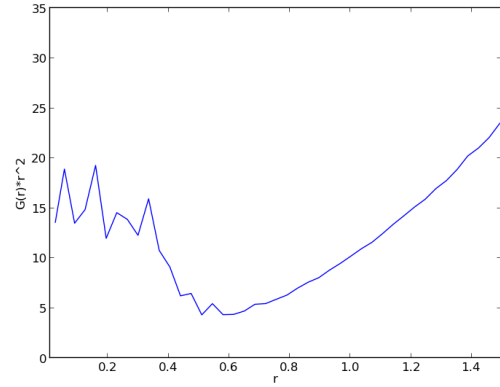
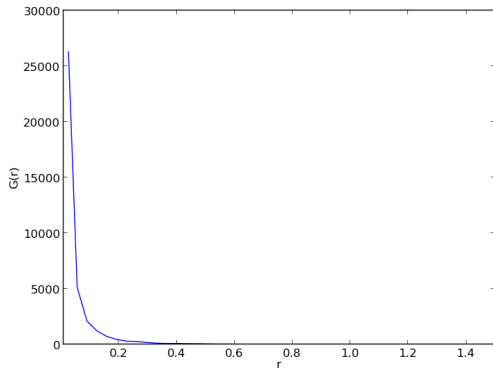(b) Radial distribution function times r^2 of spin-up and spin-down particles at $T = 4.5\epsilon_0$
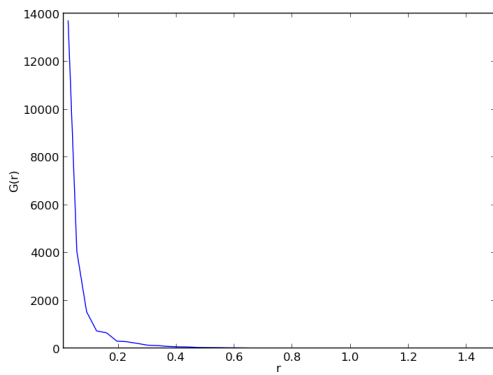
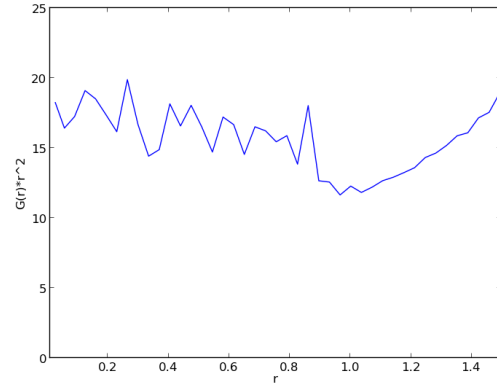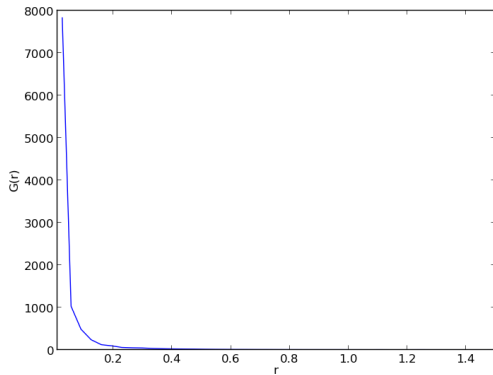(c) Radial distribution function of spin-up and spin-down particles at $T = 2.5\epsilon_0$

(d) Radial distribution function times r^2 of spin-up and spin-down particles at $T = 2.5\epsilon_0$

Figure 6.4: Plots of Radial Distribution Functions at various high temperatures on the left and Radial Distribution Functions time r^2 on the right.
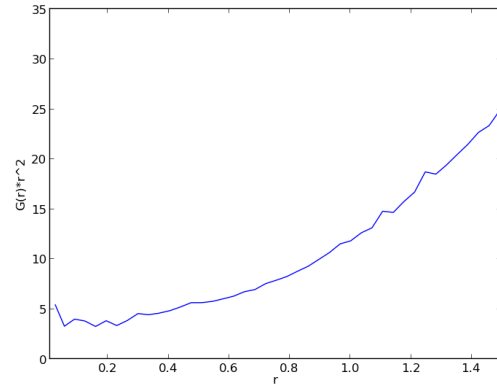
(a) Radial distribution function of spin-up and spin-down particles at $T = 0.8\epsilon_0$

(b) Radial distribution function times r^2 of spin-up and spin-down particles at $T = 0.8\epsilon_0$
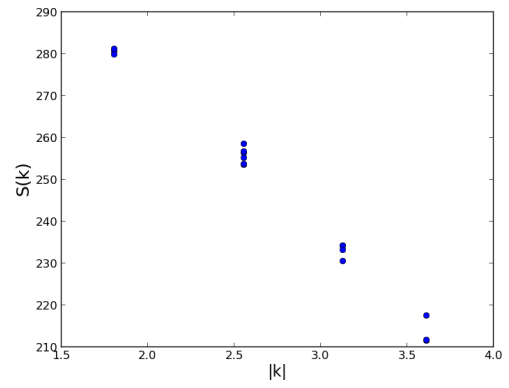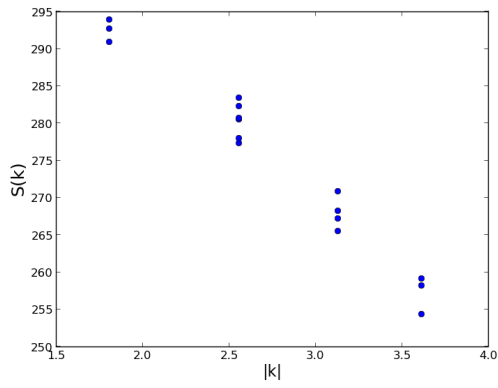

(c) Radial distribution function of spin-up and spin-down particles at $T = 0.1\epsilon_0$
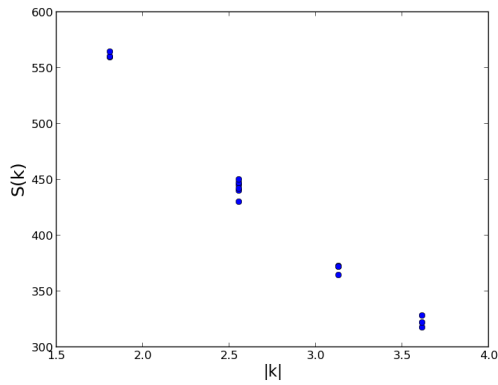

(d) Radial distribution function times r^2 of spin-up and spin-down particles at $T = 0.1\epsilon_0$

Figure 6.5: Plots of Radial Distribution Functions at various low temperatures on the left and Radial Distribution Functions time r^2 on the right.

(a) $|S(k)|$ of spin-up and spin-down particles at $T = 4.5\epsilon_0$ (b) $|S(k)|$ of spin-up and spin-down particles at $T = 2.5\epsilon_0$
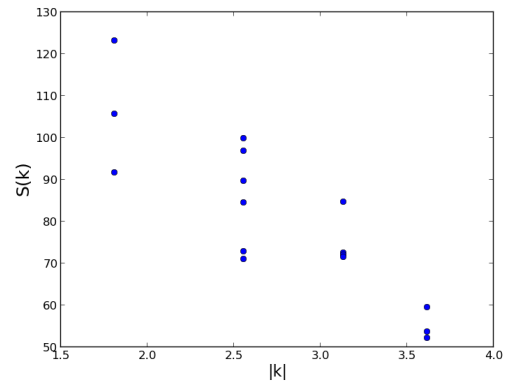
(c) $|S(k)|$ of spin-up and spin-down particles at $T = 0.8\epsilon_0$ (d) $|S(k)|$ of spin-up and spin-down particles at $T = 0.1\epsilon_0$

Figure 6.6: Plots of the Structure Factor at various temperatures as a function of $|k|$.
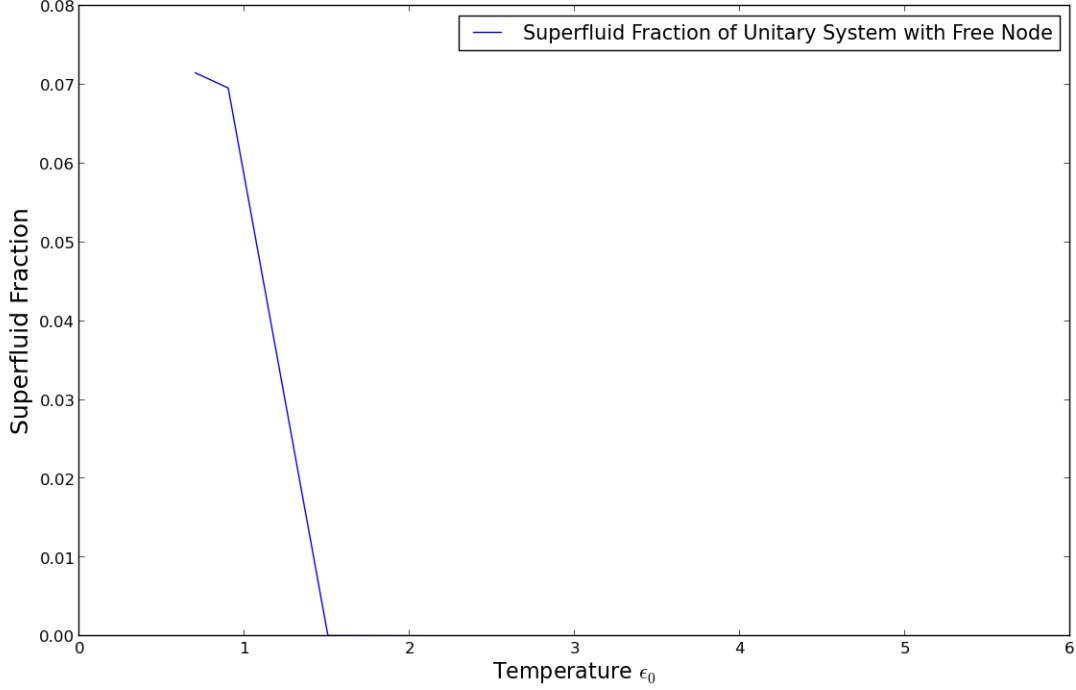
Figure 6.7: The superfluid fraction as a function of temperature. The error bars are suppressed.

6.5   Superfluid Fraction

The superfluid fraction is visualized in Fig. (6.7). The error bars are suppressed for very low temperature to make reading the plot easier. Nonetheless, it is clear that a superfluid transition does exist for this unitary fermionic system as the nascent formation of one appears to be forming in that same figure; it is even more clear from Fig. (6.8) as the superfluid fraction spans many decades of values indicating that superfluidity as measured by the superfluid fraction appears quite suddenly around a temperature, $T_{SF} \approx 1\epsilon_0$. Unfortunately, not enough data was able to be gathered to gain a true indication of this transition temperature.

6.6   Conclusion and Future Directions

This project has been a mixed success in the view of this author. While many technical challenges concerning the implementation and sampling of the delta pair propagator in the unitary limit have been overcome, this project has not yielded the "smoking gun" hoped for in determining the unitary transition. Key to this inconclusiveness is the difficulty in sampling the system in question in such a way that the extreme
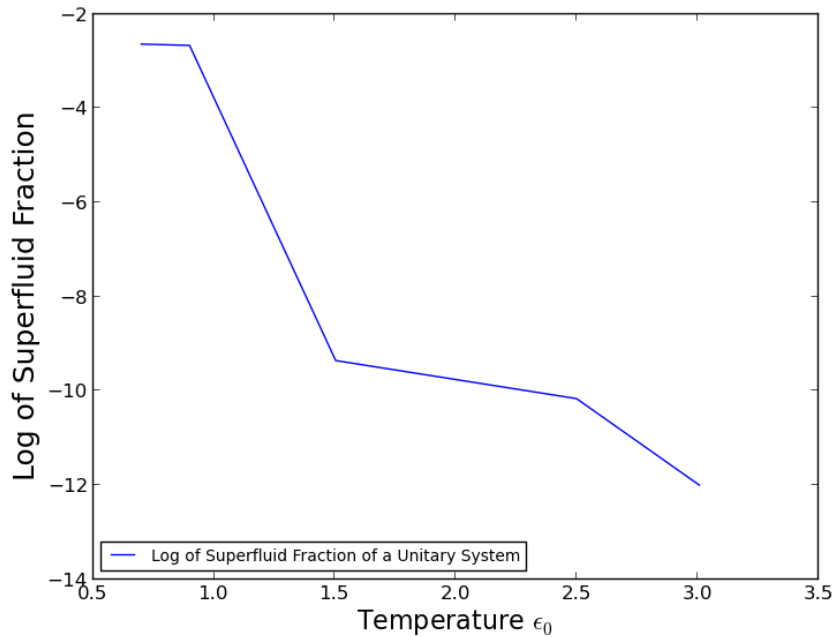
Figure 6.8: The logarithm of superfluid fraction as a function of temperature. The error bars are suppressed for covenience.

pairing observed in thesis does not occur [1]. Any future work on this problem must address this issue in a satisfactory way to move forward. Possible methods to do this include implementing alternative bulk moves that are designed to break up the tight pairing which occurs in these simulations or changing the underlying coordinate systems to spherical coordinates so that the pair divergences are canceled by the radial Jacobian term and sampling from the resultant distribution. Once this challenge is overcome, careful consideration of fermionic thermal density matrix nodes will be required to obtain accurate results. Suffice to say, it is this author's view that from the standpoint of simulation much remains to be done within the seemingly simple field of unitary fermi gas physics.

---

[1]This is challenging and problematic precisely because the physics of interest in unitarity is pairing.

References

[1] M. Lewenstein, A. Sanpera, and V. Ahufinger. *Ultracold Atoms in Optical Lattices: Simulating quantum many-body systems*. OUP Oxford, 2012.

[2] M. H. Anderson, J. R. Ensher, M. R. Matthews, C. E. Wieman, and E. A. Cornell. Observation of bose-einstein condensation in a dilute atomic vapor. *Science*, 269(5221):198–201, 1995.

[3] K. B. Davis, M. O. Mewes, M. R. Andrews, N. J. van Druten, D. S. Durfee, D. M. Kurn, and W. Ketterle. Bose-einstein condensation in a gas of sodium atoms. *Phys. Rev. Lett.*, 75:3969–3973, Nov 1995.

[4] C. C. Bradley, C. A. Sackett, J. J. Tollett, and R. G. Hulet. Evidence of bose-einstein condensation in an atomic gas with attractive interactions. *Phys. Rev. Lett.*, 75:1687–1690, Aug 1995.

[5] National Research Council Committee on AMO 2010. *Controlling the Quantum World of Atoms, Molecules, and Photons: An Interim Report*. National Academies Press, 2005.

[6] B. DeMarco and D. S. Jin. Onset of fermi degeneracy in a trapped atomic gas. *Science*, 285(5434):1703–1706, 1999.

[7] S. Gupta, Z. Hadzibabic, M. W. Zwierlein, C. A. Stan, K. Dieckmann, C. H. Schunck, E. G. M. van Kempen, B. J. Verhaar, and W. Ketterle. Radio-frequency spectroscopy of ultracold fermions. *Science*, 300(5626):1723–1726, 2003.

[8] T. Bourdel, J. Cubizolles, L. Khaykovich, K. M. F. Magalhães, S. J. J. M. F. Kokkelmans, G. V. Shlyapnikov, and C. Salomon. Measurement of the interaction energy near a feshbach resonance in a ^{6}Li fermi gas. *Phys. Rev. Lett.*, 91:020402, Jul 2003.

[9] C. Chin, M. Bartenstein, A. Altmeyer, S. Riedl, S. Jochim, J. Hecker Denschlag, and R. Grimm. Observation of the pairing gap in a strongly interacting fermi gas. *Science*, 305(5687):1128–1130, 2004.

[10] Martin W Zwierlein, Jamil R Abo-Shaeer, Andre Schirotzek, Christian H Schunck, and Wolfgang Ketterle. Vortices and superfluidity in a strongly interacting fermi gas. *Nature*, 435(7045):1047–1051, 2005.

[11] Tobias J Osborne. Hamiltonian complexity. *Reports on Progress in Physics*, 75(2):022001, 2012.

[12] Michael McNeil Forbes. The unitary fermi gas: An overview. 2012.

[13] F.H.L. Essler, H. Frahm, F. Göhmann, A. Klümper, and V.E. Korepin. *The One-Dimensional Hubbard Model*. Cambridge University Press, 2005.

[14] U. Schollwöck. The density-matrix renormalization group. *Rev. Mod. Phys.*, 77(1):259–315, Apr 2005.

[15] A. Altland and B.D. Simons. *Condensed Matter Field Theory*. Cambridge University Press, 2010.

[16] M. A. Cazalilla, R. Citro, T. Giamarchi, E. Orignac, and M. Rigol. One dimensional bosons: From condensed matter systems to ultracold gases. *Rev. Mod. Phys.*, 83:1405–1466, Dec 2011.

[17] Zoran Hadzibabic, Peter Krüger, Marc Cheneau, Baptiste Battelier, and Jean Dalibard. Berezinskii–kosterlitz–thouless crossover in a trapped atomic gas. *Nature*, 441(7097):1118–1121, 2006.

[18] The nobel prize in physics 1998. http://www.nobelprize.org/nobelprizes/physics/laureates/1998/. Accessed: 2014-10-01.

[19] B. Paredes, P. Fedichev, J. I. Cirac, and P. Zoller. $\frac{1}{2}$. *Phys. Rev. Lett.*, 87:010402, Jun 2001.

[20] M.A. Nielsen and I.L. Chuang. *Quantum Computation and Quantum Information: 10th Anniversary Edition*. Cambridge University Press, 2010.

[21] B. Douçot, M. V. Feigel'man, L. B. Ioffe, and A. S. Ioselevich. Protected qubits and chern-simons theories in josephson junction arrays. *Phys. Rev. B*, 71:024505, Jan 2005.

[22] Alexei Kitaev. Anyons in an exactly solved model and beyond. *Annals of Physics*, 321(1):2 – 111, 2006. January Special Issue.

[23] T Kraemer, M Mark, P Waldburger, JG Danzl, C Chin, B Engeser, AD Lange, K Pilch, A Jaakkola, H-C Nägerl, et al. Evidence for efimov quantum states in an ultracold gas of caesium atoms. *Nature*, 440(7082):315–318, 2006.

[24] Johann G Danzl, Manfred J Mark, Elmar Haller, Mattias Gustavsson, Russell Hart, Jesus Aldegunde, Jeremy M Hutson, and Hanns-Christoph Nägerl. An ultracold high-density sample of rovibronic ground-state molecules in an optical lattice. *Nature Physics*, 6(4):265–270, 2010.

[25] C.J. Pethick and H. Smith. *Bose-Einstein Condensation in Dilute Gases*. Cambridge University Press, 2002.

[26] L.P. Pitaevskii and S. Stringari. *Bose-Einstein Condensation*. International Series of Monographs on Physics. Clarendon Press, 2003.

[27] Shengquan Zhou. *Numerical methods for cold atom systems*. PhD thesis, University of Illinois at Urbana-Champaign, http://hdl.handle.net/2142/34448, 9 2012.

[28] A.L. Fetter and J.D. Walecka. *Quantum Theory of Many-Particle Systems*. Dover Books on Physics. Dover Publications, 2012.

[29] A. Griffin, D.W. Snoke, and S. Stringari. *Bose-Einstein Condensation*. Cambridge University Press, 1996.

[30] W. Zwerger. *The BCS-BEC Crossover and the Unitary Fermi Gas*. Lecture Notes in Physics. Springer, 2011.

[31] N.W. Ashcroft and N.D. Mermin. *Solid State Physics*. Saunders College, Philadelphia, 1976.

[32] A.J. Leggett. *Quantum Liquids: Bose condensation and Cooper pairing in condensed-matter systems*. Oxford Graduate Texts. OUP Oxford, 2006.

[33] Oliver Penrose and Lars Onsager. Bose-einstein condensation and liquid helium. *Phys. Rev.*, 104:576–584, Nov 1956.

[34] Kerson Huang and C. N. Yang. Quantum-mechanical many-body problem with hard-sphere interaction. *Phys. Rev.*, 105:767–775, Feb 1957.

[35] D. Eagles. Possible pairing without superconductivity at low carrier concentrations in bulk and thin-film superconducting semiconductors. *Phys. Rev.*, 186:456–463, Oct 1969.

[36] V. Akkineni and University of Illinois at Urbana-Champaign. *Pairing and Superfluid Properties of Polarized Dilute Fermion Gases in the BCS-BEC Crossover*. University of Illinois at Urbana-Champaign, 2008.

[37] Y. Ohashi and A. Griffin. Bcs-bec crossover in a gas of fermi atoms with a feshbach resonance. *Phys. Rev. Lett.*, 89:130402, Sep 2002.

[38] DS Petrov, C Salomon, and GV Shlyapnikov. Diatomic molecules in ultracold fermi gasesnovel composite bosons. *Journal of Physics B: Atomic, Molecular and Optical Physics*, 38(9):S645, 2005.

[39] Aurel Bulgac, Paulo F Bedaque, and Antonio C Fonseca. A dilute atomic fermi system with a large positive scattering length. *arXiv preprint cond-mat/0306302*, 2003.

[40] Yusuke Nishida and Dam Thanh Son. ? expansion for a fermi gas at infinite scattering length. *Phys. Rev. Lett.*, 97:050403, Aug 2006.

[41] Joaquín E Drut. Improved lattice operators for nonrelativistic fermions. *Physical Review A*, 86(1):013604, 2012.

[42] Michael G Endres, David B Kaplan, Jong-Wan Lee, and Amy N Nicholson. Lattice monte carlo calculations for unitary fermions in a harmonic trap. *Physical Review A*, 84(4):043644, 2011.

[43] Jiunn-Wei Chen and David B Kaplan. Lattice theory for low energy fermions at nonzero chemical potential. *Physical review letters*, 92(25):257002, 2004.

[44] Dean Lee. Ground state energy at unitarity. *Physical Review C*, 78(2):024001, 2008.

[45] Michael G Endres, David B Kaplan, Jong-Wan Lee, and Amy N Nicholson. Lattice monte carlo calculations for unitary fermions in a finite box. *Physical Review A*, 87(2):023615, 2013.

[46] Silas R Beane, Paulo F Bedaque, Asumpta Parreno, and Martin J Savage. Two nucleons on a lattice. *Physics Letters B*, 585(1):106–114, 2004.

[47] Mark JH Ku, Ariel T Sommer, Lawrence W Cheuk, and Martin W Zwierlein. Revealing the superfluid lambda transition in the universal thermodynamics of a unitary fermi gas. *Science*, 335(6068):563–567, 2012.

[48] D Rakshit, KM Daily, and D Blume. Natural and unnatural parity states of small trapped equal-mass two-component fermi gases at unitarity and fourth-order virial coefficient. *Physical Review A*, 85(3):033634, 2012.

[49] J. Carlson, S.-Y. Chang, V. Pandharipande, and K. Schmidt. Superfluid fermi gases with large scattering length. *Phys. Rev. Lett.*, 91:050401, Jul 2003.

[50] J. Carlson and Sanjay Reddy. Asymmetric two-component fermion systems in strong coupling. *Phys. Rev. Lett.*, 95:060401, Aug 2005.

[51] B.L. Hammond, W.A. Lester, and P.J. Reynolds. *Monte Carlo Methods in Ab Initio Quantum Chemistry.* Lecture and Course Notes In Chemistry Series. World Scientific, 1994.

[52] Vamsi K. Akkineni, D. M. Ceperley, and Nandini Trivedi. Pairing and superfluid properties of dilute fermion gases at unitarity. *Phys. Rev. B*, 76:165116, Oct 2007.

[53] Renato Pessoa, S. A. Vitiello, and K. E. Schmidt. Monte carlo calculations for fermi gases in the unitary limit with a zero-range interaction. Nov 2014.

[54] S. Y. Chang, V. R. Pandharipande, J. Carlson, and K. E. Schmidt. Quantum monte carlo studies of superfluid fermi gases. *Phys. Rev. A*, 70:043602, Oct 2004.

[55] G. E. Astrakharchik, J. Boronat, J. Casulleras, Giorgini, and S. Equation of state of a fermi gas in the bec-bcs crossover: A quantum monte carlo study. *Phys. Rev. Lett.*, 93:200404, Nov 2004.

[56] L. Bachelier, M. Davis, A. Etheridge, and P.A. Samuelson. *Louis Bachelier's Theory of Speculation: The Origins of Modern Finance.* Princeton University Press, 2011.

[57] M. Chaichian and A. Demichev. *Path Integrals in Physics: Volume I Stochastic Processes and Quantum Mechanics.* Institute of physics series in mathematical and computational physics. Taylor & Francis, 2001.

[58] H. Kleinert. *Path Integrals in Quantum Mechanics, Statistics, Polymer Physics, and Financial Markets.* World Scientific Publishing Company, Incorporated, 2009.

[59] Edward Nelson. Feynman integrals and the schrdinger equation. *Journal of Mathematical Physics*, 5(3):332–343, 1964.

[60] R.P. Feynman, A.R. Hibbs, and D.F. Styer. *Quantum Mechanics and Path Integrals: Emended Edition.* Dover Books on Physics. Dover Publications, 2010.

[61] Kenneth P. Esler. Advancements in the path integral monte carlo method for many-body quantum systems at finite temperature, 2006. Copyright - Copyright UMI - Dissertations Publishing 2006; Last updated - 2013-04-19; First page - n/a; M3: Ph.D.

[62] L.B. Barberà, J.B. Medico, and Universitat Politècnica de Catalunya. Departament de Física Aplicada. *Path integral Monte Carlo[: algorithms and applications to quantum fluids.* Universitat Politència de Catalunya, 2002.

[63] P.A.M. Dirac. *The Principles of Quantum Mechanics.* International series of monographs on physics. Clarendon Press, 1947.

[64] Richard Phillips Feynman and Albert R. Hibbs. *Quantum mechanics and path integrals.* International series in pure and applied physics. McGraw-Hill, New York, St. Louis, San Francisco, 1965.

[65] R.P. Feynman and L.M. Brown. *Feynman's thesis: a new approach to quantum theory.* World Scientific Publishing Company Incorporated, 1942.

[66] L.S. Schulman. *Techniques and Applications of Path Integration.* Dover Publ., New York, 2nd edition, 2005.

[67] H. Kleinert. *Path Integrals in Quantum Mechanics, Statistics, and Polymer Physics, and Financial Markets.* World Scientific Publishing Company Incorporated, 2004.

[68] T. Kashiwa, Y. Ohnuki, and M. Suzuki. *Path Integral Methods.* Oxford Science Publications. Clarendon Press, Oxford, UK, 1st edition, 1997.

[69] J. Thijssen. *Computational Physics.* Cambridge University Press, 2007.

[70] B J Berne and D Thirumalai. On the simulation of quantum systems: Path integral methods. *Annual Review of Physical Chemistry*, 37(1):401–424, 1986.

[71] Minoru Takahashi and Masatoshi Imada. Monte carlo calculation of quantum systems. *Journal of the Physical Society of Japan*, 53(3):963–974, 1984.

[72] D. M. Ceperley. *Monte Carlo and Molecular Dynamics of Condensed Matter Systems*, chapter Path Integral Monte Carlo Methods for Fermions. Bologna, Italy, 1996.

[73] D. M. Ceperley. Fermion nodes. *Journal of Statistical Physics*, 63:1237–1267, 1991. 10.1007/BF01030009.

[74] D. M. Ceperley. Path-integral calculations of normal liquid ^{3}He. *Phys. Rev. Lett.*, 69:331–334, Jul 1992.

[75] David Ceperley. Path integrals in the theory liquid helium. *Rev. Mod. Phys.*, 67(2):279–355, 1995.

[76] A. D. Klemm and R. G. Storer. The structure of quantum fluids: helium and neon. *Australian Journal of Physics*, 26:43, February 1973.

[77] Nicholas Metropolis, Arianna W Rosenbluth, Marshall N Rosenbluth, Augusta H Teller, and Edward Teller. Equation of state calculations by fast computing machines. *The Journal of Chemical Physics*, 21:1087, 1953.

[78] W. K. Hastings. Monte Carlo sampling methods using Markov chains and their applications. *Biometrika*, 57(1):97–109, April 1970.

[79] David Chandler and Peter G Wolynes. Exploiting the isomorphism between quantum theory and classical statistical mechanics of polyatomic fluids. *The Journal of Chemical Physics*, 74:4078, 1981.

[80] Jianshu Cao and Gregory A. Voth. The formulation of quantum statistical mechanics based on the feynman path centroid density. i. equilibrium properties. *The Journal of Chemical Physics*, 100(7):5093–5105, 1994.

[81] Jianshu Cao and Gregory A. Voth. The formulation of quantum statistical mechanics based on the feynman path centroid density. ii. dynamical properties. *The Journal of Chemical Physics*, 100(7):5106–5117, 1994.

[82] Seogjoo Jang and Gregory A. Voth. A derivation of centroid molecular dynamics and other approximate time evolution methods for path integral centroid variables. *The Journal of Chemical Physics*, 111(6):2371–2384, 1999.

[83] Ian R. Craig and David E. Manolopoulos. Quantum statistics and classical mechanics: Real time correlation functions from ring polymer molecular dynamics. *The Journal of Chemical Physics*, 121(8):3368–3373, 2004.

[84] Ian R. Craig and David E. Manolopoulos. A refined ring polymer molecular dynamics theory of chemical reaction rates. *The Journal of Chemical Physics*, 123(3):034102, 2005.

[85] Bastiaan J. Braams and David E. Manolopoulos. On the short-time limit of ring polymer molecular dynamics. *The Journal of Chemical Physics*, 125(12):124105, 2006.

[86] Ian R. Craig and David E. Manolopoulos. Chemical reaction rates from ring polymer molecular dynamics. *The Journal of Chemical Physics*, 122(8):084106, 2005.

[87] Scott Habershon, David E. Manolopoulos, Thomas E. Markland, and Thomas F. Miller. Ring-polymer molecular dynamics: Quantum effects in chemical dynamics from classical trajectories in an extended phase space. *Annual Review of Physical Chemistry*, 64(1):387–413, 2013. PMID: 23298242.

[88] Wolfhard Janke and Tilman Sauer. Path integral monte carlo using multigrid techniques. *Chemical Physics Letters*, 201(56):499 – 505, 1993.

[89] Art E. Cho, J. D. Doll, and David L. Freeman. Wavelet formulation of path integral monte carlo. *The Journal of Chemical Physics*, 117(13):5971–5977, 2002.

[90] Michiel Sprik, Michael L Klein, and David Chandler. Staging: A sampling technique for the monte carlo evaluation of path integrals. *Physical Review B*, 31(7):4234, 1985.

[91] M. F. Herman, E. J. Bruskin, and B. J. Berne. On path integral monte carlo simulations. *The Journal of Chemical Physics*, 76(10):5150–5155, 1982.

[92] Bruce J. Berne and D. Thirumalai. On the simulation of quantum systems: Path integral methods. *Annu. Rev. Phys. Chem.*, 37:401–424, 1986.

[93] Jianshu Cao and Bruce J. Berne. On energy estimators in path integral monte carlo simulations: Dependence of accuracy on algorithm. *The Journal of Chemical Physics*, 91(10):6359–6366, 1989.

[94] Karl J. Runge and Geoffrey V. Chester. Solid-fluid phase transition of quantum hard spheres at finite temperatures. *Phys. Rev. B*, 38:135–162, Jul 1988.

[95] D. Thirumalai and B.J. Berne. Methods for simulating time correlation functions. *Cmpt. Phys. Com.*, 63:415–426, 1991.

[96] Bruce J. Berne and D. Thirumalai. On the simulation of quantum systems: Path integral methods. *Annu. Rev. Phys. Chem.*, 37:401–424, 1986.

[97] J. Grujic, A. Bogojevic, and A. Balaz. Energy estimators and calculation of energy expectation values in the path integral formalism. *Physics Letters A*, 360(2):217 – 223, 2006.

[98] Yosihiko Ogata. A monte carlo method for high dimensional integration. *Numerische Mathematik*, 55(2):137–157, 1989.

[99] D. Frenkel and B. Smit. *Understanding Molecular Simulation: From Algorithms to Applications.* Computational Science Series, Vol 1. Academic Press, 2002.

[100] E. L. Pollock and D. M. Ceperley. Path-integral computation of superfluid densities. *Phys. Rev. B*, 36:8343–8352, Dec 1987.

[101] L.G. Valiant. The complexity of computing the permanent. *Theoretical Computer Science*, 8(2):189 – 201, 1979.

[102] Mark R. Jerrum, Leslie G. Valiant, and Vijay V. Vazirani. Random generation of combinatorial structures from a uniform distribution. *Theoretical Computer Science*, 43(0):169 – 188, 1986.

[103] D. M. Ceperley. *Monte Carlo and Molecular Dynamics of Condensed Matter Systems*, chapter Path integral Monte Carlo methods for fermions. Editrice Compositori, 1996.

[104] Matthias Troyer and Uwe-Jens Wiese. Computational complexity and fundamental limitations to fermionic quantum monte carlo simulations. *Phys. Rev. Lett.*, 94(17):170201, May 2005.

[105] Alexander P Lyubartsev. Interacting electrons in one dimension: a path integral monte carlo study. *Journal of Physics A: Mathematical and Theoretical*, 40(26):7151, 2007.

[106] R. Egger, L. Mühlbacher, and C. H. Mak. Path-integral monte carlo simulations without the sign problem: Multilevel blocking approach for effective actions. *Phys. Rev. E*, 61:5961–5966, May 2000.

[107] Nancy Makri. Information guided noise reduction for monte carlo integration of oscillatory functions. *Chem. Phys. Lett.*, 400:446–452, 2004.

[108] D. E. Gonzalez Trotter, F. Salinas Meneses, W. Tornow, C. R. Howell, Q. Chen, A. S. Crowell, C. D. Roper, R. L. Walter, D. Schmidt, H. Witała, W. Glöckle, H. Tang, Z. Zhou, and I. Šlaus. Neutron-deuteron breakup experiment at $E_n = 13$ MeV: Determination of the $^1S_0$ neutron-neutron scattering length a_{nn}. *Phys. Rev. C*, 73:034001, Mar 2006.

[109] S.M. Zemyan. *The Classical Theory of Integral Equations: A Concise Treatment.* SpringerLink : Bücher. Birkhäuser/Springer, 2012.

[110] E B Manoukian. Explicit derivation of the propagator for a dirac delta potential. *Journal of Physics A: Mathematical and General*, 22(1):67, 1989.

[111] James M Yearsley. The propagator for the step potential and delta function potential using the path decomposition expansion. *Journal of Physics A: Mathematical and Theoretical*, 41(28):285301, 2008.

[112] K. Wódkiewicz. Fermi pseudopotential in arbitrary dimensions. *Phys. Rev. A*, 43:68–76, Jan 1991.

[113] M. Abramowitz and I.A. Stegun. *Handbook of Mathematical Functions: with Formulas, Graphs, and Mathematical Tables.* Dover Books on Mathematics. Dover Publications, 2012.

[114] W.H. Press. *Numerical Recipes in FORTRAN: The Art of Scientific Computing.* Number v. 1-2. Cambridge University Press, 1992.

[115] S. Fujita. Pair distribution function and two-body propagator. *Phys. Rev.*, 115:1335–1341, Sep 1959.

[116] R. G. Storer. Radial distribution function for a quantum plasma. *Phys. Rev.*, 176:326–331, Dec 1968.

[117] Mohit Randeria, Nandini Trivedi, Adriana Moreo, and Richard T. Scalettar. Pairing and spin gap in the normal state of short coherence length superconductors. *Phys. Rev. Lett.*, 69:2001–2004, Sep 1992.